FUNCTIONAL CHARACTERIZATION OF FORMIN-DEPENDENT ACTIN POLYMERIZATION AT ADHERENS JUNCTIONS

MEGHA VAMAN RAO

M.Sc. (Pondicherry University, 2010)

A THESIS SUBMITTED

FOR THE DEGREE OF DOCTOR OF PHILOSOPHY

MECHANOBIOLOGY INSTITUTE

NATIONAL UNIVERSITY OF SINGAPORE

2016

DECLARATION

I hereby declare that this thesis is my original work and has been written by me in its entirety. I have duly acknowledged all sources of information that have been used in this thesis.

This thesis has not been submitted for any degree in any university previously.

Megha Vaman Rao

29 March 2016

ACKNOWLEDGEMENTS

This thesis could not have been completed without the support, encouragement and inspiration provided by several people.

I wish to express my deepest gratitude to Dr. Ronen Zaidel-Bar for being a wonderful mentor during the course of my PhD, and for his insightful suggestions and guidance that have helped me through this journey. It has truly been a great pleasure to work and interact with Dr. Zaidel-Bar over the past 5 years.

My sincere thanks to members of my Thesis Advisory Committee – Prof. Alexander Bershadsky and Dr. Edward Manser – for their suggestions, feedback and guidance throughout the years.

Many thanks to everyone at the Mechanobiology Institute who have helped me with learning new techniques, sharing reagents, providing feedback or for just being good friends! Thank you in particular to Dr. Yusuke Toyama, Leyla, Andrea, Cristina, Kee Chua, Kabir, Shiqiong and Hui Ting.

Thank you to all current and former members of the Zaidel-Bar group for numerous suggestions and advice through the years. Special thanks to Wu Yao for all the discussions and help with experiments. Thank you to Anup, Wei Yung, Jason, Pei Yi, Thang and Aish for being such great lab mates and friends!

TABLE OF CONTENTS

SUMMARY

Trans-membrane E-cadherin receptors mediate cell-cell adhesion via a complex called the Adherens Junctions (AJ) that is crucial for maintenance of epithelial integrity in homeostasis, during development, morphogenesis and tissue repair. Linkage of the cytoplasmic tail of E-cadherin to the actomyosin cytoskeleton is essential for the stability of cadherin clusters, as well as to confer on the AJ force-sensing and force-generating capabilities. Actin polymerization that provides the driving force for AJ formation and remodeling is predominantly mediated by two classes of actin nucleators – the Arp2/3 complex and formins. The Arp2/3 complex has a well-characterized role in the turnover of actin at the AJ, while the role of formins is less clear. In this study, we investigated the function of formin-dependent actin polymerization at the AJ, in both quiescent and collectively migrating monolayers.

Using siRNA-mediated knockdown (KD) and live-cell imaging approaches, we identified Diaphanous-related formin-1 (mDia1) and Formin-like 3 (Fmnl3) as key regulators of junctional actin turnover in cultured mammary epithelial cells. Knockdown of either mDia1 or Fmnl3 resulted in several striking phenotypes including: (a) ~30% reduction in F-actin and E-cadherin at the AJ, (b) 2-fold increase in cell area and loss of columnar epithelial architecture, and (c) weaker cell-cell adhesion strength. Fluorescence Recovery After Photobleaching measurements of E-cadherin and F-actin at the AJ revealed increased stability of E-cadherin facilitated by formin-polymerized actin. Endogenous mDia1 exhibited diffuse localization in

epithelial cells, while both endogenous and exogenous Fmnl3 localized prominently to cell-cell contacts. Expression of exogenous Fmnl3 led to a ~25% increase in F-actin and E-cadherin at the AJ. Further, activation of Fmnl3 was dependent on Cdc42 binding, which in turn was found to function downstream of Src-kinase at the AJ.

In monolayers subjected to an *in vitro* scratch assay, depletion of Fmnl3 resulted in poor cohesion and dispersion of leader cells during migration, while double KD (mDia1 and Fmnl3) led to complete failure in migration. Importantly, time-course analysis during migration revealed up-regulation of *Fmnl3* expression and increased junctional localization of the protein, implicating Fmnl3 in AJ reinforcement under conditions of increased strain. Indeed, using drug treatments to alter cellular contractility, we show that Fmnl3 is recruited to the AJ in a force-dependent manner.

In summary, this study identifies essential roles for mDia1 and Fmnl3 in reinforcing cell-cell junctions. We also show, for the first time, loss of epithelial cohesion in a collective migration model and weakening of cell-cell adhesion strength associated with perturbation of formin activity. Overall, we demonstrate the importance of formin-dependent actin polymerization in supporting adhesion and cohesion, which is vital for dynamic processes such as wound repair.

LIST OF TABLES

LIST OF FIGURES

LIST OF ABBREVIATIONS

AJ	Adherens Junctions
ANOVA	ANOVA
BSA	Bovine Serum Albumin
cDNA	Complementary DNA
DAD	Diaphanous Auto-regulatory Domain
DID	Diaphanous Inhibitory Domain
DMEM	Dulbecco's Modified Eagle Medium
DRF	Diaphanous Related Formin
E-cad	E-cadherin
EGTA	Ethylene Glycol Tetra-acetic Acid
EMT	Epithelial-Mesenchymal Transition
FH	Formin Homology
FRAP	Fluorescence Recovery After Photobleaching
GFP	Green Fluorescence Protein
KD	Knockdown
LJ	Lateral Junctions
MT	Microtubules
NPF	Nucleation Promoting Factor
PCR	Polymerase Chain Reaction
PFA	Paraformaldehyde
ROI	Region of Interest
RT-PCR	Reverse Transcription Polymerase Chain Reaction
siRNA	Small Interfering RNA
SMIFH2	Small molecule inhibitor of FH2 domains
WASP	Wiskott-Aldrich Syndrome Protein
WAVE	WASP-family verprolin-homologous protein
ZA	Zonula Adherens

Chapter 1

Introduction

1. INTRODUCTION

1.1 Adherens Junctions – Composition and Organization

Evolution of multi-cellularity in animals and the maintenance of tissue integrity can be attributed to the development of a variety of inter-cellular linkages. Based on tissue origin, epithelial cells often possess a combination of different junctions including Adherens Junctions (AJ), Tight Junctions, Desmosomes and Gap Junctions (Evans and Martin, 2002; van Roy and Berx, 2008; Anderson and Van Itallie, 2009; Desai *et al.*, 2009). In this study, we focus primarily on the AJ found in epithelial cells, description of which follows hereafter.

Adherens junctions are the earliest to appear during embryonic development (Green *et al.*, 2010), and are calcium-dependent cell-cell adhesion complexes built around cadherin receptors as the core adhesion molecule. While the AJ in its entirety is a complex structure (Zaidel-Bar, 2013; Guo *et al.*, 2014), it can be broadly divided into three components: (i) Adhesion receptors that bind to their receptor partners on apposing cells, (ii) an intracellular actomyosin cytoskeleton that anchors the receptors, and generates contractile force, and (iii) Adaptor proteins that link the adhesion receptors to the cytoskeleton. Further, regulation of all these components is facilitated through the activity of regulatory modules comprised of RhoGTPases (Watanabe *et al.*, 2009), kinases and phosphatases (McLachlan and Yap, 2007; Bertocchi *et al.*, 2012; Padmanabhan *et al.*, 2015).

E-cadherin (E-cad), the primary receptor at the epithelial AJ, is transcribed from the *CDH1* gene (16q22.1), and the protein can be divided into five tandemly repeated extracellular cadherin domains (EC1-EC5), a trans-membrane domain, and an intracellular cytoplasmic domain **(Figure 1.1A)** (van Roy and Berx, 2008). The cytoplasmic domain consists of a membrane proximal p120-catenin-binding juxta-membrane domain (Yap *et al.*, 1998), followed by a β-catenin binding domain **(Figure 1.1A)** (Aberle *et al.*, 1994). AJ formation occurs when cadherin receptors on apposing cells interact with each other through *trans*-interactions between their EC1 domains (Harrison *et al.*, 2011). Formation of a "strand-swapped dimer" that is anchored by exchange of tryptophan residues between two EC1 domains allows for *trans*-interactions between two E-cad receptors (Harrison *et al.*, 2011). In addition, the EC1 domain of one cadherin receptor can interact in *cis* with the EC2 domain of an adjacent cadherin receptor, resulting in the assembly of a molecular layer at the AJ (Harrison *et al.*, 2011). On the intracellular surface, E-cad binds to several catenins, including β-catenin and α-catenin, which anchor E-cad to the cytoskeleton, directly or indirectly through numerous adaptor proteins **(Figure 1.1B)**. The study of α-catenin in particular has received great attention after it was demonstrated with *in vitro* reconstituted proteins that α-catenin cannot interact with the E-cad-β-catenin complex and actin simultaneously (Drees *et al.*, 2005; Yamada *et al.*, 2005). These findings were puzzling because *in vivo* studies showed α-catenin is essential for linking E-cad to the actin cytoskeleton (Desai *et al.*, 2013). The conundrum was resolved when it was found that the α-catenin-β-catenin complex could bind F-actin also *in vitro* when force is introduced to the system (Buckley *et*

al., 2014). More recent evidence also suggests a mechanosensory role for α-catenin at the AJ, through its ability to bind proteins such as vinculin (le Duc *et al.*, 2010; Yonemura *et al.*, 2010), and EPLIN (Taguchi *et al.*, 2011) following a force-dependent conformational change.
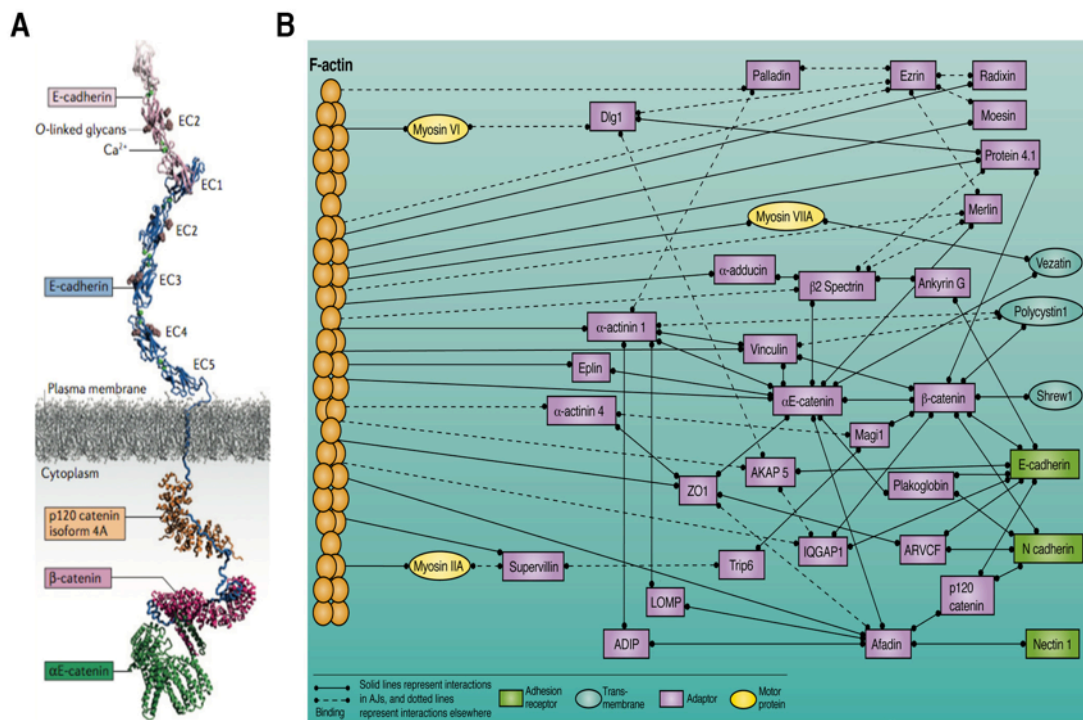
Figure 1.1: Architecture of the Adherens Junction and linkage to the cytoskeleton

(A) A model of the core cadherin-catenin complex that constitutes the AJ is shown here. EC: Extra-cellular domain[1].
(B) Structural components and adaptor proteins that link the adhesion receptors at the AJ with the actin cytoskeleton are shown here[2].

[[1]Figure 1.1A reproduced with permission from (Takeichi, 2014). [2]Figure1.1B reproduced with permission from (Zaidel-Bar, 2013). Refer Appendix 6.2.]

1.2 Actin polymerization is key for AJ assembly and maturation

While establishment of the AJ requires homophilic binding interactions between cadherin receptors, connections to the cytoskeleton and generation of contractility are crucial to strengthen nascent adhesions, and allow for AJ assembly and turnover in numerous dynamic processes (Mege *et al.*, 2006; Miyake *et al.*, 2006; Hong *et al.*, 2013). Cell-cell contact in epithelial cells is established by actin polymerization dependent processes, such as, the formation of lamellipodia (Adams *et al.*, 1998; Yamada and Nelson, 2007) or by filopodial protrusions in primary keratinocytes (Vasioukhin *et al.*, 2000) and *in vivo* in the *Caenorhabditis elegans* (Raich *et al.*, 1999) and mouse (Fierro-Gonzalez *et al.*, 2013) embryos.

Actin polymerization within lamellipodial protrusions in epithelial cells enables cells to meet, leading to coalescence of highly diffuse and mobile E-cad into immobile puncta and subsequently into larger cadherin plaques (Adams *et al.*, 1998). The RhoGTPase, Rac1, and the actin nucleator, Ap2/3 complex (discussed in greater detail in the following section), have been implicated in driving actin polymerization in lamellipodial protrusions (Yamada and Nelson, 2007). Expansion of cell-cell contacts is then dependent on a second wave of RhoGTPase activity (RhoA) that increases myosin-II-dependent contractility flanking the contact zones (Yamada and Nelson, 2007). Besides the Arp2/3 complex, the actin remodeling protein Ena/VASP has also been localized to sites of nascent cell-cell adhesions (Scott *et al.*, 2006).

Regulation of actin polymerization and stability of actin at the AJ is in turn, achieved through the action of RhoGTPases. For instance, actin nucleation and stabilization at the AJ appear to be dependent on Rac1 and Cdc42 that regulate Arp2/3-dependent actin polymerization through their signaling effectors (Otani *et al.*, 2006; Kovacs *et al.*, 2011; Verma *et al.*, 2012). Further, members of another class of actin nucleators, the Formins (discussed in greater detail in the following sections), are also known to function downstream of RhoGTPase activation.

While the large number of players involved makes actin regulation at the AJ a seemingly complex process (as illustrated in **Figure 1.2**), literary evidence so far suggests general principles for the interplay between actin and cadherin at the AJ: (i) actin polymerization based cell protrusions facilitate cell-cell contact, (ii) actin polymerization and reorganization is required for nascent adhesions to mature into a stable AJ, and (iii) actin networks associate with mature AJs to stabilize them and allow for AJ turnover. Further, as alluded to previously, cadherin ligation also stimulates actin polymerization through signaling effectors downstream of E-cad, thus establishing a feedback loop between cell-cell adhesion and actin dynamics **(Figure 1.2)**; also reviewed in (Padmanabhan *et al.*, 2015).
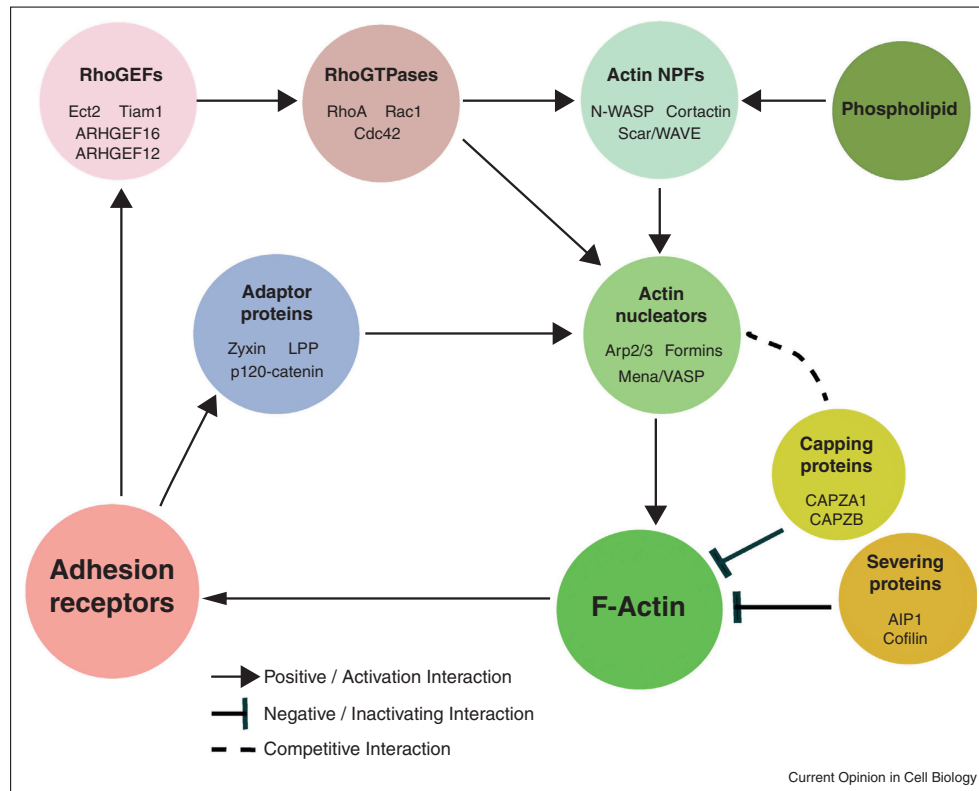
Figure 1.2: Actin dynamics regulation at the AJ

Schematic illustration of a feedback loop between actin dynamics and cell-cell adhesion. Interaction between adhesion receptors promotes downstream signaling (through RhoGTPases, actin NPFs, adaptor proteins) that in turn stimulates actin polymerization by actin nucleators. Further, as described in the text, actin polymerization provides the driving force for adhesion receptor ligation, thereby completing a feedback loop at the AJ.

[Original figure prepared by myself, and reproduced with permission from (Padmanabhan *et al.*, 2015). Refer Appendix 6.2.]

1.3 Organization and polymerization of actin at the AJ

At the ultra-structural level, E-cad and F-actin are organized as a tightly packed belt called the "Zonula Adherens (ZA)" at the apical side of epithelial cells, and amorphous networks below the ZA called "Lateral Junctions (LJ)", present along the lateral membranes. Further, electron microscopy has revealed the presence of two distinct pools of F-actin at the ZA – the commonly observed F-actin bundles running parallel to the membrane (responsible for contractile force generation), and structurally unresolved F-actin filaments closely associated with E-cad at the membrane that possibly stabilize adhesion complexes (Zhang *et al.*, 2005; Yonemura, 2011). More recent evidence using 3D-Stochastic Optical Reconstruction Microscopy (STORM) revealed the presence of qualitatively and quantitatively similar E-cad clusters at both the ZA and LJ, except for increased inter-cluster distance at the LJ (Wu *et al.*, 2015). In addition, F-actin at the nano-scale was found to 'fence' and de-limit E-cad clusters, while bundles of F-actin could also be resolved at the apical ZA (Wu *et al.*, 2015).

Despite the crucial role played by the actin cytoskeleton, spontaneous initiation of actin assembly at the AJ or elsewhere in a cell is a kinetically unfavorable process. To overcome this hurdle, cells use 'actin nucleators' and elongation factors to facilitate actin nucleation and polymerization, which include the Actin-related protein 2/3 (Arp2/3) complex, and members of the formin family (Goley and Welch, 2006; Chesarone *et al.*, 2010). While several other actin nucleators have come to light recently as discussed in (Quinlan *et al.*, 2005; Qualmann and Kessels, 2009; Firat-Karalar and Welch,

2011), in the following sections we focus on the two major groups of cellular actin nucleators - the Arp2/3 complex and formins - and their functions at the AJ.

1.3.1 Arp2/3-dependent actin polymerization and its function at the AJ

The Arp2/3 complex is a highly conserved actin nucleator comprised of seven polypeptides, including Arp2, Arp3 and ArpC1-5 subunits **(Figure 1.3)**. Studies using purified proteins have revealed the Arp2/3 complex binds to the side of an existing actin filament where it initiates assembly of a new filament (Goley and Welch, 2006) **(Figure 1.3)**. This results in the polymerization of a branched actin network such as that found in the lamellipodium, where filaments are placed at ~70° to each other (Goley and Welch, 2006).
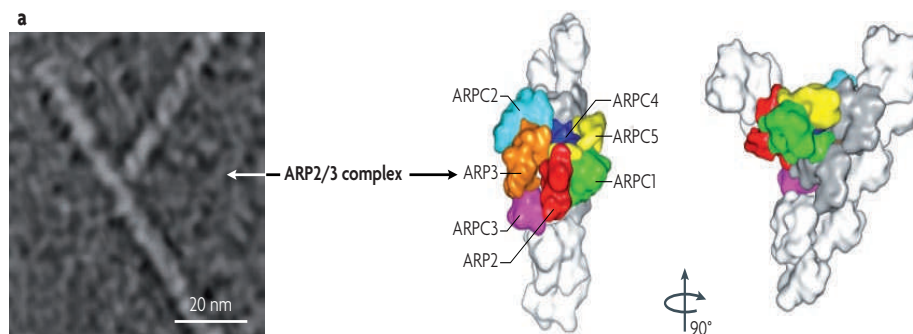
Figure 1.3: Branched actin polymerization by the Arp2/3 complex
Electron micrograph and electron tomography based structural models illustrating a Y-shaped branched actin filament polymerized by the Arp2/3 complex.

[Reproduced with permission from (Campellone and Welch, 2010). Refer Appendix 6.2.]

Evidence from *in vitro* studies has shown an interaction between E-cad and the Arp2/3 complex, and recruitment of the Arp2/3 complex to beads coated with recombinant cadherin ectodomain, thus indicating a role for Arp2/3 complex in AJ establishment (Kovacs *et al.*, 2002; Verma *et al.*, 2004). Further, endothelial AJs are associated with intermittently-formed Arp2/3-driven lamellipodia that enable adjacent plasma membranes to seal, form new VE-cadherin adhesions and maintain junction integrity (Abu Taha *et al.*, 2014).

Owing to its poor intrinsic nucleation ability, upstream regulation of the Arp2/3 complex at the AJ is achieved by nucleation-promoting factors (NPFs) such as WASP (Wiskott-Aldrich Syndrome Protein), WAVE (WASP-family verprolin-homologous protein) and cortactin (Harris and Tepass, 2010). In epithelial cells, WAVE2 associates with E-cadherin and localizes to the AJ in a Rac-dependent manner where it serves to locally activate Arp2/3 activity (Verma *et al.*, 2012). In endothelial cell, on the other hand, N-WASP (neural-WASP) localizes to AJs via an interaction with p120-catenin, thus promoting Arp2/3-dependent actin polymerization at the AJ (Rajput *et al.*, 2013). In epithelial cells, however, N-WASP contributes to actin regulation at AJs via a mechanism independent of Arp2/3-complex activation. Specifically, N-WASP in association with WIRE (a WIP-family protein), serves to stabilize actin filaments at a post-nucleation stage to support AJ integrity (Kovacs *et al.*, 2011). Cortactin localizes at the AJ through N-WASP, and serves to integrate actin assembly at the AJ by recruiting WAVE2 and Arp2/3 (Han *et al.*, 2014).

1.3.2 Actin polymerization by formins

A second major class of cellular actin nucleators is composed of members of the formin family. Formins are large (120-200kDa), multi-domain proteins, characterized by the presence of highly conserved Formin Homology (FH) domains, FH1 and FH2. *In vitro* and *in vivo*, the FH2 domain serves as the primary catalytic domain that triggers actin nucleation (Pruyne *et al.*, 2002; Sagot *et al.*, 2002). While the FH2 domain is capable of nucleating actin filaments *in vitro* from actin monomers, the precise mechanism for nucleation has remained elusive (Sagot *et al.*, 2002; Pring *et al.*, 2003). Modeling studies suggest that the FH2 domain binds to and stabilizes spontaneously formed actin dimers or trimers (Pring *et al.*, 2003). Further, homodimers of FH2 domains bind as processive caps to the barbed end of actin filaments, thus preventing other capping proteins from terminating elongation **(Figure 1.4)** (Copeland *et al.*, 2004; Harris *et al.*, 2004; Moseley *et al.*, 2004). The FH1 domain is a proline-rich domain that interacts with profilin, an actin monomer binding protein, and accelerates actin filament elongation by increasing local G-actin concentration for use by the FH2 domain **(Figure 1.4)** (Romero *et al.*, 2004; Vavylonis *et al.*, 2006; Paul and Pollard, 2008).
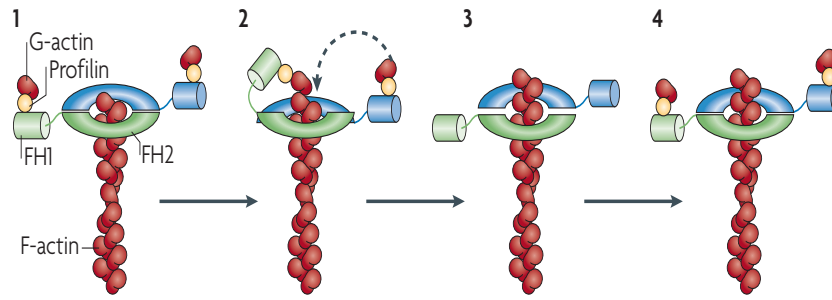
Figure 1.4: Model for actin polymerization by formins

(1) Association of the FH2 domain with the barbed end of an actin filament, and recruitment of profilin-actin by the FH1 domain.
(2) Delivery of profilin-actin to the barbed end, followed by the FH2 domain stepping towards the barbed end.
(3) & (4) The second FH2 domain repeats the above steps.

[Reproduced with permission from (Campellone and Welch, 2010). Refer Appendix 6.2.]

Mammalian formins are of 15 distinct types **(Table 1.1)** that are classified into 7 subfamilies **(Figure 1.5)**. The Diaphanous-Related Formins (DRFs), which are the focus of our study, comprise 4 subfamilies (Dia, Daam, Fhod and Fmnl/Frl), members of which are frequently characterized by an intra-molecular auto-inhibition **(Figure 1.5A)**. The N-terminus of these formins consists of a RhoGTPase-binding domain (RBD or GBD), followed by a Diaphanous inhibitory domain (DID), while at the C-terminus is present a Diaphanous auto-regulatory domain (DAD) **(Figure 1.5A-B)**. Interaction between the DID and DAD results in auto-inhibition and prevents actin assembly by the FH1-FH2 domains. In some cases, binding of RhoGTPases to the GBD relieves auto-inhibition and activates the formin (Chesarone *et al.*,

2010; Kuhn and Geyer, 2014), while other formins are activated by phosphorylation (Takeya *et al.*, 2008).

Besides functioning as an actin nucleator and elongation promoting factor, some formins also bundle actin filaments, sever actin filaments or depolymerize F-actin (Harris *et al.*, 2004; Chhabra and Higgs, 2006; Esue *et al.*, 2008; Schonichen *et al.*, 2013). Actin filaments polymerized by formins are found in lamellipodial and filopodial protrusions, stress fibers, cytokinetic rings, phagocytic cups, and at cell-cell junctions, as reviewed in (Chesarone *et al.*, 2010). In addition, formins also influence microtubule dynamics and stabilization, independent of their actin polymerizing functions (Bartolini and Gundersen, 2010). Furthermore, diverse expression profiles of formins in a wide variety of tissues (Krainer *et al.*, 2013), suggests multiple cellular functions for formins.
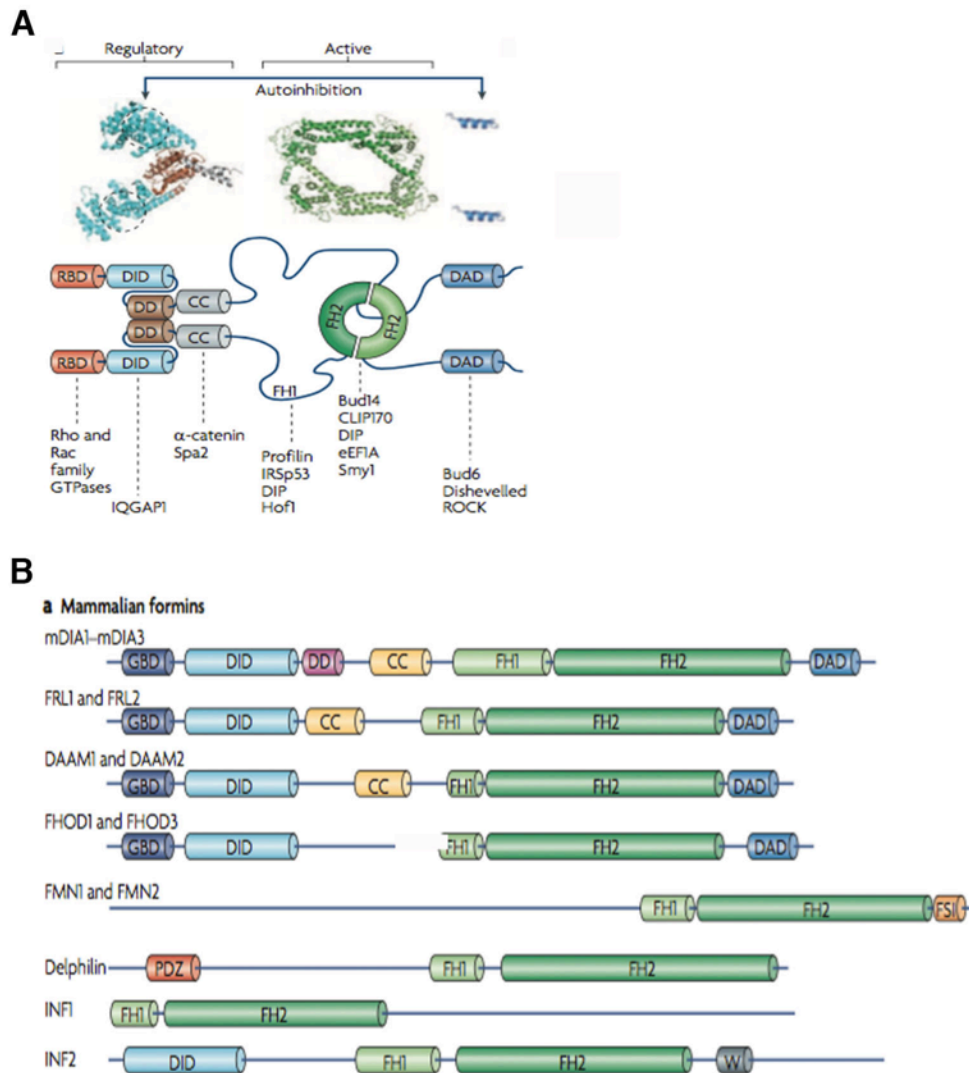
Figure 1.5: Domain organization and regulation of formins

(A) Crystal structure, schematic and binding partners of various domains in a formin.

(B) Illustration of the 7 subfamilies of formins and their domain organization. RBD/GBD- RhoGTPase/GTPase binding domain; DID- Diaphanous inhibitory domain; DD- Dimerization domain; CC- Coiled coil; DAD- Diaphanous autoregulatory domain; FH1, FH2- Formin Homology 1, 2; FSI- Formin-Spire interaction domain; W- WASP homology 2 domain

[Figure 1.5A reproduced with permission from (Chesarone *et al.*, 2010), 1.5B reproduced with permission from (Campellone and Welch, 2010). Refer Appendix 6.2.]

Table 1.1: Mouse DRFs and Non-DRFs

Formin	Full name	Gene symbol	NCBI Gene ID
Diaphanous-Related Formins (DRFs)			
mDia1/Diaph1	Diaphanous related formin 1	*Diaph1/Diap1*	13367
mDia2/Diaph3	Diaphanous related formin 3	*Diaph3/Diap3*	56419
mDia3/Diaph2	Diaphanous related formin 2	*Diaph2/Diap2*	54004
Daam1	Dishevelled associated activator of morphogenesis 1	*Daam1*	208846
Daam2	Dishevelled associated activator of morphogenesis 2	*Daam2*	76441
Fhod1/Fhos1	Formin Homology 2 Domain Containing 1	*Fhod1*	234686
Fhod3	Formin Homology 2 Domain Containing 3	*Fhod3*	225288
Fmnl1	Formin-like 1	*Fmnl1*	57778
Fmnl2	Formin-like 2	*Fmnl2*	71409
Fmnl3	Formin-like 3	*Fmnl3*	22379
Non-DRFs			
Delphilin	Delphilin/Glutamate receptor, ionotropic, delta 2 (Grid2) interacting protein 1	*Grid2ip*	170935
Inf1	Inverted formin 1	*Inf1*	-
Inf2	Inverted formin 2	*Inf2*	70435
Fmn1	Formin 1	*Fmn1*	14260
Fmn2	Formin 2	*Fmn2*	54418

1.3.2.1 Role of formins at the AJ

Historically, the Arp2/3 complex and its NPFs have been the focus of investigation with regards to actin polymerization at the AJ. However, in recent times, several studies have uncovered roles for formins at the AJ. Diaphanous-related formin 1 (mDia1) has been the most widely studied formin for its role in strengthening E-cad-based cell-cell adhesions in cultured mammalian cells (Carramusa *et al.*, 2007; Ryu *et al.*, 2009). Besides playing a role in augmenting the AJ, Dia also plays a role in junctional E-cad turnover by regulating endocytosis (Levayer *et al.*, 2011). Dia and myosin-II have been shown to regulate lateral clustering of E-cad and initiation of endocytosis at cell-cell contacts in *Drosophila* embryos, downstream of RhoGEF2 (Levayer *et al.*, 2011). Further, *dia* mutants in *Drosophila* exhibit profound defects during germband retraction as a result of destabilized AJs and increased protrusive activity of migrating amnioserosal cells (Homem and Peifer, 2008).

More recently, another member of the DRF family, Formin-like 2 (FMNL2), was localized to the AJ in 3D cultures of MCF10A where it regulates actin turnover and the formation of an epithelial lumen (Grikscheit *et al.*, 2015). FMNL2 was found to associate with E-cad and α-catenin, and localized to the AJ in a Rac1-dependent manner (Grikscheit *et al.*, 2015). Another closely related formin, FMNL3, was shown to localize to endocytic punctae in close proximity to N-cadherin-based cell-cell contacts (Gauvin *et al.*, 2015). In addition, FMNL3 was also enriched in filopodia that presumably contributed to establishment of cell-cell adhesions (Gauvin *et al.*, 2015). Further, FMNL3-comtaining filopodia were also observed in endothelial cells during

angiogenesis in zebrafish, with depletion of FMNL3 resulting in failure of blood vessel lumenization (Hetheridge *et al.*, 2012; Phng *et al.*, 2015). While the study of formins at the AJ has received greater attention lately, detailed characterization of the molecular mechanisms underlying the effect of formins on cell-cell adhesion remains poorly elucidated.

Table 1.2: Summary of literary evidence for roles of formins at cell-cell junctions

Formin	Function	Cell type/Model Organism	Reference
mDia1	Localizes and reinforces cell-cell junctions in a RhoA-dependent manner	Breast cancer epithelial cells (MCF7)	(Carramusa *et al.*, 2007)
Dia1	Dia localizes at the AJ with Abi, a core component of the WAVE complex	Human squamous carcinoma (A431)	(Ryu *et al.*, 2009)
mDia (1&3)	Required for integrity of AJ and polarity of neuroepithelial cells	Developing mouse brain	(Thumkeo *et al.*, 2011)
Dia	Stabilizes AJ and inhibits cell protrusiveness	Various stages of *Drosophila* morphogenesis	(Homem and Peifer, 2008)
Dia	Dia and Myosin-II regulate initiation of E-cadherin endocytosis at cell-cell contacts, downstream of RhoGEF2	*Drosophila* morphogenesis	(Levayer *et al.*, 2011)
FMNL2	Supports actin turnover at the AJ and lumen development downstream of Rac1	Human mammary epithelial cell line (MCF10A)	(Grikscheit *et al.*, 2015)
FMNL3	Promotes actin polymerization at endothelial cell-cell junctions and facilitates lumen development *in vivo*	Zebrafish angiogenesis	(Phng *et al.*, 2015)
FMNL3	Enriched in filopodia and endocytic punctae underneath plasma membrane protrusions	Human osteosarcoma cells (U2OS) Mouse Fibroblasts (NIH3T3)	(Gauvin *et al.*, 2015)

1.4 Intercellular adhesion and collective cell migration

Maintenance of cell-cell junction integrity is essential not just during homeostasis, but also to facilitate tissue rearrangement during embryo morphogenesis, wound repair and tissue regeneration (Friedl and Gilmour, 2009; Shaw and Martin, 2009; Scarpa and Mayor, 2016). All these processes are characterized by the coordinated movements of a collective of cells, and are referred to as collective cell migration. In this regard, the AJ plays a crucial role in maintaining cell-cell cohesion and mechanical integrity, and is also a site for cell-cell signaling and regulation of front-back cell polarity (Ilina and Friedl, 2009).

For a long time, collective cell migration was thought to be largely driven by the formation of 'leader' cells and a multicellular finger-like projection at the front end of the migrating cell sheet (Poujade *et al.*, 2007). Further, at the sides of the finger was present an actin belt that likely coupled mechanical signaling between the leader cell and the followers (Poujade *et al.*, 2007). However, more recent analysis of monolayer dynamics using traction force or monolayer stress microscopy has revealed propagation of forces deep into the monolayer behind the leading edge (Tambe *et al.*, 2011). Treatment of migrating monolayers with EGTA (calcium chelator) prevents force transmission across the cell sheet due to weakening of cadherin-based cell-cell junctions, resulting in uncoordinated migration (Tambe *et al.*, 2011). More recently, P-cadherin was demonstrated to increase intercellular mechanical forces and promote collective migration (Bazellieres *et al.*, 2015), through the recruitment of β-PIX (guanine nucleotide exchange factor) to the

AJ and activation of Cdc42 (Plutoni *et al.*, 2016). Hence, these studies illustrate the requirement of cell-cell adhesion integrity in enabling directed migration in a cohort of cells. Despite the importance of AJs in supporting collective migration, our understanding of the mechanisms controlling adhesion and actin polymerization at cell-cell junctions during migration is still preliminary. Furthermore, while several studies are increasingly exploring roles for formin-dependent actin polymerization at the AJ, it has largely been in the context of stationary monolayers.

1.5 Thesis Outline

In this study, we used siRNA-mediated knockdown and live-cell imaging approaches to elucidate the role of formins at cell-cell junctions in cultured mammalian epithelial cells. In particular, we focused on identifying and characterizing formins responsible for junctional actin turnover, stabilizing E-cad at the AJ and reinforcing cell-cell junction strength. Further, we extended our assessment of formin function to cell-cell junctions under stress in a collective cell migration model. In addition, we also explored upstream regulators of formin activity at the AJ.

Following this introduction, experimental procedures are outlined in Chapter 2. Major findings of this study are presented in Chapter 3, followed by discussion and concluding remarks in Chapter 4.

Chapter 2
Materials
&
Methods

2. MATERIALS & METHODS

2.1 Cell culture

Cell lines used in this study and the appropriate culture media are listed in **Table 2.1**. All cell lines were maintained at 37°C in 5% CO_2 atmosphere during routine passages and sample preparation steps.

Table 2.1: Cell lines used in this study

SNo.	Name of cell line	Organism	Tissue/Cell Type	Culture medium
1.	EpH4	Mouse	Mammary Epithelium	Dulbecco's Modified Eagle Medium (DMEM; Invitrogen) +10% Fetal Bovine Serum (FBS; Invitrogen) +1% Penicillin-streptomycin (P/S; Invitrogen)
2.	EpH4 E-cadherin-GFP stable cell line	Mouse	Mammary Epithelium	DMEM +10% FBS +1% P/S
3.	MCF10A	Human	Mammary Epithelium	DMEM/F12 (Invitrogen) +5% Horse Serum (Invitrogen) +20ng/ml Epidermal Growth Factor (Peprotech) +100ng/ml Cholera toxin (Sigma) +0.5mg/ml Hydrocortisone (Sigma) +10μg/ml Insulin (Sigma) +1% P/S
4.	IOSE-523	Human	Ovarian Surface Epithelium	Roswell Park Memorial Institute (RPMI)-1640 (Invitrogen) +10% FBS
5.	PEO1	Human	Ovarian (Epithelial phenotype)	RPMI-1640 +10% FBS
6.	HeyA8	Human	Ovarian (Mesenchymal phenotype)	RPMI-1640 +10% FBS
7.	OVCA429WT	Human	Ovarian (Intermediate EMT phenotype)	DMEM +10% FBS
8.	SKOV3	Human	Ovarian (Intermediate EMT phenotype)	DMEM +10% FBS

2.2 Chemical Inhibitors

Drug treatments were performed on overnight cultures of confluent EpH4 monolayers as per the conditions outlined in **Table 2.2**, followed by fixation with pre-warmed 4% paraformaldehyde (PFA), and processed for immunofluorescence staining thereafter.

Table 2.2: Chemical inhibitors used in this study

S.No.	Drug Name	Drug Target	Concentration and duration of application	Source
1.	SMIFH2	Formin family (actin nucleators)	20μM 12hr	Tocris Biosciences
2.	PP2	Src-kinase	20μM 1hr	Sigma Aldrich
3.	CK666	Arp2/3 complex inhibitor	100μM 1hr	Calbiochem
4.	CK689	Arp2/3 complex inhibitor Negative control	100μM 1hr	Calbiochem
5.	Blebbistatin	Non-muscle myosin II ATPase inhibitor	50μM 1hr	Sigma Aldrich
6.	Nocodazole	Microtubule polymerization inhibitor	10μM 1hr	Sigma Aldrich

2.3 Plasmids

Plasmids encoding full-length Fmnl3 and Fmnl3-I111D (both GFP-tagged) were a gift from Dr. Shigetomo Fukuhara (National Cerebral and Cardiovascular Center Research Institute, Osaka, Japan) (Wakayama *et al.*, 2015). Activation of endogenous mDia1 activity was achieved by expression of the Diaphanous Auto-regulatory domain (DAD) from mDia1 (AA 1177-1222) fused to an mVenus fluorescent tag (mVenus-DAD). Plasmids for expression of constitutive active mutants of RhoA (V14), Cdc42 (L61) were provided by Dr. Alexander Bershadsky (Mechanobiology Institute, Singapore), while active Rac1 (L61) was obtained from the Lemichez group (C3M University of Nice Sophia Antipolis, France). The following constructs were obtained from The Michael Davidson Collection (Florida State University, USA): GFP-c-Src (Full-length chicken c-Src cloned into the EGFP-N1 vector) and tdTomato-Actin (Full-length human beta-actin cloned into the tdTomato-N1 vector).

2.4 Transfection – Plasmids and Small Interfering RNA (siRNA)

For plasmid transfections, EpH4 monolayers were cultured overnight to 70-80% confluence, followed by transfection with 0.75-1μg purified plasmid of choice using Lipofectamine 2000 (Invitrogen).

Knockdown of gene expression was performed by introducing mouse or human gene-specific ON-TARGET Plus siRNA oligonucleotides or a non-targeting control siRNA (GE Dharmacon) using Lipofectamine 2000

(Invitrogen). All siRNAs (listed in **Table 2.3**) were used at a final concentration of 50nM. Cells were fixed and processed for immunofluorescence labeling or live-cell imaging 26-28hr or 36hr post-transfection for EpH4 or MCF10A, respectively. Duplicate samples were prepared for collection of cell lysates and analysis of gene knockdown efficiency via semi-quantitative PCR analysis.

Table 2.3: List of siRNA oligonucleotides used for gene knockdown

S.No	Gene Symbol	Species	Gene ID	Gene Accession	Sequence
1.	*Diap1*	Mouse	13367	NM_007858	AGGUCGGGCUUGCGGGAUA GGGAGAUGGUGUCGCAAUA UCACACUGCUGGUCGGAAA UGGAUGAGGUCGAACGCUU
2.	*Diap3*	Mouse	56419	NM_019670	CAUAAAUGCUCUCGUUACA GUGCAUUGUCGGCGAGGAA CAGGAUAGCGAAAGAGCGA GUGGAAGGCCUCCGGCAUA
3.	*Diap2*	Mouse	54004	NM_017398	CCGCAUGCCAUACGAGGAA GAUGAGAAAUACCGGGAUA GCAAUAUGUUGAAGCUCUA CCUAGAUGCUUGUGUAAAU
4.	*Daam1*	Mouse	208846	NM_172464	AGCGAAGAGUUGCGGGAUA CAGGAGAGGUGUUCGACAA GAUGAAAUCAAGCGGGCAA GCCCAAAGUAGAAGCGAUU
5.	*Fhod1*	Mouse	234686	NM_177699	CUACAUACCGUGAGCGCAA GUAUCGGACUUGUCGGGAA UCGCAUGAUUACCGAGACA UGAGAGUGCCCUUCGGUUA
6.	*Fhod3*	Mouse	225288	NM_175276	GGAACAAAUUCAACCGGGA GCAGAGGAUAGAACGGGAA GAGCCGAGGCGGAUCAGAA CGGCAAGAGAGAGAGGAAA
7.	*Fmnl1*	Mouse	57778	NM_019679	GGGUUUAGGAGGCGAGUUC UUACACAGGUGCUGCGGGA AGAGAGAGUUUGUGCGGCA CCUACAAGAAAGCGGAACA
8.	*Fmnl2*	Mouse	71409	NM_172409.2	UGUUAAUGGUGCCGAAAUA GGACUUAAAUGUGGACGAA CAAAGUCGACAGACCGAAA GCGGAGAAAAGCAGCGUUU
9.	*Fmnl3*	Mouse	22379	NM_011711	GUAAAGAACUGCAUCGGUU ACAACAGCGUCCUUCGAAA AGUAUGAGCGUGAACGACA CCACUAAAGUCCUACGGGA
10.	*Src*	Mouse	20779	NM_001025395	GCACGGGACAGACCGGUUA GGGAGCGGCUGCAGAUUGU UCAGAUCGCUUCAGGCAUG GCUCGUGGCUUACUACUCC
11.	*DIAP1*	Human	1729	NM_005219.4	GAAGUGAACUGAUGCGUUU GAAGUUGUCUGUUGAAGAA GAUAUGAGAGUGCAACUAA GCGAGCAAGUGGAGAAUAU
12.	*FMNL3*	Human	91010	NM_175736.4	AAGAACAGCUGGAGCGAUA CCUCAUUACUUACGAGAGA AGGUAAAGCUGCUGCGGCA GCAUGGUGGUCUUGGCUAU
13.	Neg siRNA	Mouse/ Human	-	-	UGGUUUACAUGUCGACUAA UGGUUUACAUGUUGUGUGA UGGUUUACAUGUUUUCUGA UGGUUUACAUGUUUUCCUA

2.5 RNA extraction and semi-quantitative PCR

RNA extraction was performed using Trizol Reagent (Ambion), as per manufacturer's instructions, from confluent epithelial monolayers cultured overnight on 35mm dishes. Purified RNA (1µg) was then used as template for oligo-dT-primed reverse transcription and cDNA synthesis using the reagents available in the SuperScript$^®$ III First-strand synthesis kit (Invitrogen). Equal volumes of cDNA were subsequently used to amplify genes of interest using gene-specific PCR primer sets (listed in **Table 2.4**) for quantification of endogenous expression levels or knockdown levels post-siRNA transfection. PCR products were analyzed and imaged on agarose gels using the ChemidocMP imaging system (Biorad). Quantitative analysis of expression levels was then performed using the 'Gel Analyzer' plug-in built into ImageJ/Fiji (NIH).

Table 2.4: List of gene-specific primers used for semi-quantitative PCR analysis

S. No	Gene	Species	Forward Primer (5'-3')	Reverse Primer (5'-3')
1.	*Diap1*	Mouse	GGCCTAAATGGTCAAGGAGATAG	CAGAGGTGACAGCAGTGAAA
2.	*Diap3*	Mouse	GTGGACGATTTGGCACATTTAG	CTCTTTCTCTGCTCGCTCTTT
3.	*Diap2*	Mouse	CGCCATCTGAAGACAGGATAAT	CCGATAGGAGGAAGTGAAGAAAG
4.	*Daam1*	Mouse	CAGGCAGAGAAGATGAGGAAAG	GAACTCCTGCTGTCTTTGGTAG
5.	*Fhod1*	Mouse	TCTCCCTTCCTGTCATCTCTATC	CCTTGGCTCTGGACTCAAATAG
6.	*Fhod3*	Mouse	GTTCCTTCTCACACTCTCTTCC	GCGTCTCTCCATCTGACATAAA
7.	*Fmnl1*	Mouse	CAGCCTATGGTTTCCGACTT	GGGATGTGGTCTTGGGATTT
8.	*Fmnl2*	Mouse	CCGTGTTCTTCCCTGTCTTT	CTCGTCTGTAGGGTTGGTTTC
9.	*Fmnl3*	Mouse	AAATACCCGGAACTGGCTAAC	CGCATTACCTCCTCTTGTTTCT
10.	*Src*	Mouse	CTCGTGGCTTACTACTCCAAAC	CATAGTTCATCCGCTCCACATAG
11.	*Gapdh*	Mouse	AACAGCAACTCCCACTCTTC	TGGGTGCAGCGAACTTTAT
12.	*DIAP1*	Human	CTCTCCTGGCTGTGGTTATTT	CACCTCCCATTTCCTTGTAGAC
13.	*FMNL3*	Human	CAAGAAGCAGGAGGAGGTAATG	CTACAGACCTAGTGCCCATAGT
14.	*GAPDH*	Human	GGTCGGAGTCAACGGATTT	TCTTGAGGCTGTTGTCATACTT

2.6 Dispase-based dissociation assay

For this assay, epithelial cells were plated until 90-95% confluent on 60mm dishes. Cells were washed twice with PBS, and treated with 2ml Dispase solution (2.4U/ml; Gibco) at 37°C for 40-45min. Subsequently, all cells (either single or clumps) released from each sample were collected and washed twice with PBS. Cell pellets were collected by centrifugation, re-suspended in 500µl PBS and subject to mechanical disruption by vortexing. The number of single cells released into suspension after vortexing were counted using a Countess® automated cell counter (Invitrogen). Next, all samples were treated with TrypLE Express (Gibco, Life Technologies) for 3-4min at 37°C to dissociate cell clumps and release all cells into suspension. Cell counts were quantified post-trypsinization and used for assay normalization. As a control for low adhesion strength monolayer, EGTA treatment was performed (4mM for 2hr) on confluent monolayers prior to sample processing for the dispase assay.

2.7 Fibronectin patterning

Cell confinement experiments were performed by plating cells on circular fibronectin patterns, following the protocol outlined in (Doxzen *et al.*, 2013). For preparation of circular patterns, a silanized wafer was used as template to generate PDMS stamps with circular features of 100µm. A mixture of fibronectin and Cy5-conjugated fibronectin (Sigma Aldrich) was then placed on the PDMS stamps and incubated at 37°C for 1hr. Next, the stamps were washed three times with PBS, air-dried and then gently pressed against a

glass-bottom dish (Ibidi 81151) to imprint circular patterns on to the dish. Areas outside the circular patterns were rendered passive to cell adhesion by treatment with 0.2% Pluronic acid (Sigma) for 1hr, followed by 2-3 washes with PBS prior to seeding cells.

2.8 *In vitro* scratch assay

To assess collective migration using an *in vitro* scratch assay, epithelial cells were cultured post-siRNA transfection on 35mm glass-bottom dishes at 37°C for 26-28hr (EpH4) or up to 36hr (MCF10A). Then, a p10 pipette tip was used to generate a "scratch" in the monolayer. The dishes were then processed for live-cell image acquisition by washing thrice with sterile PBS to remove cell debris, followed by addition of imaging medium. Image acquisition for cell migration and gap closure was then performed as outlined below, with images captured at 15min intervals for up to 12-13hr for EpH4 or up to 24hr for MCF10A.

2.9 Immunofluorescence staining

For all immunofluorescence experiments, samples were prepared by seeding cells on glass coverslips or glass-bottom dishes at a density of $2\text{-}4\text{x}10^{5}$ cells/ml in 2ml of growth medium. Based on the experiment, transfection with necessary plasmids was performed using Lipofectamine 2000. Following overnight incubation for 20-22hr, cells were fixed using warm 4% PFA for 20min and permeabilized with 0.2% Triton X-100 for 3min at room

temperature (RT). Samples were then processed for immunolabeling by incubating with 1% bovine serum albumin (BSA) for 1hr/RT, followed by primary antibody diluted in 1% BSA for 1hr at RT, and lastly, incubation with secondary antibody, phalloidin and/or DAPI for 30min at RT in dark conditions. Samples were then coated with FluorSave mounting media (Merck Millipore) for preservation of fluorescence labeling and to facilitate short-term storage (2-4 weeks). Antibodies and phalloidin conjugates used in this study are listed in **Table 2.5**.

Table 2.5: Reagents used for immunofluorescence labeling in this study

S.No	Antibody	Source	Dilution
1.	E-Cadherin	Sigma Aldrich U3254	1:1600
2.	E-Cadherin	BD Biosciences 610181	1:100
3.	Fmnl3	Santa Cruz Biotechnology sc-66770	1:100
4.	mDia1	BD Biosciences 610848	1:100
5.	Alpha-catenin	Sigma Aldrich C2081	1:1000
6.	Conformation sensitive Alpha-catenin (Alpha-18)	Shigenobu Yonemura (gift)	1:100
7.	Anti-rat/rabbit/goat Alexa-Fluor 488/568/647 conjugated secondary antibodies	Life Technologies	1:500
8.	Phalloidin Alexa-Fluor 488/568/647	Life Technologies	1:1000
9.	4',6-diamidino-2-phenylindole (DAPI)	Life Technologies	300nM

2.10 Microscopy

2.10.1 Image acquisition: Fixed samples and Live-cell imaging

Image acquisition was performed on a Spinning Disk confocal microscope (Model CSU-X1 Yokogawa Corporation; Model Ti, Nikon), equipped with a laser launch unit (iLas2, Roper Scientific), CCD camera (Evolve Rapid-Cal, Photometrics), Perfect Focus System (Nikon) for control of z-axis movement, and MetaMorph software (Molecular Devices) for image acquisition. All fixed samples were imaged using a 60X/1.40NA Plan-Apo objective (Nikon), while phase contrast imaging for the *in vitro* scratch assay was performed using a lower magnification 20X/0.75NA Plan-Apo objective (Nikon). For all live imaging experiments, the microscope chamber was set to 37°C, and imaging was performed in DMEM lacking phenol red, supplemented with 25mM HEPES (Invitrogen) for EpH4 cells, or complete growth medium for MCF10A.

2.10.2 Fluorescence Recovery After Photo-bleaching (FRAP)

For photo-bleaching experiments (performed on the microscope setup described above), EpH4 cells with stable expression of E-Cadherin-GFP or transient expression of tdTomato-actin were used. In accordance with a typical FRAP set-up, images were acquired for the pre-bleach and post-bleach phases using the appropriate laser (GFP - 491nm laser, 20% laser power, 100ms exposure time; tdTomato - 561nm laser, 15% laser power, 100ms exposure). To locally bleach an area along the cell-cell junction, a rectangular ROI (10 μm^2) was exposed to a 405nm laser pulse set to 100% transmittance,

with an exposure time of 600ms (GFP) or 700ms (tdTomato). During the post-bleach (or recovery) phase, images were acquired at 1s intervals for 5min, followed by 3s for 7min. Pre-bleach and post-bleach fluorescence intensity values were then extracted using a plug-in in MetaMorph, followed by exponential curve fitting in Prism 6 (GraphPad). Data obtained from the recovery curves were fit using the exponential function:

$$Y=Y0+a*(1-exp(-b*x))$$

Next, the half-time of fluorescence recovery ($t_{1/2}$) and immobile fractions (F_i) were computed from the exponential curve fit.

$$t_{1/2} = ln2/b$$

$$Fi =100*(1-a/(1-Y0))$$

All data were subjected to the Student's t-test to assess statistical significance between experimental groups being compared.

2.11 Image analysis

2.11.1 MATLAB Algorithm

In this study, quantification of fluorescence intensities at the junction and other cellular parameters were performed using a custom MATLAB algorithm, described in detail as follows.

The MATLAB algorithm segments the image into *junction region* and *cell region* using a local thresholding method. Based on the segmentation results, the image was then analyzed on a per-cell basis such that the properties of each cell and its junctions were measured.

First, each image was background subtracted with a rolling ball (with radius of *50* pixels). Next, *niblack thresholding* (with *k = -0.1* and window size = *55*) was applied to generate a *binary mask*, where *1* represented the *junction region* and *0* represented the *cell region*. The *binary mask* was further processed by some morphological operations to get a final smooth *mask*. Each *connected cell region* (or *cell segment*) was then assigned with a different label and the *junction region* was labeled with *0* in the *label map*. In order to segment the *junction region* into meaningful *junction segments*, the *branch points* were identified, which are the connecting points of *junction segments*. This was done by applying a thinning operation on the *binary mask* to generate a skeleton of the junctions. From the skeleton, we obtained the *branch points* and these *branch points* were then connected to the *cell segments* nearest to them.

For each *cell segment*, we obtained a set of *boundary pixels* that are located on the boundary of the *cell segment*. The *boundary pixels* were then divided into *N* sub-sets of *boundary pixels* if we had *N junction segments*, i.e., the *boundary pixels* for *junction n* is the sub-set of *boundary pixels* bounded by *branch point n* and *branch point n+1*. Assuming the sub-set of *boundary pixels* for *junction n* contained *K boundary pixels*, for each of these pixels, denoted as $b_k = \{b_1, b_2, \ldots, b_K\}$, we defined a *normal line,* $l_k = \{l_1, l_2, \ldots, l_K\}$ that started from each pixel $b_k = \{b_1, b_2, \ldots, b_K\}$ and crossed over to another cell. These *normal lines* were perpendicular to *junction n* and with a fixed length of *50* pixels. Each *normal line,* l_k when overlaid on the *mask*, gave us the *normal line pixels* that belonged to the *junction region*, denoted as $p_{kj} =$

$\{p_{k1}, p_{k2}, \ldots, p_{kJ}\}$. The number of these pixels, J, gave us thickness, t_k. The *junction thickness* was thus computed as the average of t_k, for $k = \{1, 2, \ldots, K\}$.

Next, we calculated the intensity $i_{kj} = \{i_{k1}, i_{k2}, \ldots, i_{kJ}\}$ for $\{p_{k1}, p_{k2}, \ldots, p_{kJ}\}$ by overlaying these pixels on the background subtracted image. With this, we could quantify the *junction intensity* as well as the *intensity variations across the junction* and the *intensity variations along the junction*. The computation of *junction intensity* was straightforward, i.e., by averaging the intensity of all the pixels that belonged to the *junction segment*.

For analysis of junction length in time-lapse movies, the *skeleton* of the *junction mask* was partitioned into *junction skeleton segments* by using *branch points* as separation points. The length of each junction was estimated from the number of pixels of each *junction skeleton segment* scaled by the pixel size. For each time point, a *junction length map* was generated. The map was used for tracking length changes over time in Fiji.

2.11.2 Statistics and Figure Preparation

Data generated in this study were analyzed using Microsoft Excel and Prism 6 (GraphPad). Prism 6 was used for preparation of all graphs and for performing statistical analyses (Student's t-test for two datasets; One-way ANOVA for more than two datasets). All figures were prepared using Adobe Photoshop CS6 v13.0 (Adobe Systems).

Chapter 3

Results

3. RESULTS

3.1 Formin-dependent actin polymerization is essential for AJ organization and dynamics

3.1.1 Actin polymerization by formins is essential for AJ organization

Polarized epithelial monolayers are characterized by the presence of distinct AJs that can be visualized by immunofluorescence labeling to detect E-cadherin (E-cad) and F-actin. Both F-actin and E-cad are organized as a belt-like structure at the apical-most portion of the membrane, termed the 'Zonula Adherens' (ZA), as well as sparsely distributed along the lateral membranes comprising the 'Lateral Junctions' or 'Lateral Contacts' **(Figure 3.1A)**. Establishment of cadherin-actin interactions is crucial for both the stability as well as the re-organization of the AJ, as illustrated in several studies (Mege *et al.*, 2006; Miyake *et al.*, 2006; Hong *et al.*, 2013). While several lines of evidence conclusively demonstrate a role for the Arp2/3 complex and its nucleation-promoting factors in supporting actin polymerization at the AJ (Verma *et al.*, 2004; Kovacs *et al.*, 2011; Verma *et al.*, 2012), here, we chose to dissect a role for members of the formin family at the AJ. To this end we tested the effect of a pan-formin inhibitor SMIFH2 (Rizvi *et al.*, 2009) on confluent EpH4 monolayers. As illustrated in **Figure 3.1A**, inhibiting formin activity in polarized monolayers resulted in reduced F-actin and E-cad fluorescence intensity at the AJ, increase in cell area due to flattening of cells, and a visible reduction of the lateral junctions. Reduction of F-actin and E-cad fluorescence intensity was further substantiated by quantitative analysis using

an in-house MATLAB algorithm, revealing 30% and 21% decrease in junctional F-actin and E-cad respectively ($p<0.0001$ and $p<0.001$ respectively, Student's t-test) **(Figure 3.1B-C)**. SMIFH2-treatment also resulted in significant increase in cell-spread area, with cells in treated monolayers exhibiting areas $>1200\mu m^{2,}$ in comparison to control cells that largely had areas $<800 \mu m^2$ **(Figure 3.1D)**.
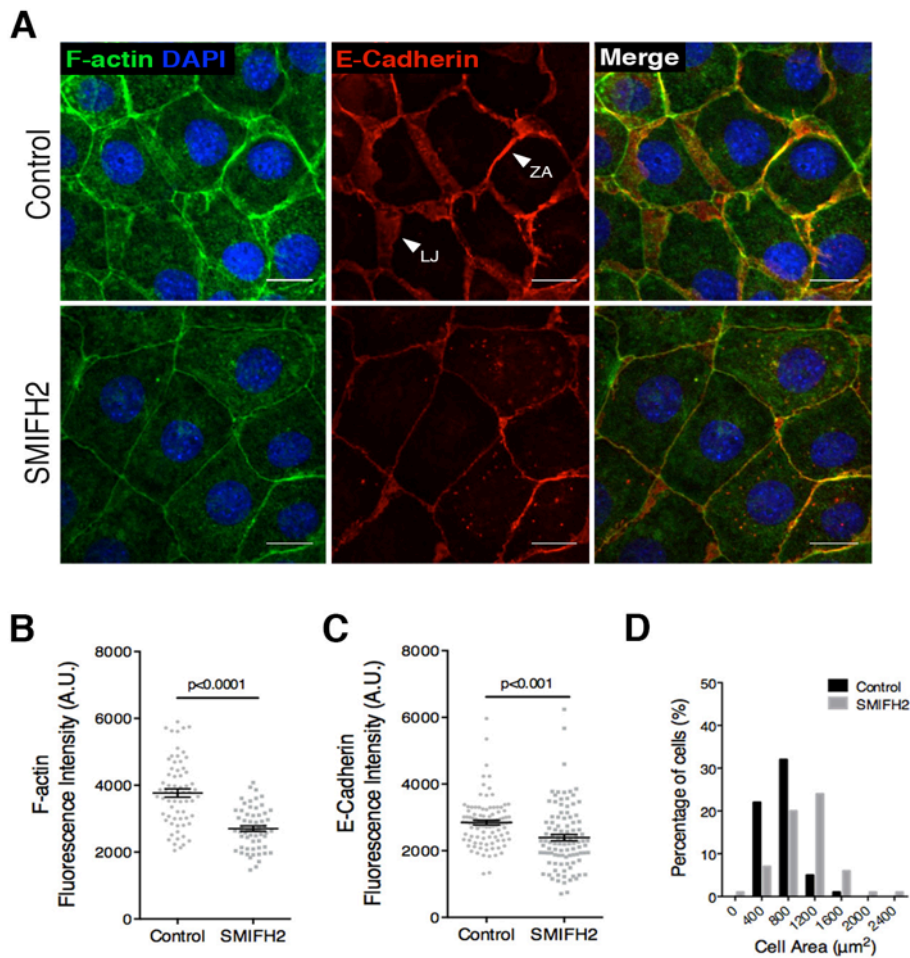
FIGURE 3.1: Actin polymerization by formins is essential for AJ organization

(A) Representative images for F-actin and E-cadherin (E-cad) immuno-labeling in EpH4 monolayers, in control (DMSO) and SMIFH2-treated conditions (12hr treatment). ZA: Zonula Adherens, LJ: Lateral Junctions. Scale bar, 20μm.

(B) Quantification of F-actin fluorescence intensity at cell-cell junctions for **(A)** using an automated MATLAB algorithm for image analysis. Here and in subsequent figure panels, unless otherwise specified, data for every junction is represented as a single gray dot, with Mean±SEM. n≥100 junctions from 3 experiments.

(C) Quantification of E-cad fluorescence intensity at cell-cell junctions for **(A).** n≥100 junctions from 3 experiments.

(D) Histogram of cell areas in control vs. SMIFH2-treated monolayers. n=100 junctions from 3 experiments.

Statistical significance tested using Student's t-test in **(B)** & **(C)**.

3.1.2 Formin-dependent actin polymerization is required for the maintenance of columnar cell morphology

As illustrated in **Figure 3.1A & 3.1D**, inhibition of formin activity resulted in increased spreading of cells within a monolayer. Interestingly, this phenomenon was only true of EpH4 monolayers, since SMIFH2 application on isolated EpH4 cells did not lead to excessive cell spreading **(Figure 3.2A-B)**. Thus, we hypothesized that cell spreading may be an active process, likely driven by Arp2/3 complex mediated actin polymerization. To test this, we performed double inhibition experiments, using a combination of SMIFH2 and CK666 inhibitors **(Figure 3.2C)**. Indeed, cell spreading was abrogated with inhibition of both formin and Arp2/3 complex activities, demonstrating that spreading in the absence of formin activity was an active Arp2/3-driven process **(Figure 3.2C)**.

Next, we hypothesized that the disappearance of lateral junctions upon formin inhibition (as shown in **Figure 3.1A**) could result either as an indirect consequence of cell spreading or due to lower formin activity at the AJ. To differentiate between these two possibilities, we cultured cells on fibronectin islands of fixed diameter (100μm) to limit the area available for cell spreading **(Figure 3.3A)**. Importantly, when cells on such islands were subjected to SMIFH2 treatment, we observed negligible spreading outside the fibronectin patterns, and preservation of lateral junctions **(Figure 3.3A-B)**. These results demonstrate that the disappearance of lateral junctions occurred as a secondary consequence of cell spreading and loss of columnar morphology induced by formin inhibition. It is worthwhile to note, however, that cells on

SMIFH2-treated islands that remained columnar did exhibit a small yet significant reduction in E-cad levels at the AJ ($p < 0.05$, Student's t-test) **(Figure 3.3C)**.

Altogether, these results indicate an essential role for formin polymerized actin in maintaining AJ organization and columnar morphology in epithelial monolayers.
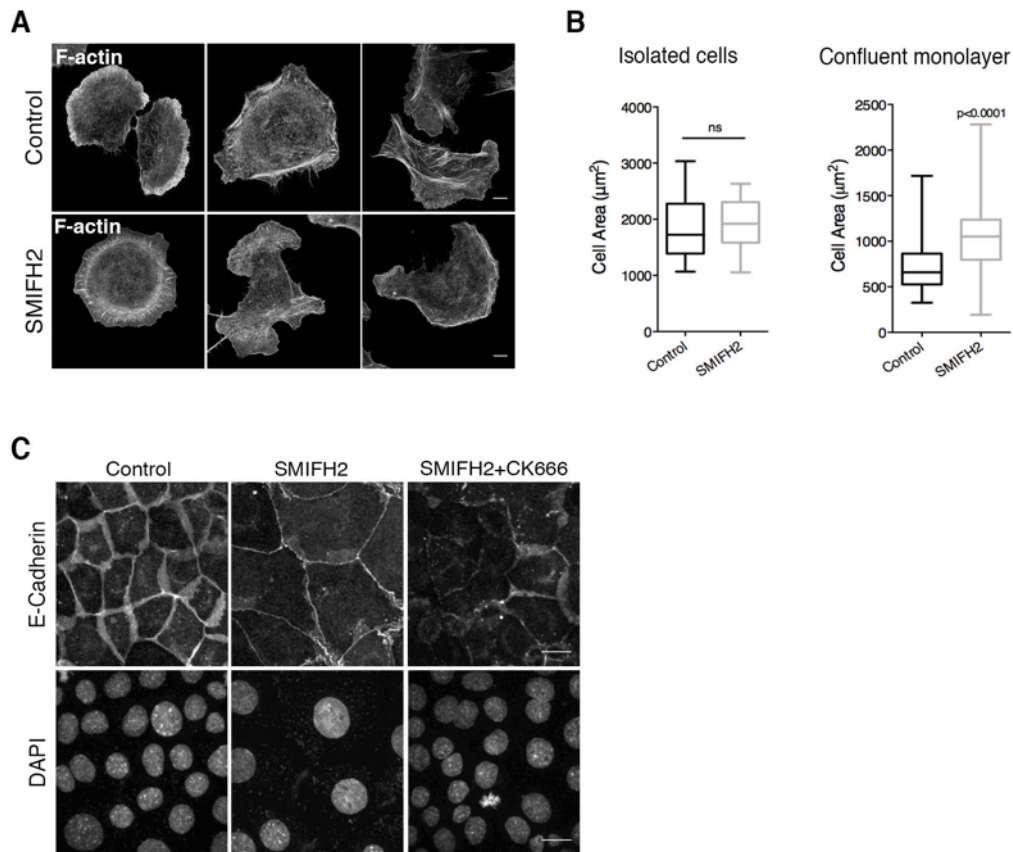
Figure 3.2: Cell spreading associated with formin inhibition is driven by Arp2/3 complex activity

(A) F-actin labeling in isolated EpH4 cells with and without SMIFH2 treatment (three examples shown for each condition). Scale bar, 10μm.
(B) Comparison of cell area changes associated with SMIFH2-treament in isolated cells or confluent EpH4 monolayers. n=30 isolated cells or 100 cells in a monolayer.
(C) Double inhibition of Arp2/3 complex and formin activity (SMIFH2+CK666) prevents cell spreading, otherwise seen with SMIFH2-treatment alone (middle panel). DAPI labeling is shown as a reference. Scale bar, 20μm.
Statistical significance tested using Student's t-test in **(B)**.
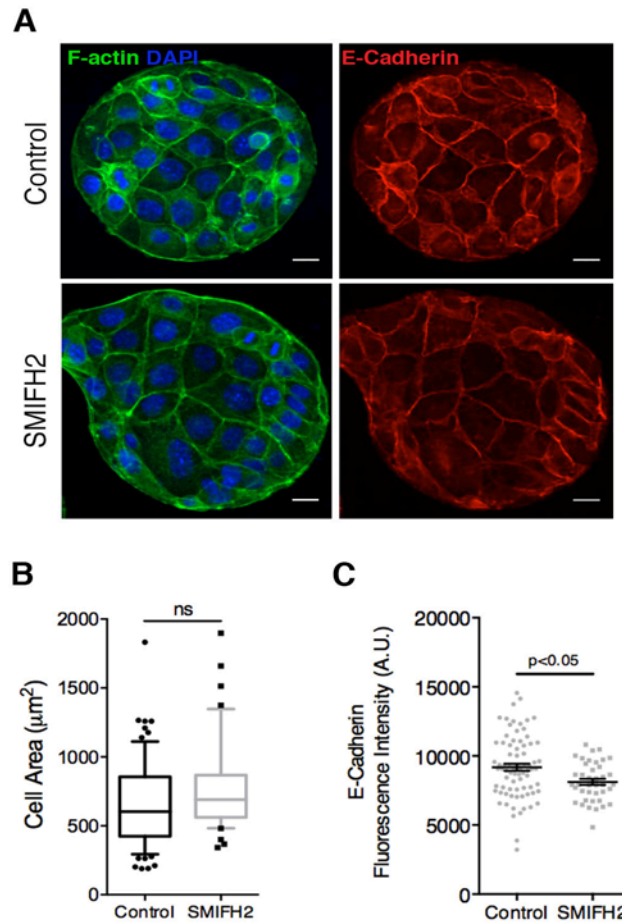
Figure 3.3: Reduction in lateral junctions following SMIFH2 treatment is due to increased cell spreading

(A) F-actin and E-cad labeling for islands of EpH4 cells formed on circular fibronectin patterns, with or without SMIFH2 treatment. Region surrounding each island was rendered passive to cell spreading by treatment with pluronic acid. Scale bar, 10μm.

(B) Cell area quantification for **(A)**. Data collected from 10 islands assessed for each condition, presented as box and whisker plot showing median and 10-90th percentile, and outliers as individual data points.

(C) Quantification of junctional E-cad fluorescence intensity for **(A)**, with Mean±SEM.

Statistical significance tested using Student's t-test in **(B)** & **(C)**.

3.1.3 Formin activity is required for stability of cell-cell junctions

While long-term inhibition of formin activity (12hr) resulted in lower F-actin and E-cad levels at the AJ, we observed that monolayer integrity was not entirely perturbed. However, short-term live cell imaging (40-45min) of EpH4 monolayers stably expressing E-cadherin-GFP revealed stark differences upon treatment with the SMIFH2 inhibitor for 2hr. At the apical ZA, we found extremely stable junctions in control monolayers, which did not undergo significant rearrangement during the course of imaging **(Figure 3.4A-B)**. On the contrary, the apical ZA in SMIFH2-treated monolayers were more prone to extensions or shortening, and thus remodeled to a greater extent than control junctions **(Figure 3.4A, C)**. As illustrated in **Figure 3.4B-C**, fluctuations in junction length in SMIFH2-treated monolayers were significantly greater than in control monolayers. Similarly, analysis of maximum change in junction length (either increase or decrease) in 40min also indicated more variability for SMIFH2 vs. control **(Figure 3.4D)**.

At baso-lateral regions of contact, we observed numerous filopodial extensions labeled by E-cadherin-GFP in control monolayers **(Figure 3.5A)**. Treatment with SMIFH2 completely abolished these filopodial protrusions, and instead resulted in the formation of prominent lamellipodial protrusions **(Figure 3.5A-B)**. Almost all lamellipodial protrusions formed were observed to terminate at regions of tri-cellular contacts. It is likely that elevated Arp2/3 complex activity associated with inhibiting cellular formins may be responsible for the increase in lamellipodial protrusions described here.
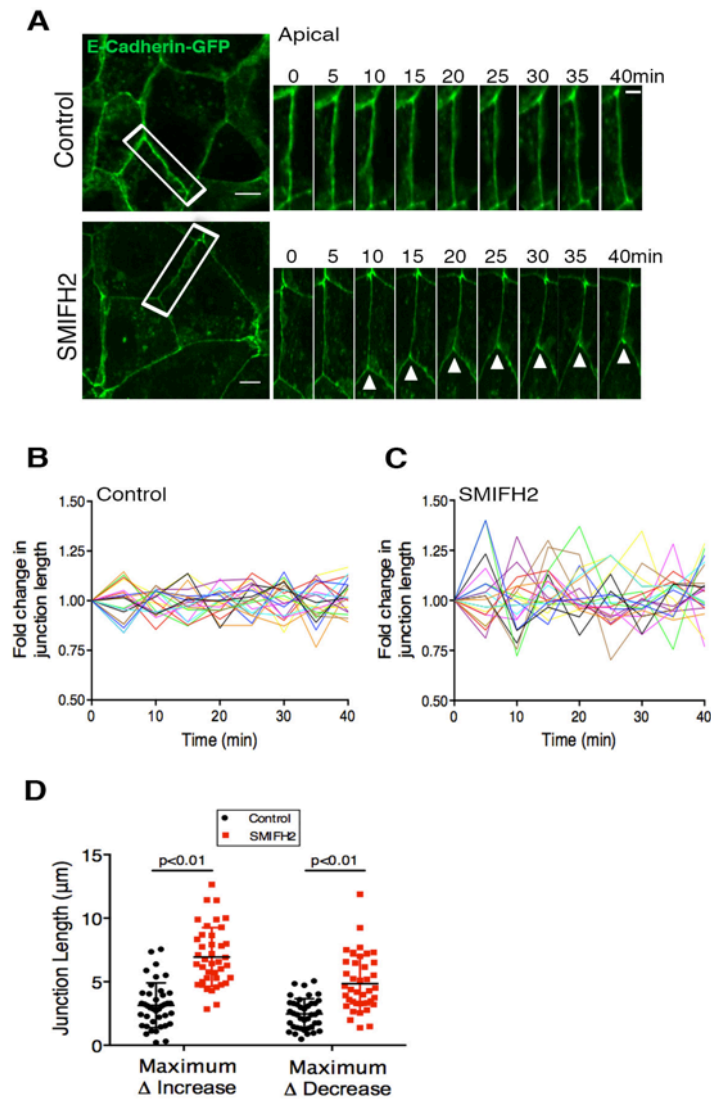
Figure 3.4: Apical junctions undergo significant remodeling following formin inhibition

(A) Montage from time-lapse movies of E-cadherin-GFP labeled apical Zonula Adherens (ZA), in control and SMIFH2-treated (2hr) conditions. Note the stability of apical junctions in control in comparison to SMIFH2 treatment. Scale bar, 10μm.

(B) & **(C)** Quantification of fold change in apical junction length over time, in Control or post-SMIFH2 treatment, respectively. Data for 20 junctions is shown here, with every single line representing one junction.

(D) Quantification of maximum increase or decrease in apical junction length, relative to junction length at T0, for control and SMIFH2-treated monolayers. n≥40 junctions per condition from 2 experiments, with Mean±SD.

Statistical significance tested using Student's t-test in **(D).**
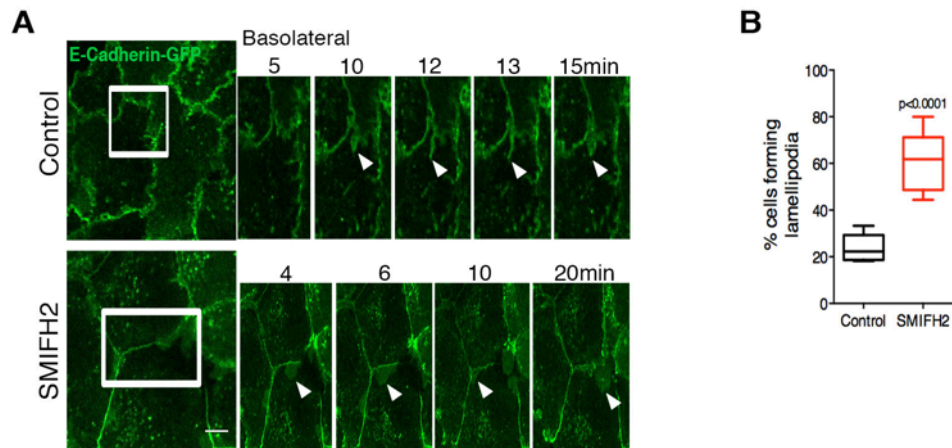
Figure 3.5: Formin inhibition leads to increased lamellipodial activity at baso-lateral contacts

(A) Montage from time-lapse movies of E-cadherin-GFP labeled baso-lateral contacts, in control and SMIFH2-treated (2hr) conditions. Note the formation of filopodial protrusions in control vs. lamellipodial protrusions after SMIFH2 treatment. Scale bar, 10μm.

(B) Quantification of cells forming lamellipodia (%) at basolateral contacts. Box plot represents minimum to maximum and median.

Statistical significance tested using Student's t-test in **(B).**

3.2 Identification and characterization of formin(s) and their upstream regulators with roles at the epithelial AJ

3.2.1 Identification of candidate formins using an siRNA-based screen

As the SMIFH2 inhibitor used so far was a pan-formin inhibitor, we focused our efforts on identifying specific members of the formin family that were involved in regulating actin polymerization and cadherin organization at the AJ. We primarily focused our search of candidate formins to those belonging to the Diaphanous-related family of formins, which includes Dia, FMNL, DAAM and FHOD classes.

First, we tested endogenous expression levels of the above-mentioned classes of formins using semi-quantitative Reverse Transcription Polymerase Chain Reaction (RT-PCR). For this, total RNA was extracted from EpH4 cells and reverse transcribed to cDNA using oligo-dT primers; subsequently, gene-specific primers **(Table 2.4)** were used to amplify each of the formins using cDNA as template. As shown in **Figure 3.6A**, we first tested a range of PCR amplification cycles (ranging from 22 to 42) to optimize detection of expression levels (for example, *Fmnl3* expression could be detected from cycle 27 onwards, while *Diap2* expression was undetectable even up to 42 amplification cycles). Based on this analysis, we chose to perform PCR amplification for all formins at 42 cycles and quantify endogenous expression levels. PCR analysis revealed mDia1 and Fmnl3 as the two most abundant formins in EpH4 cells, with mDia2, Daam1, Fmnl1, Fmnl2 and Fhod1 being

expressed at very low levels, and negligible expression of mDia3 and Fhod3 (all data normalized to GAPDH) **(Figure 3.6B)**.

Next, we introduced in EpH4 cells siRNAs **(Table 2.3)** to individually knockdown (KD) each of the above formins and scored for knockdowns that phenotypically resembled SMIFH2-mediated inhibition. Here, we used a SMARTpool comprising of a mixture of four siRNAs targeting every single gene to achieve higher potency and specificity of KD (all siRNA sequences are provided in **Table 2.3**). Phenotypic characterization of AJ morphology revealed that KD of *Diap1* and *Fmnl3* resulted in reduced E-cad at the AJ and increased cell spread area **(Figure 3.7A;** representative gel images for *Diap1* and *Fmnl3* KD shown in **Figure 3.7C-D)**, as was previously observed with SMIFH2 treatment. Knockdown of all other formins tested did not produce any significant changes in AJ organization when compared to non-targeting control siRNA (Neg siRNA) **(Figure 3.7A)**. Efficiency of knockdown for each formin was assessed by RT-PCR as presented in **Figure 3.7B**, with expression of each formin being reduced to ~20% 26-28hr post-siRNA transfection. Furthermore, we also performed double KD experiments to simultaneously deplete mDia1 and Fmnl3, and observed severe defects in the assembly of cell-cell junctions and monolayer formation **(Figure 3.8A)**. While quantification of junctions was not possible for the double KD condition, individual KD of mDia1 or Fmnl3 resulted in reduced F-actin (29-31% lower) and E-cad (30% lower) fluorescence intensities at the AJ **(Figure 3.8B-C)**.

Next, we asked if a role for formins mDia1 and Fmnl3 at the AJ was a general feature of epithelial cells. To verify this, we chose to KD DIA1 and FMNL3 in a human mammary epithelial cell line, MCF10A. As illustrated in **Figure 3.9A**, depletion of DIA1 or FMNL3 had marked effects on cell-cell junctions in MCF10A, resulting in lower E-cad and increased cell spread area (representative gel images for *DIAP1* and *FMNL3* KD shown in **Figure 3.9B-C**). Taken together, these results indicate a general role for formins mDia1/DIA1 and Fmnl3/FMNL3 at the AJ in epithelial cells.
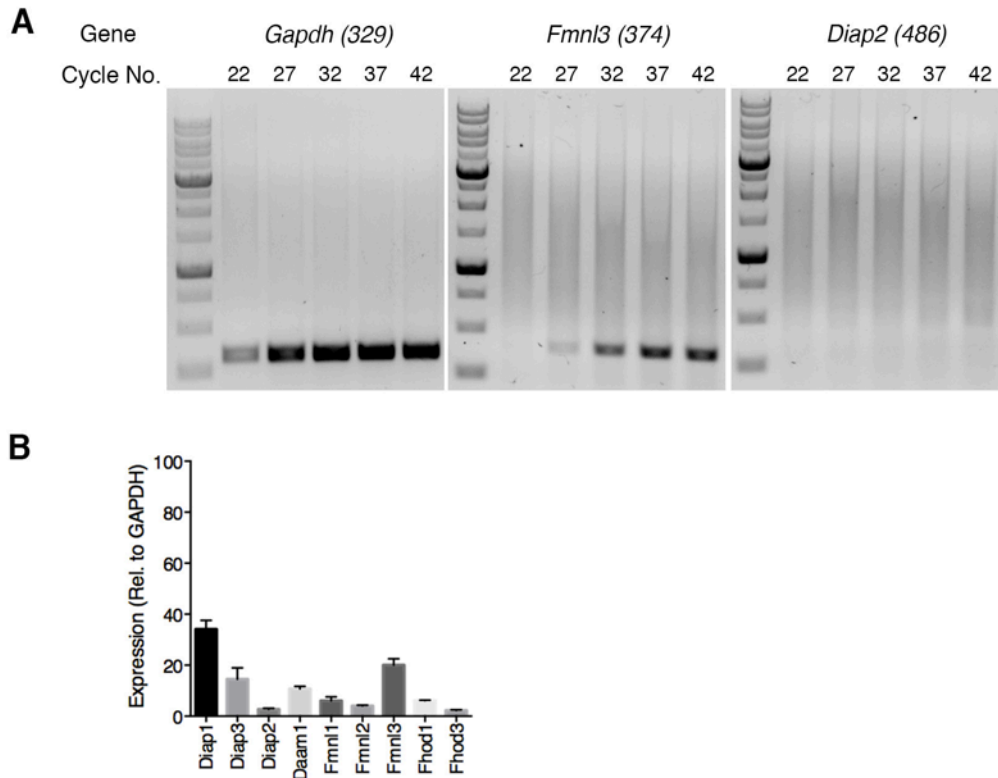
Figure 3.6: Expression profile of Diaphanous-related family of formins in EpH4 epithelial cells

(A) Examples of PCR amplification for endogenous *Gapdh* (house-keeping gene control), *Fmnl3* (positive amplification) and *Diap2* (negligible amplification) for up to 42 cycles.

(B) Endogenous expression levels of Diaphanous-related family of formins in EpH4 cells normalized to Gapdh expression (all measured at 42 PCR amplification cycles). Error bars indicate SEM, n=2 independent experiments.
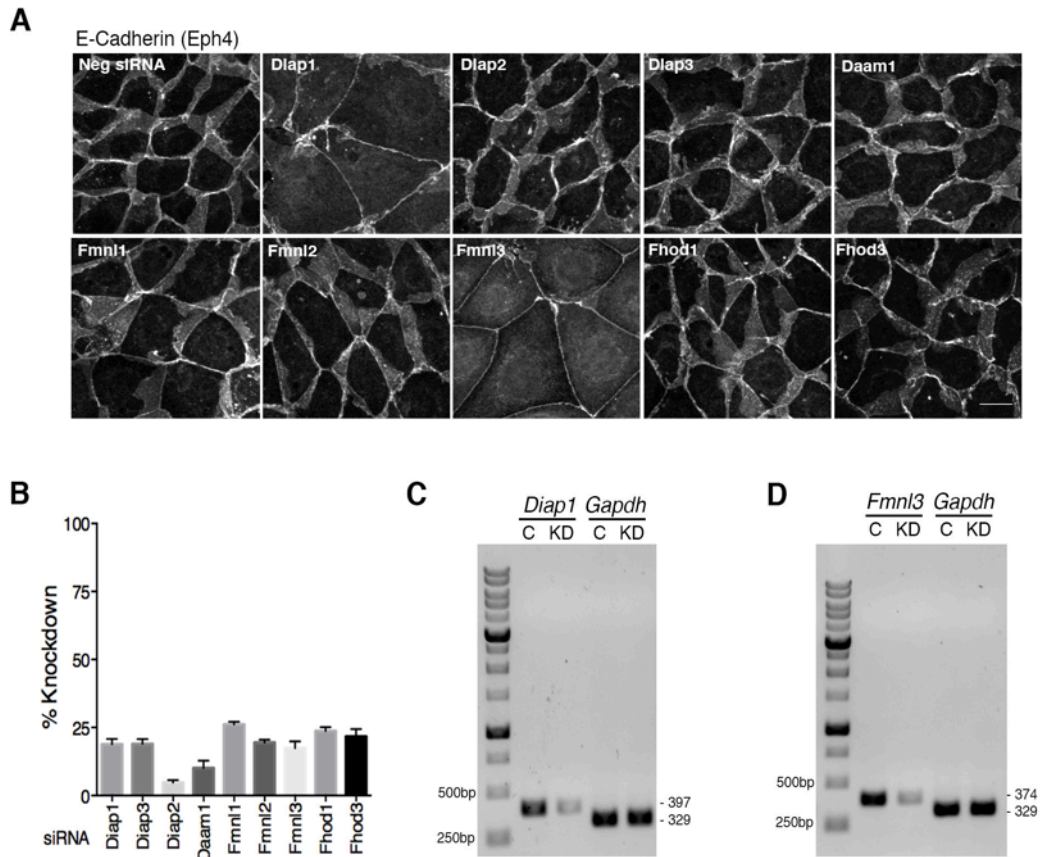
Figure 3.7: siRNA-mediated knockdown screen for Diaphanous-related family of formins

(A) Representative images of AJ morphology (visualized by E-cad labeling) in EpH4 monolayers following KD of formins as indicated. Scale bar, 20μm.

(B) Quantification of KD efficiency for individual formins in EpH4 cells, error bars represent SEM. n=2-3 independent experiments.

(C) & **(D)** Representative gel images showing KD efficiency for *Diap1* and *Fmnl3* in EpH4, with *Gapdh* used as control. C: Non-targeting siRNA control, KD: Knockdown.
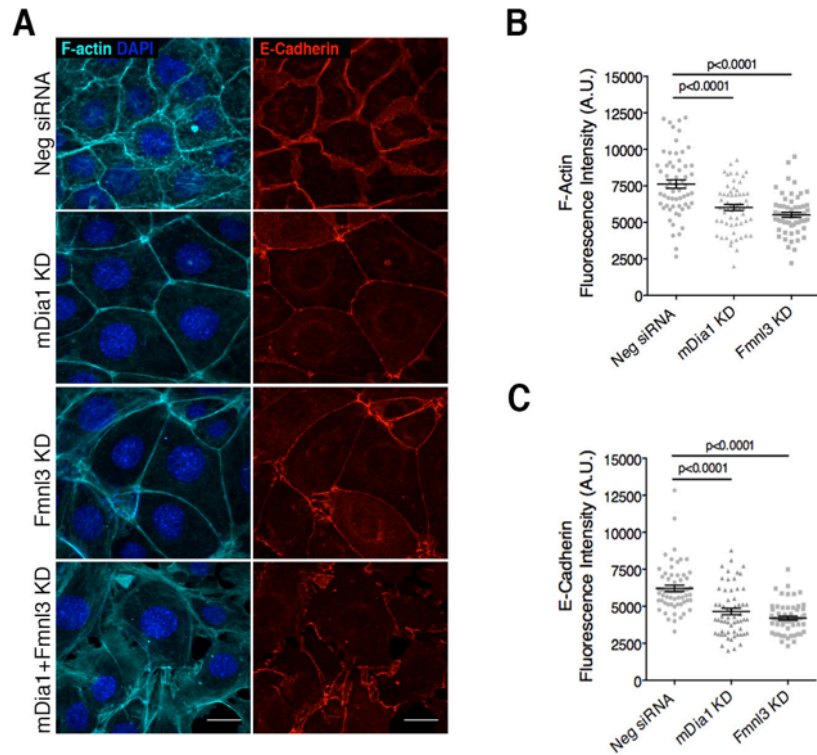
Figure 3.8: Double KD of mDia1 and Fmnl3 results in severe defects in AJ formation

(A) Individual KD of mDia1 or Fmnl3 phenocopies SMIFH2-treatment (as visualized by F-actin and E-cad staining), while double KD (mDia1+Fmnl3 KD) leads to severe defects in AJ formation, resulting in a sparse monolayer. Scale bar, 20μm.

(B) Quantification of F-actin intensity at the AJ for **(A)**.

(C) Quantification of E-cad intensity at the AJ for **(A)**.

n=60-70 junctions per condition from 3 experiments for **(B)** & **(C)**, with Mean±SEM.

Statistical significance tested using one-way ANOVA in **(B)** & **(C)**.
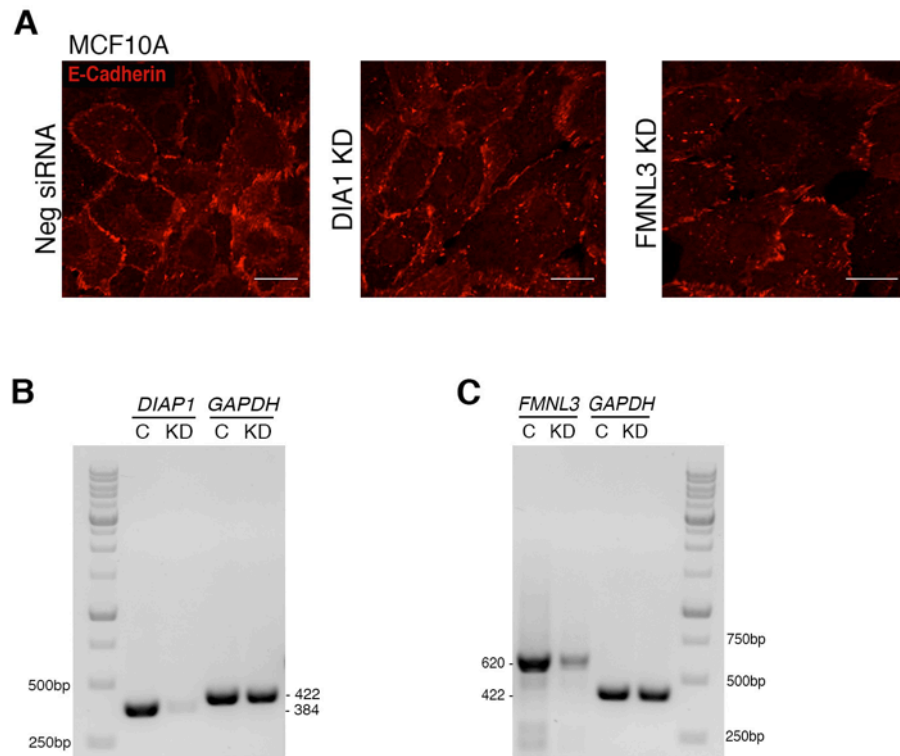
Figure 3.9: DIA1 or FMNL3 KD in MCF10A recapitulates phenotypes in EpH4 monolayers

(A) Individual KD of DIA1 or FMNL3 leads to reduction in E-cad labeling at the AJ and increased cell spreading in MCF10A monolayers. Scale bar, 20μm.

(B) & **(C)** Representative gel images showing KD efficiency for *DIAP1* and *FMNL3* in MCF10A, with *GAPDH* used as control. C: Non-targeting siRNA control, KD: Knockdown.

3.2.2 Localization and characterization of mDia1/DIA1 and Fmnl3/FMNL3

in epithelial cells

Given the striking effects observed in KD experiments, we explored for possible localization of mDia1/DIA1 and Fmnl3/FMNL3 at the AJ in epithelial cells.

Immuno-labeling for endogenous mDia1/DIA1 detection in EpH4 or MCF10A cells revealed no particular enrichment at the AJ **(Figure 3.10A)**. Endogenous Fmnl3/FMNL3, however, was distinctly enriched at the AJ in both EpH4 and MCF10A monolayers **(Figure 3.10B)**. In addition, Fmnl3 labeling was also detected in the primary cilium in EpH4 monolayers **(Figure 3.10B, top panel)**, and calls for further investigation to elucidate its function in this structure. In line with endogenous protein localization, introduction of GFP-tagged Fmnl3 in EpH4 monolayers resulted in its junctional localization, co-localization with E-cad, and an associated increase in F-actin and E-cad content at the AJ (p<0.0001 and p<0.001 respectively, Student's t-test) **(Figure 3.10C-E)**.

Furthermore, we also tested a role for mDia1 at the AJ despite being unable to detect specific localization. To do so, we introduced in cells a Diaphanous auto-regulatory domain (DAD) from mDia1, which is known to stimulate endogenous mDia1 activity (Alberts, 2001; Rao *et al.*, 2013) **(Figure 3.10F)**. Activation of endogenous mDia1 activity resulted not only in augmentation of F-actin content at the AJ (50% increase vs. GFP-transfected control; p<0.0001, Student's t-test) **(Figure 3.10G)**, but also a concomitant increase in

E-cad fluorescence intensity at the junction (33% higher compared to GFP-transfected cells; p<0.0001, Student's t-test) **(Figure 3.10H)**.

Altogether, these results suggest a role for both mDia1 and Fmnl3 in regulating F-actin and E-cad organization at epithelial cell-cell junctions.
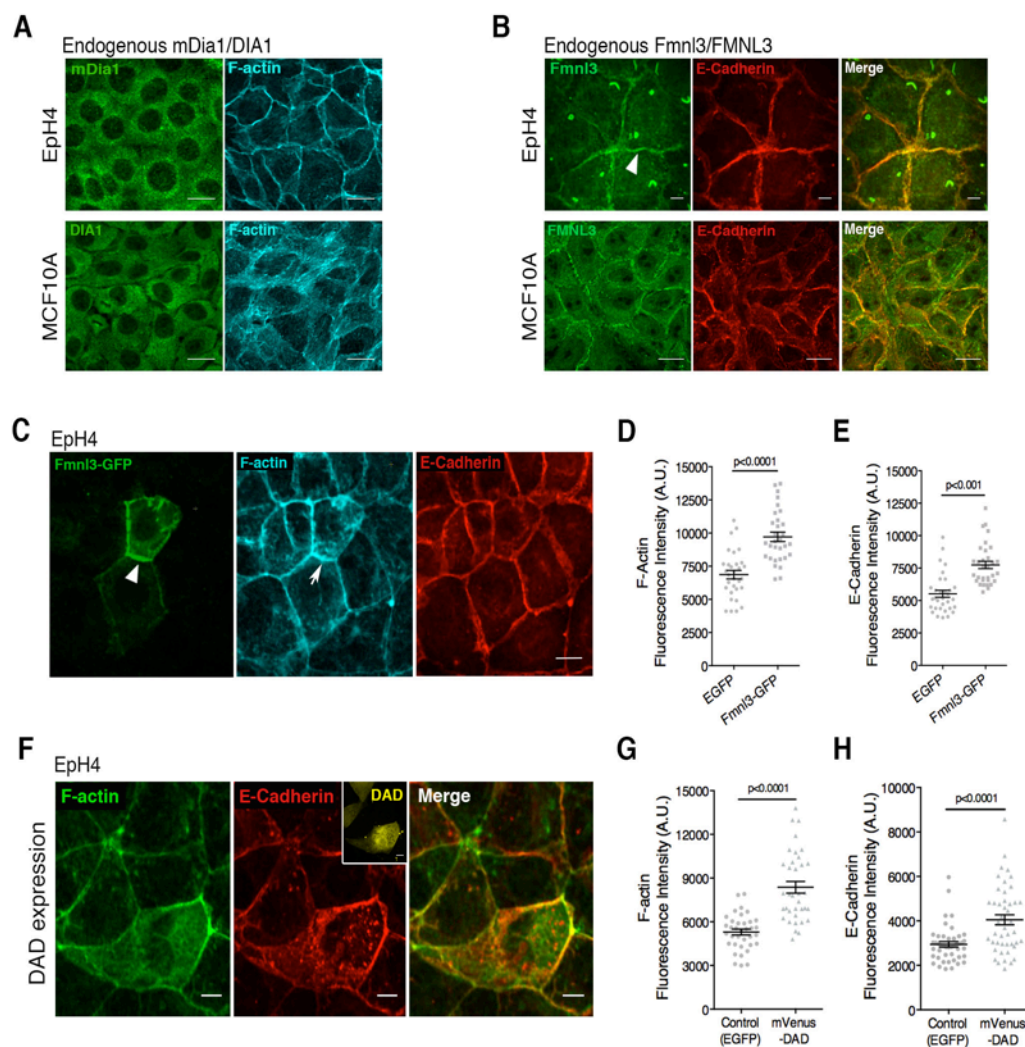
Figure 3.10: Localization and characterization of mDia1/DIA1 and Fmnl3/FMNL3 in epithelial cells

(A) Endogenous mDia1 or DIA1 exhibits diffuse localization in EpH4 or MCF10A monolayers, respectively. Scale bar, 20μm.

(B) Endogenous Fmnl3 or FMNL3 localizes prominently to cell-cell junctions in EpH4 (white arrowhead) or MCF10A monolayers, respectively. Scale bar, 20μm.

(C) Fmnl3-GFP localizes to the AJ (white arrowhead) in EpH4 cells, leading to increase in F-actin (white arrow) and E-cad at cell-cell junctions in transfected cells. Scale bar, 10μm.

(D) & (E) Quantification of junctional fluorescence intensities of F-actin and E-cad, respectively, for **(C)**. n=30 cells/condition from 3 experiments, with Mean±SEM.

(F) EpH4 cells transfected with mVenus-DAD (mVenus fluorescence shown in inset) demonstrate elevated levels of F-actin and E-cad in comparison to non-transfected neighbors. Scale bar, 10μm.

(G) & (H) Quantification of junctional fluorescence intensities of F-actin and E-cad, respectively, for **(F)**. n≥30 cells/condition from 3 experiments, with Mean±SEM.

Statistical significance tested using Student's t-test in **(D), (E), (G) & (H)**.

3.2.3 Src kinase inhibition phenocopies mDia1/Fmnl3 KD and Src kinase acts upstream of formin activity at the AJ

Having identified mDia1 and Fmnl3 as important regulators of actin polymerization at the AJ, we next sought to determine upstream regulators of these formins.

A variety of upstream regulators of formin activity have been identified and characterized so far, which include kinases and RhoGTPases. For instance, the non-receptor tyrosine kinase Src has been shown to regulate several cellular functions of the formin FHOD1 (Koka *et al.*, 2005), and also interacts with DAAM1 to regulate actin filament dynamics in mammalian cells (Aspenstrom *et al.*, 2006). Interestingly, an siRNA screen for kinases that function at the AJ revealed phenotypically similar results for Src KD as we have described here for mDia1 or Fmnl3 KD. As shown in **Figure 3.11A**, inhibition of Src kinase activity via the drug PP2 or siRNA-mediated KD **(KD levels shown in Figure 3.11B)** resulted in a change in junction organization akin to that observed with mDia1 or Fmnl3 KD.

Given that Src inhibition resulted in reduced E-cad at the AJ, we asked if this translated to monolayers possessing weaker cell-cell adhesions. To test adhesion strength, we performed the dispase-based dissociation assay, which uses the enzyme dispase to disrupt cell-ECM attachments without perturbing cell-cell junctions. Post-dispase incubation, the mechanical disruption of cell sheets into single cells is inversely correlated with adhesion strength. As illustrated in **Figure 3.11C**, incubation with dispase for 20min resulted in

higher percentage of cells dissociating from a confluent monolayer pre-treated PP2, in comparison with an unperturbed control (Note the larger cell-free areas in 'EGTA' (low adhesion strength control) and 'PP2', **Figure 3.11C**). Quantification of single cells after a 45min incubation period, revealed 16±3.7% single cells dissociated from control EpH4 monolayers **(Figure 3.11C)**. Pre-treatment with the calcium chelator EGTA, that severely perturbs cadherin-dependent cell-cell adhesion, resulted in nearly complete (95±2.9%) dispersal of the monolayer into single cells **(Figure 3.11C)**. In comparison to untreated control, PP2-treated monolayers produced significantly higher number (32±3.1%; $p<0.0001$, Student's t-test) of single cells after incubation with dispase **(Figure 3.11C)**. Hence, these results suggest that perturbation of Src activity resulted in compromised cell-cell adhesion strength in EpH4 monolayers.

As alluded to previously, Src kinase activity has been demonstrated to act upstream of formins in a variety of cellular contexts. Hence, we sought to identify in our system if Src kinase was also an upstream regulator of mDia1 or Fmnl3. As a direct test, we attempted to rescue the effects of Src inhibition by activation of endogenous mDia1 via DAD expression. Interestingly, DAD expression resulted in dramatic increase in E-cad levels and augmentation of the AJ in transfected cells **(Figure 3.12A-B)** in comparison to non-transfected neighbors that exhibited the Src inhibition phenotype. Hence, we could place formin activity at the AJ downstream of Src kinase activity.

Next, we also tested for regulation of Fmnl3 by Src, by combining Src-GFP expression with siRNA-mediated KD of Fmnl3. In control conditions, co-transfection of full-length Src-GFP and non-targeting siRNA resulted in prominent junctional localization of Src-GFP **(Figure 3.12C top panel)**. This was also associated with robust enrichment of F-actin and E-cad at junctions between transfected cells **(Figure 3.12C top panel, 3.12D-E).** On the contrary, while co-transfection of Src-GFP and Fmnl3 siRNA did not abolish Src localization, we observed no change in F-actin or E-cad levels at the AJ **(Figure 3.12C bottom panel, 3.12D-E)**.

Overall, these data demonstrate a role for Src kinase an as upstream regulator of formin activity at cell-cell junctions.
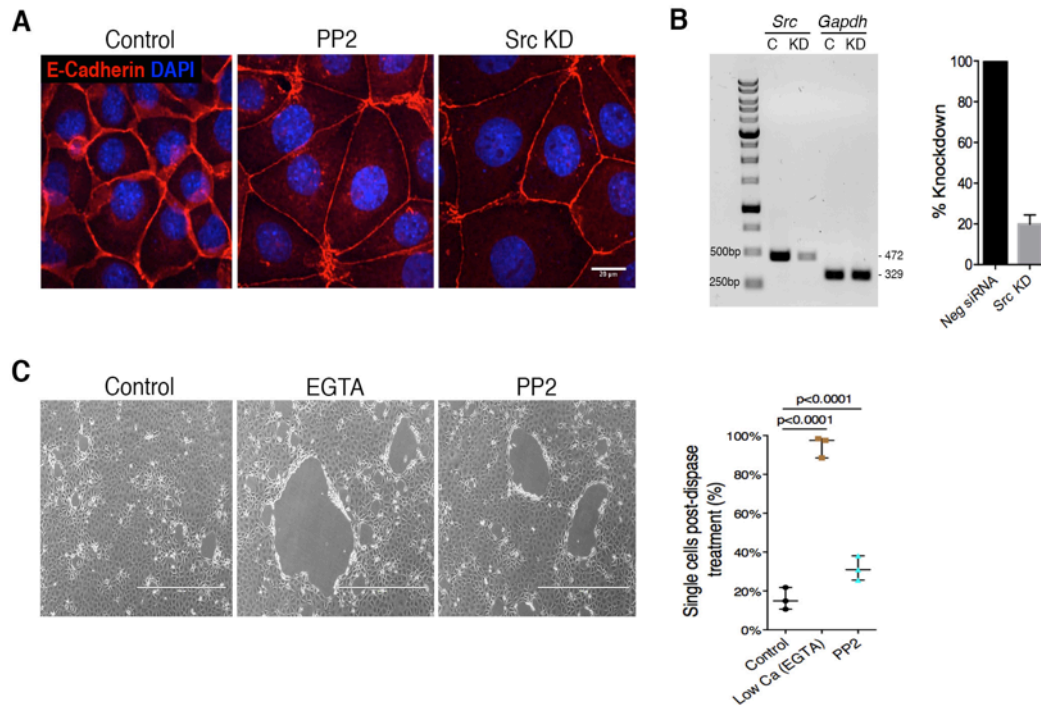
Figure 3.11: Src kinase inhibition phenocopies formin inhibition

(A) Inhibition of Src kinase activity via PP2 treatment or siRNA-mediated knockdown results in reduced E-cad and increased cell spreading, similar to phenotypes associated with mDia1 or Fmnl3 KD. Scale bar, 20μm.

(B) Representative gel image and quantification of KD efficiency for *Src* in EpH4, with *Gapdh* used as control. C: Non-targeting siRNA control, KD: Knockdown.

(C) Dispase assay for PP2 treated monolayers to assess cell-cell adhesion strength. Note the large gaps formed in EGTA (low adhesion strength control) or PP2-treated monolayers in comparison to control, indicating increased dissociation of cells. Quantification of single cells released from each sample is shown alongside. n=3 independent experiments, with Mean±SD.

Statistical significance tested using one-way ANOVA in **(C)**.
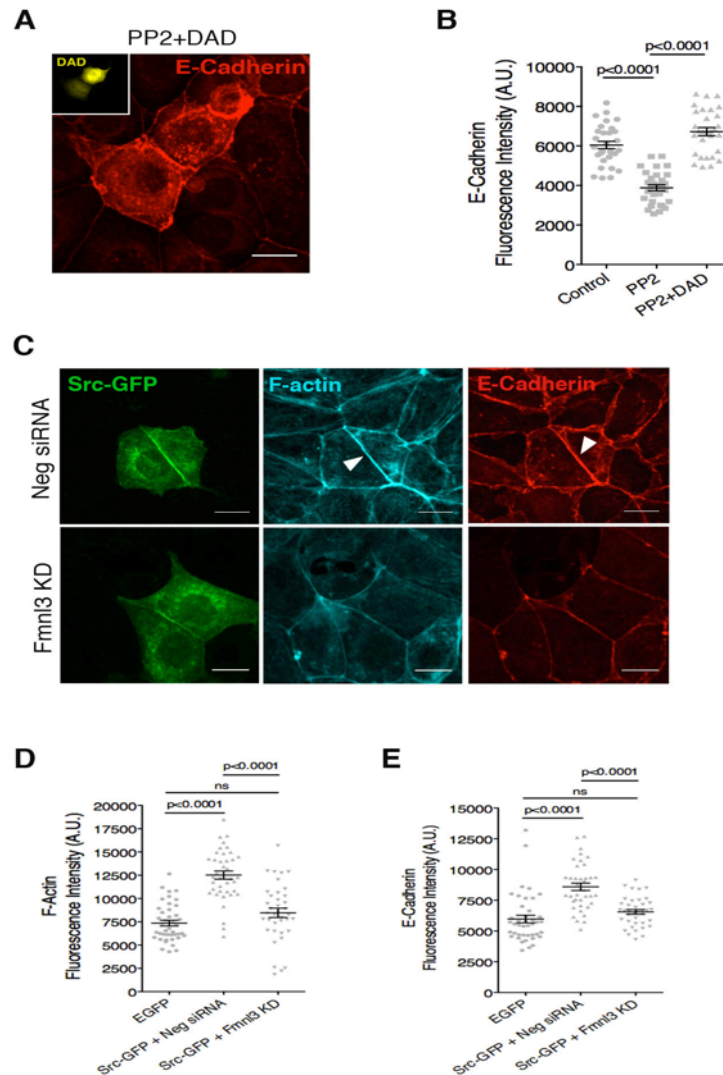
Figure 3.12: Src kinase acts upstream of formin activity at the AJ

(A) Reduction in junctional E-cad levels associated with Src inhibition (PP2) can be rescued by activation of endogenous mDia1 via DAD expression (mVenus fluorescence shown in inset). Note the significant increase in E-cad at the AJ in transfected cells vs. non-transfected counterparts. Scale bar, 20μm.

(B) Quantification of junctional E-cad related to **(A)**. n≥30 cells/condition from 3 experiments, with Mean±SEM.

(C) Expression of Src-GFP (full-length) results in its junctional localization, associated with higher F-actin and E-cad levels at the AJ (arrowheads, top panel). Junction augmentation is abrogated when Src-GFP expression is combined with Fmnl3 KD (bottom panel). Scale bar, 20μm.

(D) & (E) Quantification of junctional fluorescence intensities of F-actin and E-cad, respectively, for **(C)**. n≥35 cells/condition from 3 experiments, with Mean±SEM.

Statistical significance tested using one-way ANOVA in **(B), (D) & (E)**.

3.2.4 Cdc42 is a signaling intermediate between Src kinase and formin activity at the AJ

An overwhelming body of evidence has implicated RhoGTPases as upstream regulators of Diaphanous-related family of formins that are typically auto-inhibited and require activation through RhoGTPase binding, as reviewed in (Chesarone *et al.*, 2010). Several previous studies have also implicated Src kinase as a regulator of RhoGTPase activity at the AJ (Fukuhara *et al.*, 2004; Bertocchi *et al.*, 2012). Hence, we hypothesized a RhoGTPase intermediate existed in the signaling cascade from Src to formin activity.

To test this, we used constitutive active mutants of RhoA (V14), Rac1 (L61), and Cdc42 (Q61L), and tested their ability to rescue the phenotype of Src inhibition with PP2. Expression of active Cdc42 was effective in rescuing defects in AJ morphology that were otherwise observed with Src kinase inhibition **(Figure 3.13A-B)**. We also detected increased E-cad levels at the AJ in Cdc42 (Q61L)-expressing cells compared to non-transfected neighbors **(Figure 3.13A-B)**. On the other hand, active RhoA or Rac1 did not rescue PP2 inhibition, and failed to restore E-cad fluorescence levels at cell-cell junctions **(Figure 3.13C-D)**. Thus, we identified Cdc42 as a key intermediate between Src and formin activity at the AJ.

In a recent study, Cdc42 was demonstrated to regulate Fmnl3 activation and promote filopodia production during zebrafish angiogenesis (Wakayama *et al.*, 2015). We hypothesized that this may be true of cell-cell junctions as well, and used a mutant Fmnl3 to test the same. Mutation I111D in Fmnl3

abolishes binding to Cdc42, as previously shown in (Wakayama *et al.*, 2015). Fmnl3-GFP (I111D) exhibited diffuse cytoplasmic localization when transfected in EpH4 cells, with no particular enrichment at the AJ **(Figure 3.13E)**. Further, this mutant did not affect either F-actin or E-cad levels at the AJ **(Figure 3.13F-G)**, unlike wild-type Fmnl3-GFP that induced substantial increase in F-actin/E-cad at the AJ **(**refer **Figure 3.10C-E)**. Thus, our results confirm the RhoGTPase Cdc42 to be an important intermediate between Src kinase activity and formin activation, particularly Fmnl3, at the AJ.
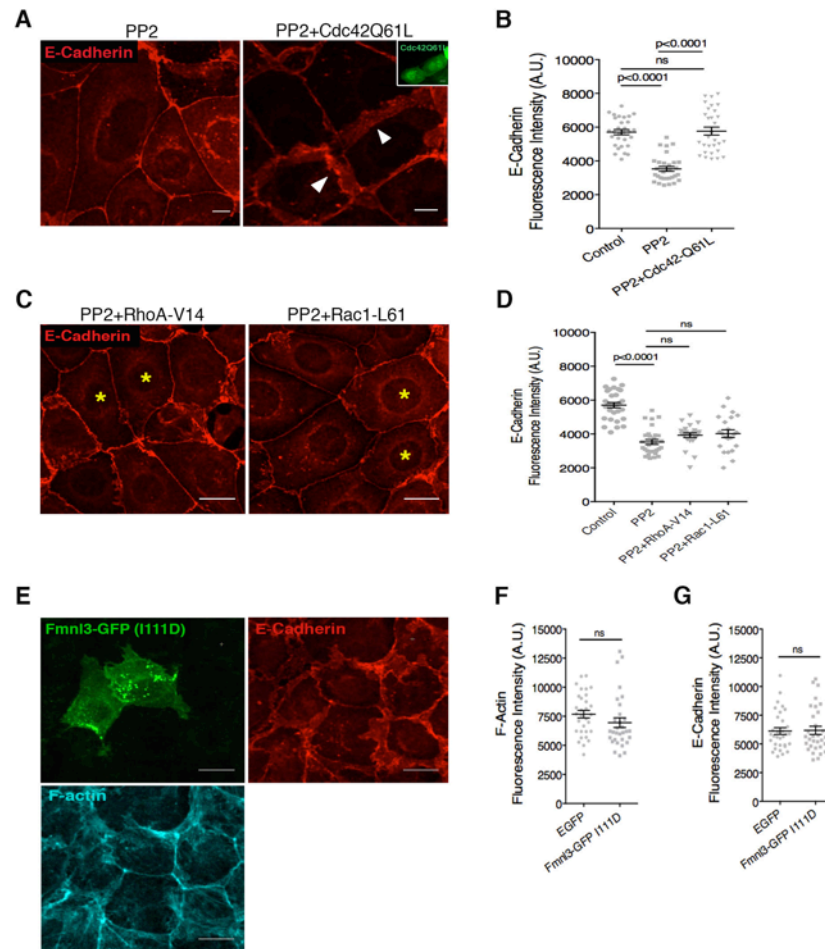
Figure 3.13: Cdc42 is a signaling intermediate between Src kinase and formin activity at the AJ

(A) Constitutively active Cdc42 expression (GFP shown in inset) rescues Src inhibition phenotype. Note the difference in AJ morphology in transfected cells (white arrowheads) compared to non-transfected neighbors. Scale bar, 10μm.

(B) Quantification of E-cad fluorescence intensity for **(A)**. n≥29 cells per condition from 3 experiments, with Mean±SEM.

(C) Constitutively active RhoA or Rac1 expression (transfected cells marked with asterisk) does not rescue Src inhibition phenotype. Scale bar, 20μm.

(D) Quantification of E-cad fluorescence intensity for **(C)**. n≥25 cells per condition from 3 experiments, with Mean±SEM.

(E) Fmnl3-GFP (I111D) does not localize to the AJ or affect F-actin/E-cad levels. Scale bar, 20μm.

(F) & (G) Quantification of junctional fluorescence intensities of F-actin and E-cad, respectively, for **(E)**. n≥26 cells/condition from 3 experiments, with Mean±SEM.

Statistical significance tested using one-way ANOVA in **(B) & (D)**, Student's t-test in **(F) & (G)**.

3.3 Formin activity affects molecular and monolayer dynamics in epithelial cells

3.3.1 Formin activity affects E-cadherin and F-actin dynamics at the AJ

Given the strong correlation between formin activity and F-actin/E-cad content at the AJ, we proceeded to perturb formin activity and test the effects on molecular dynamics using Fluorescence Recovery After Photobleaching (FRAP). This technique is used to characterize protein dynamics by bleaching a region of interest (ROI) along a cell-cell junction, followed by time-lapse observation of fluorescence recovery within the bleached ROI. Quantitative analysis of molecular dynamics is then achieved by fitting fluorescence intensity measurements in the recovery phase to a reaction-diffusion equation (Sprague and McNally, 2005; Erami *et al.*, 2015).

In a recent study, FRAP analysis was used to identify distinct populations of E-cad at cell-cell junctions based on their dynamics; and elegantly demonstrated that a large fraction of E-cad molecules were immobilized through interactions facilitated by the extracellular domain (EC1) and/or cytoplasmic domain-mediated interactions with actin (Erami *et al.*, 2015). Perturbation of EC1 domain mediated *cis* (V81D+V175D mutations) or *trans* (W2A mutation) interactions or deletion of the cytoplasmic domain to prevent actin binding resulted in poorer immobilization of E-cad at cell junctions (Erami *et al.*, 2015). Given their direct role in polymerizing actin, we chose to modulate levels of formin activity and performed FRAP experiments on EpH4 monolayers stably expressing E-cadherin-GFP **(Figure 3.14A)**.

Data from our FRAP analysis are summarized in **Table 3.1**, while recovery curves and quantification of mobile fractions are illustrated in **Figure 3.14B-C**. In control monolayers, FRAP analysis on E-cad revealed the half-life of recovery ($t_{1/2}$) to be 151s and a mobile fraction of 53±1.43%. In comparison, E-cad in SMIFH2-treated monolayers recovered at a much faster rate ($t_{1/2} =$ 112s), with a significantly higher mobile fraction (65±2.63%; p<0.001, Student's t-test). Stimulation of endogenous mDia1 and actin polymerization via DAD expression, however, resulted in a significantly slower recovery rate with a $t_{1/2}$ of 173s and 43±1.89% mobile fraction (p<0.01, Student's t-test).

Next, we also assessed F-actin dynamics at the AJ by performing FRAP on EpH4 cells transiently expressing tdTomato-actin **(Figure 3.14D-F,** summarized in **Table 3.2)**. Here, we focused our efforts on characterizing Fmnl3 KD or over-expression conditions, given the clear localization of Fmnl3 we observed previously. At control junctions, the recovery curve for tdTomato-actin exhibited bi-phasic characteristics, with an initial rapid recovery phase and second phase consisting of G-actin monomer integration into the F-actin pool, as has been previously described in other systems (Tardy *et al.*, 1995). Based on our analysis, $t_{1/2}$ for F-actin at control junctions was quantified to be 19.95s **(Table 3.2, Figure 3.14D-F)**. Cellular depletion of Fmnl3 led to an accelerated recovery phase initially ($t_{1/2}$=12.2s), indicating that a reduction in F-actin polymerization by Fmnl3 likely shifts the G/F-actin ratio in favor of increased levels of G-actin **(Table 3.2, Figure 3.14D-F)**. Conversely, Fmnl3-GFP expression resulted in increased F-actin content at the AJ, as quantified previously **(**refer **Figure 3.10C-D)**. As expected, FRAP

analysis under these conditions led to slower tdTomato-actin turnover at the AJ ($t_{1/2}$ =25.11s) **(Table 3.2, Figure 3.14D-F)**, suggesting that the G-actin pool may be diminished due to increased formin-dependent F-actin polymerization at the AJ. Indeed, similar recovery kinetics for F-actin at the AJ has also been independently demonstrated for the formin FMNL2 in MCF10A cells cultured under 3D conditions (Grikscheit *et al.*, 2015).

Hence, these data suggest that tuning F-actin polymerization by either inhibiting or activating formins directly affects actin turnover at the AJ, which in turn impinges on the mobility of E-cad at cell junctions, further confirming the role of actin binding in the stabilization of E-cad at the AJ.

Table 3.1: Summary of FRAP analysis for E-cadherin

S.No.	Sample	Half-life ($t_{1/2}$)	Mobile Fraction
1.	Control	151s	53±1.43%
2.	SMIFH2	112s	65±2.63%
3.	DAD expression	173s	43±1.89%

Table 3.2: Summary of FRAP analysis for F-actin

S.No.	Sample	Half-life ($t_{1/2}$)	Mobile Fraction
1.	Neg siRNA (Control)	19.95s	78.7±1.45%
2.	Fmnl3 KD	12.2s	85.1±1.17%
3.	Fmnl3 over-expression	25.11s	71.03±1.84%
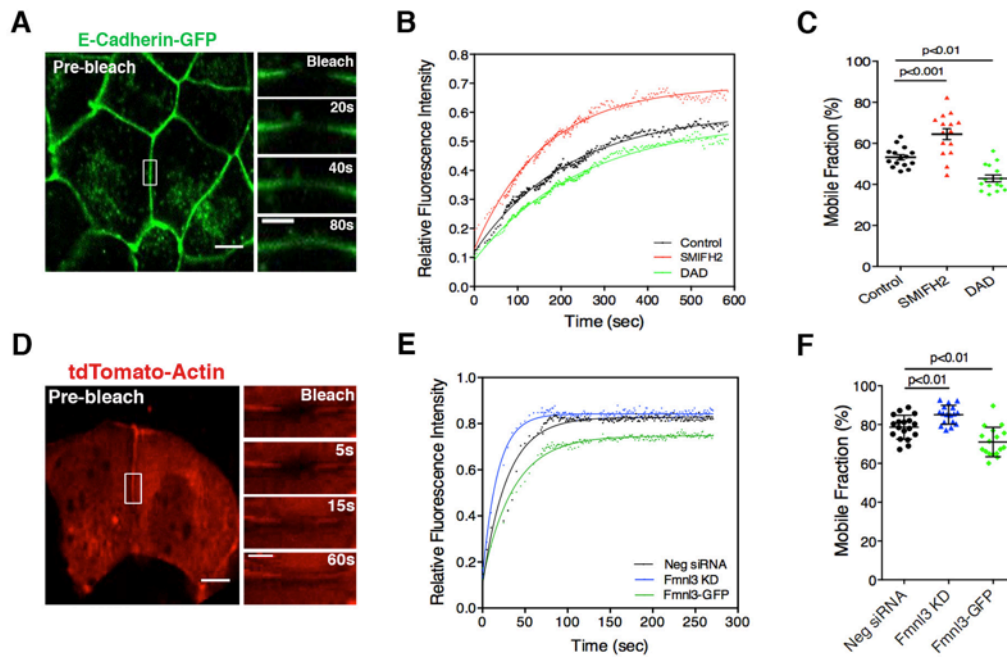
Figure 3.14: Formin activity affects E-cadherin and F-actin dynamics at the AJ

(A) FRAP analysis on E-cadherin-GFP expressing EpH4 monolayers; junctional cadherin was photo-bleached (white rectangle) and recovery of fluorescence was assessed (as shown in magnifications). Scale bar, 10μm; 5μm (magnification).

(B) Fluorescence recovery curves for E-cadherin comparing the effects of SMIFH2 treatment or DAD expression. Data are illustrated as an average for 15-16 junctions tested for each condition from 2-3 experiments.

(C) Mobile fractions corresponding to **(B)**. n=15-16 junctions from 2-3 experiments, with Mean±SEM.

(D) FRAP analysis on tdTomato-Actin expressing EpH4 cells; junctional F-actin was photo-bleached (white rectangle) and recovery of fluorescence was assessed (as shown in magnifications). Scale bar, 10μm; 5μm (magnification).

(E) Fluorescence recovery curves for F-actin comparing the effects of Fmnl3 KD or Fmnl3 overexpression (Fmnl3-GFP). Data are illustrated as an average for 17-18 junctions tested for each condition from 3 experiments.

(F) Mobile fractions corresponding to **(E)**. n=17-18 junctions from 3 experiments, with Mean±SD.

Statistical significance tested using one-way ANOVA in **(C)** & **(F)**.

3.3.2 Fmnl3 and mDia1 support monolayer cohesion during collective migration

Having found significant effects of Fmnl3 KD at the molecular level, we next analyzed effects on monolayers dynamics using an *in vitro* scratch assay to follow collective cell migration. As has been shown previously for several types of epithelial cells, EpH4 monolayers exhibited characteristic directed migration resulting in complete closure of the gap within 12hr **(Figure 3.15A-B)**. KD of Fmnl3, however, resulted in severe migration defects, primarily driven by increased dissociation of cells from the migrating fronts ($25\pm2.25\%$ in comparison to $5\pm1.23\%$ in control; $p<0.0001$, Student's t-test) **(Figure 3.15A, C)**. Failure to maintain a continuous front resulted in only 62% gap closure during the period of imaging **(Figure 3.15B)**. Further, having previously identified mDia1 as an important player at the AJ, we also tested the effect of a double KD (that is, both mDia1 and Fmnl3) on collective migration. To do so, we introduced siRNAs against both formins on pre-formed confluent EpH4 monolayers, as performing KD in suspension resulted in the formation of a sparse monolayer with punctate AJ **(**as shown previously in **Figure 3.8A, bottom panel)**. Under these conditions, we observed little to no migration **(Figure 3.15A bottom panel)**, with all gaps remaining unsealed even up to 12hr **(Figure 3.15B)**. In addition, we detected multiple cytokinesis failure events leading to numerous rounded cells that failed to re-integrate into the monolayer **(Figure 3.15A bottom panel)**. Strikingly, the double KD condition (mDia1+Fmnl3 KD) was associated with complete lack of lamellipodium formation at the migrating fronts **(Figure 3.15A bottom panel)**.

We hypothesized that the high propensity for cell detachment from migrating monolayers could be the consequence of weaker cell-cell adhesion, and tested this using the dispase-based dissociation assay. As shown in **Figure 3.15D**, control (Neg siRNA) monolayers exhibited a single cell dissociation rate of 16±2.23%, while EGTA-based calcium chelation to weaken adhesion strength resulted in increased (93±2.4%; $p<0.0001$, Student's t-test) single cell dissociation. siRNA-mediated KD of Fmnl3 led to nearly half the monolayer being dispersed into single cells (43±3.09%; $p<0.001$, Student's t-test) **(Figure 3.15D)**, while double KD of mDia1 and Fmnl3 enhanced cell dissociation to 66±3.47% **(Figure 3.15D)**.

The phenotypes described thus far were true not only of EpH4 monolayers, but also of MCF10A where KD of FMNL3 resulted in failure in migration with several instances of cell detachment at the leading edge **(Figure 3.16A, C)**. Thus, closure of the gap was also severely compromised in MCF10A monolayers, as shown in **Figure 3.16A-B**. Further, we also tested cell-cell adhesion strength in MCF10A monolayers using the dispase assay, together with a Neg siRNA control and EGTA treatment. As illustrated in **Figure 3.16D**, FMNL3 KD monolayers exhibited a single cell dissociation rate of 35±3.22% ($p<0.01$, Student's t-test) when compared to 16.46±3.47% in control monolayers.

All in all, our analysis of dynamics both at the molecular and monolayer levels, suggest that formins mDia1 and Fmnl3 facilitate actin turnover at the AJ and strengthen cell-cell adhesion, thereby preserving monolayer integrity during collective migration. Based on our data in both quiescent **(Section 3.2.2)** and migrating monolayers, we propose a co-operative role for both these formins at the AJ. Further analysis via co-immunoprecipitation and co-localization experiments is required to probe for direct interactions, if any, between these formins at the AJ.
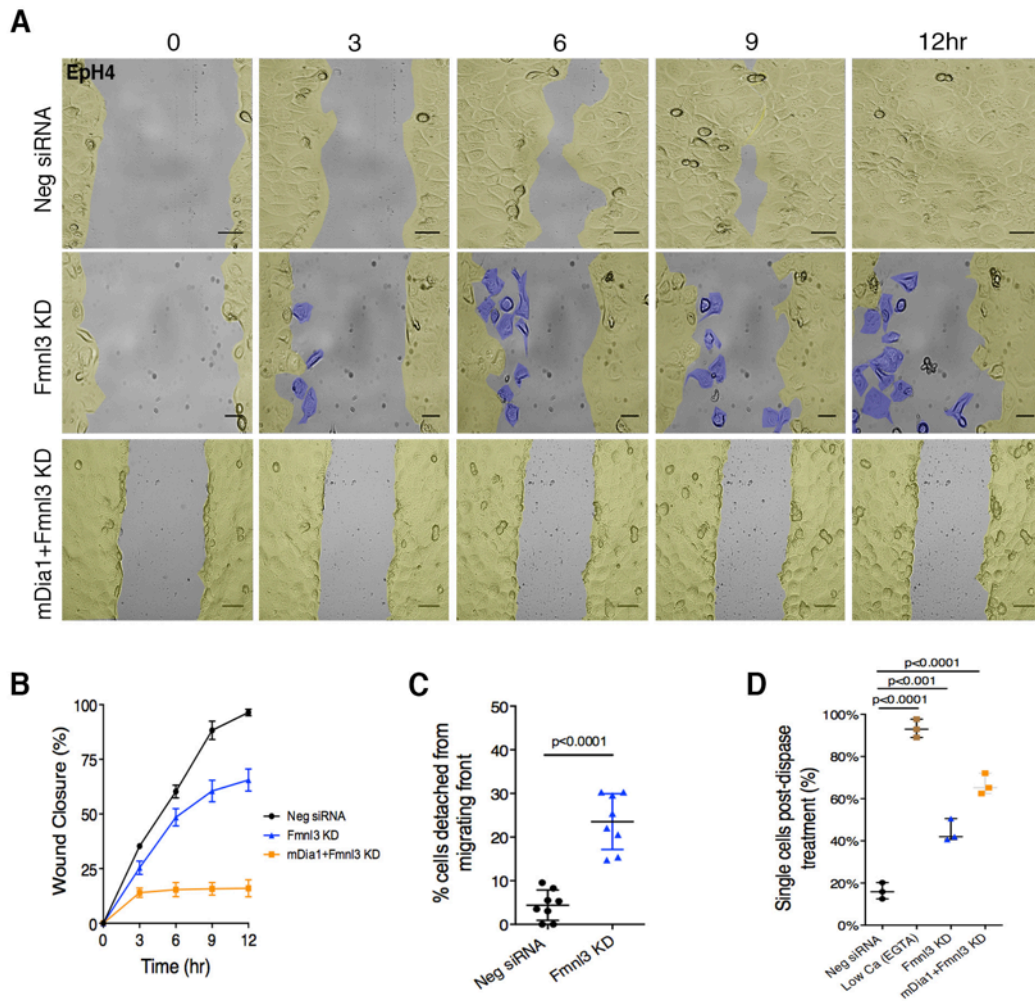
Figure 3.15: Fmnl3 and mDia1 support monolayer cohesion during collective migration in EpH4 cells

(A) *In vitro* scratch assay performed in EpH4 monolayers in three conditions: Control (Neg siRNA), Fmnl3 KD or Double KD (mDia1+Fmnl3 KD). Cohesive regions of the cell sheet are pseudo-colored in yellow in the montages shown here, while cells detached from the monolayer are highlighted in blue. Scale bar, 50μm.

(B) Wound closure quantification related to **(A)**. n=8-10 movies per condition, with Mean±SEM.

(C) Quantification of cells detached from migrating front. n=8 movies for each condition, with Mean±SD.

(D) Dispase dissociation assay corresponding to conditions tested in **(A)**, with EGTA treatment used as a low adhesion strength control. n=3 independent experiments, with Mean±SD.

Statistical significance tested using Student's t-test in **(C),** one-way ANOVA in **(D)**.
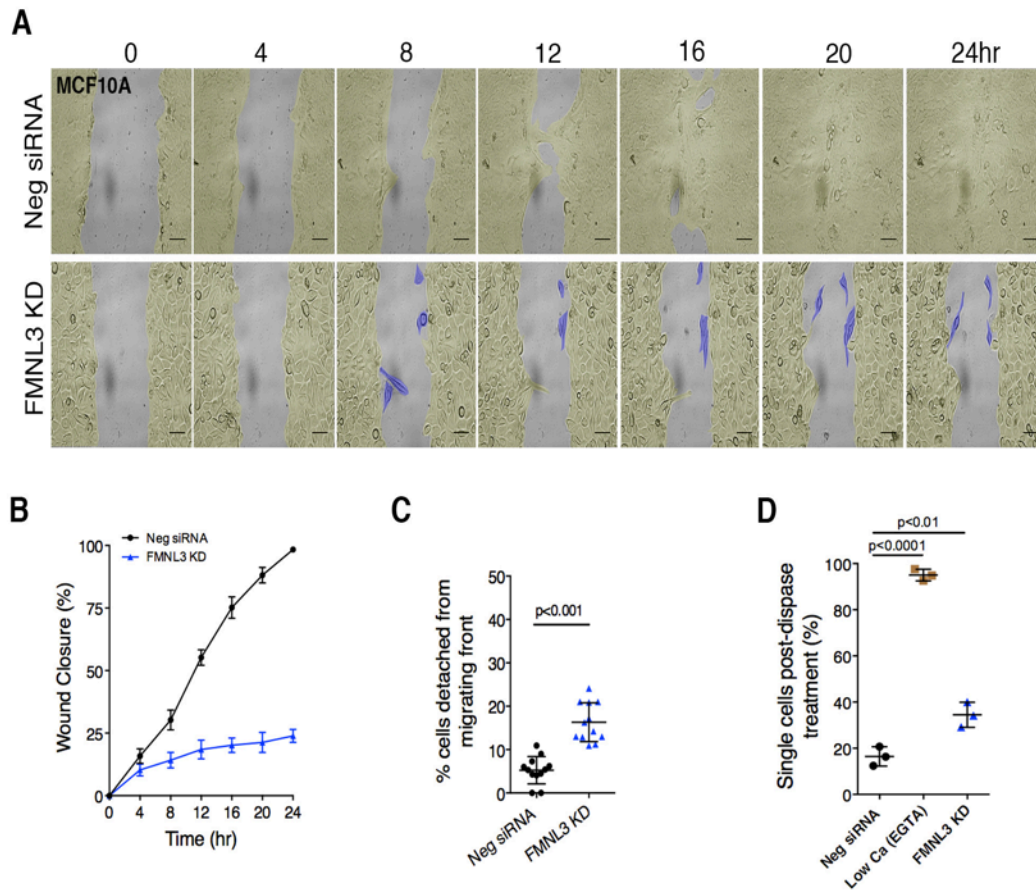
Figure 3.16: FMNL3 is required for monolayer cohesion in migrating MCF10A monolayers

(A) *In vitro* scratch assay performed in MCF10A monolayers in two conditions: Control (Neg siRNA) and Fmnl3 KD. Cohesive regions of the cell sheet are pseudo-colored in yellow in the montages shown here, while cells detached from the monolayer are highlighted in blue. Scale bar, 50μm.

(B) Wound closure quantification related to **(A)**. n=12 movies per condition, with Mean±SEM.

(C) Quantification of cells detached from migrating front. n=12 movies for each condition, with Mean±SD.

(D) Dispase dissociation assay corresponding to conditions tested in **(A)**, with EGTA treatment used as a low adhesion strength control. n=3 independent experiments, with Mean±SD.

Statistical significance tested using Student's t-test in **(C),** one-way ANOVA in **(D)**.

3.3.3 Fmnl3 localization at the AJ and expression are up regulated during collective migration

Due to the strong phenotype of cell detachment associated with Fmnl3 KD and based on its localization at the AJ in quiescent monolayers **(refer Figure 3.10B)**, we next asked if Fmnl3 localization also varied in actively migrating monolayers. To test this, we performed an *in vitro* scratch assay and assessed over time localization of Fmnl3 by immunostaining **(Figure 3.17A)**. More specifically, we analyzed localization patterns of Fmnl3 in cells that were located several cell layers behind the leading edge. Interestingly, we observed enrichment of Fmnl3 at the AJ after 4hr of wounding, with nearly 2-fold increase in localization observable between 6-10hr since migration had begun **(Figure 3.17A-B)**. Following cessation of migration between 12-14hr, there was a gradual reduction in Fmnl3 levels at the AJ **(Figure 3.17A-B)**.

Given the increased localization of Fmnl3 at cell-cell junctions during the course of migration, we questioned if this was related to up-regulation of *Fmnl3* gene expression. To verify this, we used semi-quantitative RT-PCR analysis to quantify changes in *Fmnl3* expression levels during migration. As shown in **Figure 3.17C**, we followed the process of collective migration over a 14hr time period. Migration was most active between 6-10hrs post-wounding, during which time the two opposing cell fronts began to establish cell-cell contact, and by 12hr all gaps had been completely sealed. Next, we analyzed mRNA expression levels for every time point shown in **Figure 3.17C**. Interestingly, RT-PCR analysis revealed a continuous rise in *Fmnl3* levels until ~10hr into the migration process, coinciding well with the active

phase of cell sheet migration **(Figure 3.17D-E)**. Following a peak increase of 1.4-fold at 10hr, we observed a mild reduction in expression levels between 12-14hr when long-range migration had ceased **(Figure 3.17D-E)**.

Therefore, these data support the idea that Fmnl3-dependent actin polymerization is required to reinforce junctions during collective migration, a condition that typically results in exertion of higher forces on cell-cell junctions (Tambe *et al.*, 2011).
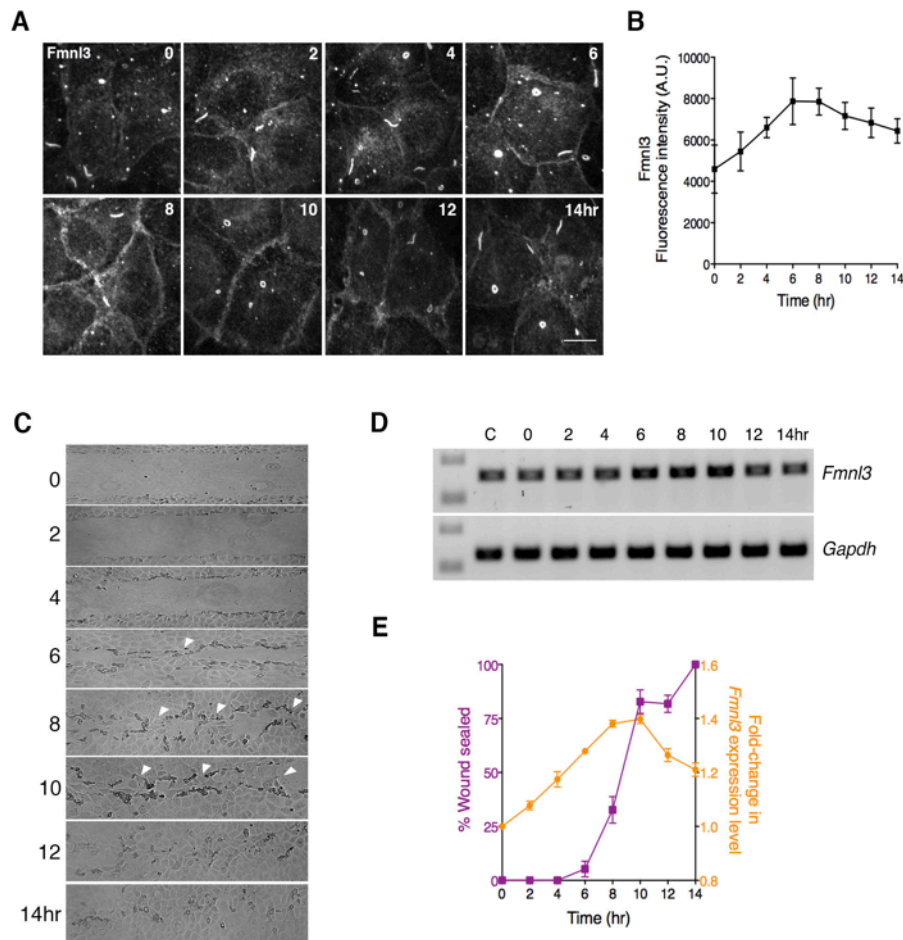
Figure 3.17: Fmnl3 localization at the AJ and expression are up-regulated to promote collective migration

(A) Detection of endogenous Fmnl3 localization during the wound closure process over 14hr. Cells shown here were situated 4-5 cells row inside the monolayer, behind the wound edge. Scale bar, 20µm.

(B) Quantification of junctional Fmnl3 fluorescence intensity corresponding to **(A)**. n=2 independent experiments, with Mean±SEM.

(C) Time series following an *in vitro* scratch assay over 14hr (low magnification, 10X). Arrowheads indicate regions of *de novo* AJ formation when opposing cell fronts establish contact.

(D) Detection of Fmnl3 expression levels using PCR amplification, corresponding to time points illustrated in **(C)**. Note the increase in intensity of bands between 6-10hr time points. C: control monolayer (unwounded).

(E) Quantification of % wound sealed from **(C)**, compared with Fmnl3 expression levels in **(D)**. Note the rise in Fmnl3 expression levels coincides with the phase of active cell sheet migration. n=2 independent experiments, with Mean±SEM.

3.3.4 Fmnl3 localization at the AJ is tension-sensitive

Increased recruitment of Fmnl3 to the AJ coincident with the duration of active migration suggested that Fmnl3 recruitment to junctions might be force-sensitive. To test this directly, we used the 'α18' monoclonal antibody that has been previously characterized (Yonemura *et al.*, 2010). The epitope recognized by the α18 antibody resides in a central domain within the AJ protein, α-catenin. Force-dependent stretching of α-catenin at the AJ allows for vinculin recruitment and exposes the central α18-binding region; thus, enabling the use of this antibody as a marker for force-dependent recruitment at the AJ.

First, we used nocodazole (increases contractility) (Chang *et al.*, 2008) or blebbistatin (decreases contractility) (Kovacs *et al.*, 2004) treatment on EpH4 monolayers to confirm that α-18 antibody staining at cell-cell junctions was indeed tension-sensitive. In line with results from (Yonemura *et al.*, 2010), we observed significantly higher α18 staining at the AJ following nocodazole treatment **(Figure 3.18A-B)**, while α18 or α-catenin labeling was significantly reduced post-blebbistatin treatment **(Figure 3.18A, bottom panel).** Therefore, these data confirm that cell-cell junctions in EpH4 were tension-sensitive which resulted in force-induced stretching of α-catenin at the AJ. Next, we used similar drug treatments to assess the localization of Fmnl3 under conditions of varying cellular contractility. As shown in **Figure 3.19A-C**, increased cellular contractility (nocodazole) resulted in an increase in Fmnl3 localization at the AJ **(Figure 3.19A middle panel, 3.19C)**, which was lost upon treatment with blebbistatin **(Figure 3.19A bottom panel)**.

Altogether, these results further demonstrate the force-dependent recruitment of Fmnl3 to cell-cell junctions, and suggest a mechanism to explain our observations of increased Fmnl3 localization to the AJ during collective cell migration. Further, it is interesting to note that previous studies have highlighted force-dependent stimulation of actin polymerization by the formins mDia1 (Higashida *et al.*, 2013) and INF2 (Shao *et al.*, 2015). Evidence from (Higashida *et al.*, 2013) implicates the FH1 and FH2 domains as likely candidates for mechano-sensitive domains, an area that warrants further investigation. The ability of formins to respond to forces and polymerize actin highlights a mechanism by which cells can quickly reinforce cellular actin structures (for instance, actin at the cortex or at the AJ) in response to tensile stress. In addition, force-dependent activation of mDia1 was also shown to be independent of Rho-GTPase binding (Higashida *et al.*, 2013). These studies provide interesting clues into alternate mechanisms for formin activation, in addition to known Rho-GTPase-dependent signaling pathways. How force is transduced within the auto-inhibited conformation of a formin remains unknown; but preliminary evidence suggests that increased cytoplasmic G-actin levels can be directly sensed and polymerized by formins such as mDia1 (Higashida *et al.*, 2013).
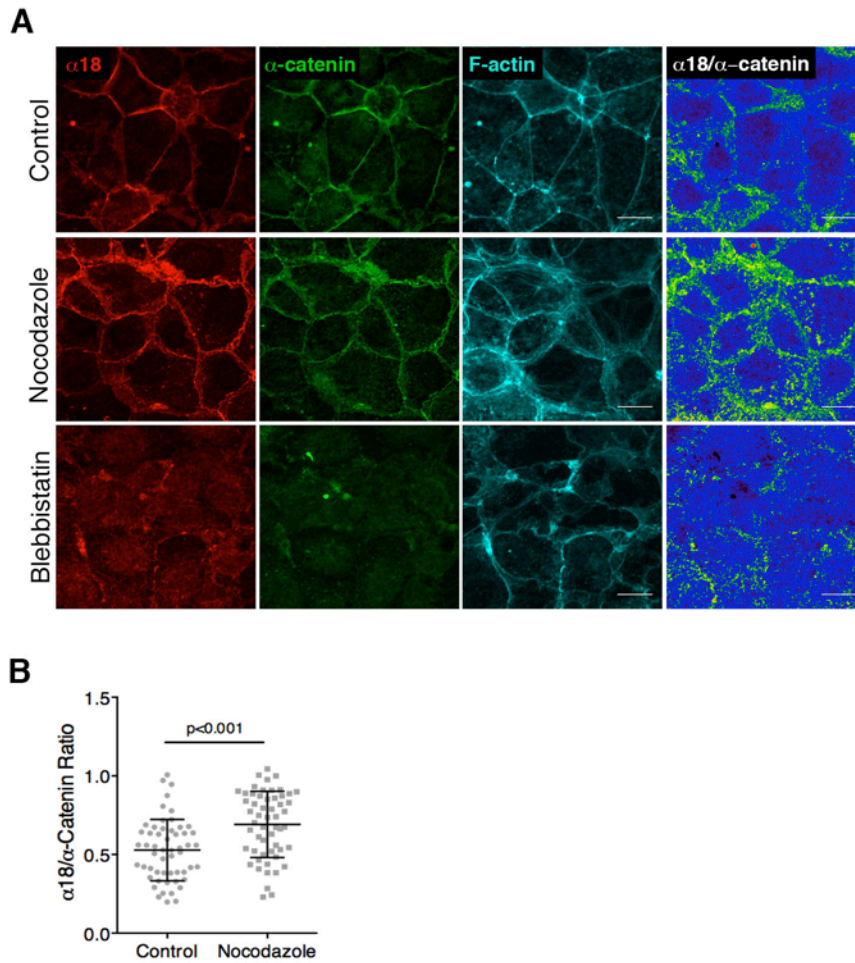
Figure 3.18: Cell-cell junctions in EpH4 are tension-sensitive

(A) EpH4 monolayers, treated with nocodazole or blebbistatin, and labeled to detect α-catenin α18, α-catenin and F-actin. α18/α-catenin ratio (last column on the right) highlights the increase or decrease in force-dependent stretching of α-catenin at cell-cell junctions. Scale bar, 20μm.

(B) Quantification of α18/α-catenin ratio for **(A)**. n>50 junctions per conditions, with Mean±SEM. Quantification could not be performed post-blebbistatin treatment due to disruption of junctions and complete loss of α18 or α-catenin labeling.

Statistical significance tested using Student's t-test in **(B)**.
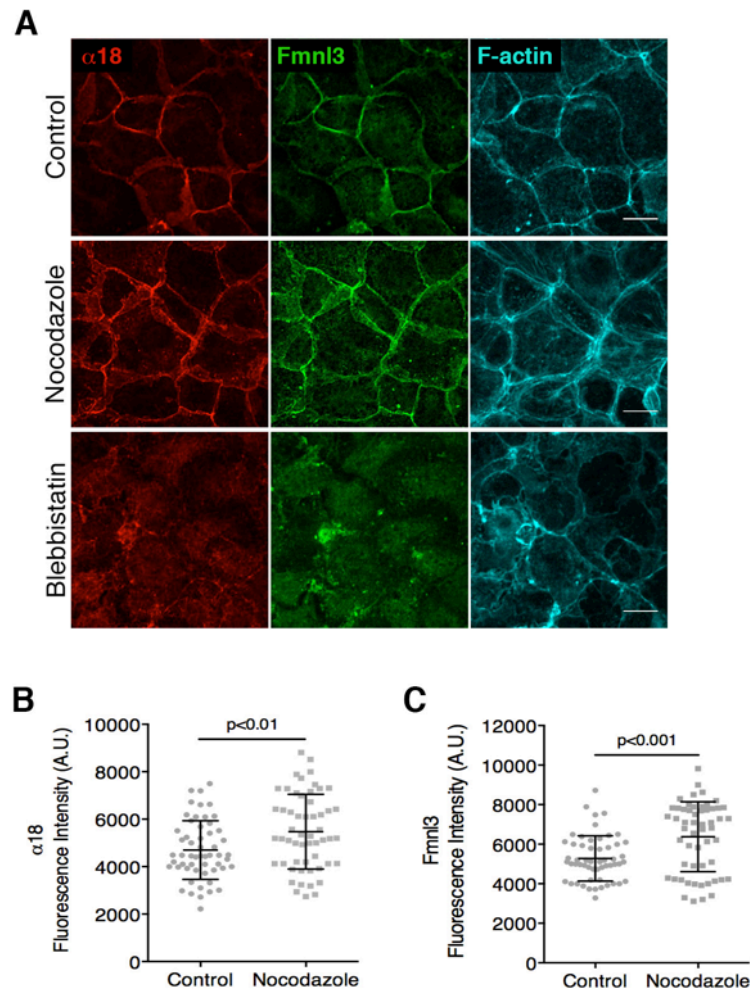
Figure 3.19: Fmnl3 localization at the AJ is tension-sensitive

(A) EpH4 monolayers, treated with nocodazole or blebbistatin, and labeled to detect α-catenin α18, Fmnl3 and F-actin. Note the increased localization of Fmnl3 at the AJ following nocodazole treatment, which is lost upon blebbistatin treatment. Scale bar, 20μm.

(B) & **(C)** Quantification of α18 and Fmnl3 fluorescence intensities, respectively, at the AJ for control and nocodazole-treated conditions illustrated in **(A)**. n>50 junctions per conditions, with Mean±SD.

Statistical significance tested using Student's t-test in **(B)** & **(C)**.

3.3.5 Fmnl3 expression is reduced as cells undergo EMT

Epithelial-Mesenchymal transition (EMT) is a biological process crucial to development that drives a polarized epithelial cell to undergo several genetic and biochemical changes resulting in a mesenchymal phenotype (Kalluri and Weinberg, 2009). These mesenchymal cells are associated with enhanced migratory abilities and invasive properties, often due to a weakening of cell-cell junctions and reorganization of the cytoskeleton, amidst other complex changes that include reprogramming of gene expression and alteration of signaling pathways (Kalluri and Weinberg, 2009; Thiery *et al.*, 2009).

The migration defects and cell detachment phenotype we observed with Fmnl3 KD in an *in vitro* scratch assay were reminiscent of phenotypes observed during EMT. Hence, we asked if there was an association between *Fmnl3* expression levels and EMT. To test this, we used a panel of human ovarian cancer lines that exhibited phenotypes resembling epithelial (PEO-1), mesenchymal (Hey-A8) or intermediate-EMT (SKOV-3 and OVCA429WT) states (All cell lines were previously characterized in (Huang *et al.*, 2013)). Non-transformed ovarian surface epithelial cells (IOSE-523) were used as a control. Using semi-quantitative RT-PCR, we probed *FMNL3* expression levels in all ovarian cell lines. Interestingly, PCR analysis detected the highest expression of *FMNL3* in the non-transformed IOSE-523 cell line, with moderate levels in epithelial ovarian cancer cells **(Figure 3.20A-B)**. Further, we failed to detect any *FMNL3* expression in the cancer cell lines of mesenchymal type **(Figure 3.20A-B)**. Overall, these results suggest that

FMNL3 expression supports the epithelial phenotype in ovarian cells, and is

lost as cells undergo EMT.
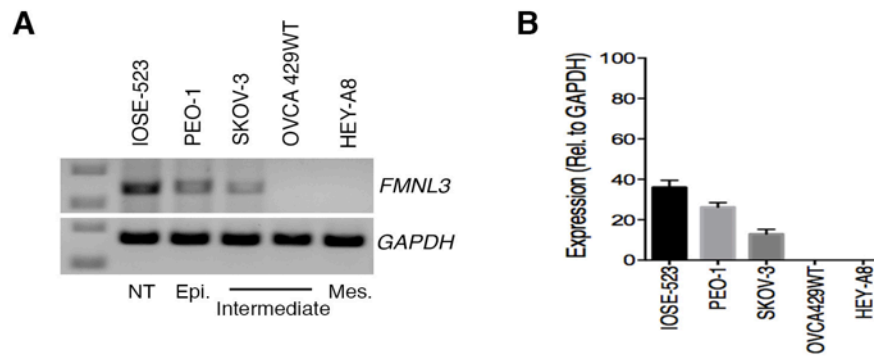
Figure 3.20: Fmnl3 expression is reduced as cells undergo EMT

(A) Detection of FMNL3 expression levels using PCR amplification in human ovarian cancer cell lines as indicated. NT: Non-transformed (control), Epi.: Epithelial, Mes.: Mesenchymal.
(B) Quantification of FMNL3 expression levels corresponding to **(A)**. n=2 independent experiments, with Mean±SEM.

Chapter 4

Discussion

4. DISCUSSION

4.1 Regulation of cell-cell adhesion by mDia1 and Fmnl3-dependent actin polymerization

The Arp2/3 complex has largely been implicated as an important actin nucleator at the AJ; however, in recent times, identifying the cellular functions of various members of the formin family has been the subject of intense research. Here, we provide evidence for formin-dependent actin polymerization in modulating actin turnover at cell-cell contacts, which in turn influences E-cadherin stabilization at the AJ. We identify two formins, mDia1 and Fmnl3, as key players in this process. Although several recent studies have independently characterized mDia1 or Fmnl3 at the AJ (Carramusa *et al.*, 2007; Homem and Peifer, 2008; Phng *et al.*, 2015), we show for the first time a crucial role for these formins in maintaining cell-cell adhesion strength and cohesion in epithelial monolayers to facilitate collective cell migration. In line with this observation, we observe force-dependent recruitment of Fmnl3 at the AJ, and demonstrate that loss of *Fmnl3* expression correlates with EMT. While our results provide various novel findings and extend our understanding of the functions of formins at the AJ, several unanswered questions remain, which are discussed in greater detail hereafter.

4.2 Regulation of formins at the AJ by kinases and RhoGTPases

Our results identify the non-receptor tyrosine kinase Src as a key upstream regulator of formin activity at cell-cell junctions. We demonstrate that Src KD phenocopies formin inhibition with SMIFH2, and Src kinase activity functions upstream of mDia1 and Fmnl3 at the AJ. Indeed, several studies have reported a positive influence of Src kinase signaling on cadherin-based junctions, via a number of downstream effectors. For instance, Src kinase signaling is required for the recruitment of phosphoinositide (PI) 3-kinase to the AJ (Pang *et al.*, 2005). Recruitment of the actin-binding protein, cortactin, is also known to occur downstream of E-cadherin-activated Src signaling at the AJ (Ren *et al.*, 2009). Phosphorylation of cortactin by Src is essential for the former to preserve the integrity of junctional actin cytoskeleton and cadherin-based cell-cell contacts (Ren *et al.*, 2009). Here, we identify formins as additional downstream effectors of Src kinase at the AJ. Furthermore, we show force-dependent recruitment of Fmnl3 to cell-cell junctions. In this regard, our data identifying Src activity upstream of formins is of particular interest since Src has also been shown to respond to mechanical stimulation, at least at cell-matrix adhesions (Wang *et al.*, 2005; Niediek *et al.*, 2012).

Further, several lines of evidence point to regulation of formins and RhoGTPase activation by Src kinase (Bertocchi *et al.*, 2012). For example, Src kinase co-localizes and associates with mDia1 in mid-bodies of dividing cells and endosomes, to facilitate cytokinesis (Tominaga *et al.*, 2000). Src activity facilitates the recruitment and activation of the RhoGTPase Cdc42 at nectin-based cell-cell adhesions via the Cdc42-GEF FRG (Fukuhara *et al.*,

2004). Src kinase activity is also upstream of Cdc42 in the formation of a cortical actin cap in HeLa cells (Kuga *et al.*, 2008), as well as in podosome assembly in HUVEC cells (Tatin *et al.*, 2006). In our results, we find that Cdc42 functions downstream of Src at the AJ, and more specifically is responsible for the activation and localization of Fmnl3 to the AJ. Just as Src kinase is known to be mechano-responsive, Cdc42 is also activated in response to fluid shear stress in endothelial cells (Tzima *et al.*, 2003). While mechano-sensitivity of both Src and Cdc42 has previously been studied with respect to cell-matrix adhesions, the recent availability of biosensors for Src and Cdc42 could aid in direct validation of the mechano-response of these proteins at the AJ (Wang *et al.*, 2005; Seong *et al.*, 2009; Hanna *et al.*, 2014).

In our study we find temporal up-regulation of *Fmnl3* expression during collective migration in EpH4 monolayers and increased localization of Fmnl3 at cell-cell junctions. Interestingly, a similar trend has also been observed for Cdc42 expression levels in *in vivo* studies during rabbit corneal epithelial wound healing **(Figure 4.1A)** (Pothula *et al.*, 2013), where Cdc42 activation is essential for proper migration and wound repair. In gastrointestinal mucosal wound healing models, up-regulation of the actin regulatory protein Annexin-2, in a Rho-dependent manner, is crucial to facilitate migration and wound closure **(Figure 4.1B)** (Babbin *et al.*, 2007). Based on our analysis, we show that increased Fmnl3 expression and localization at the AJ is particularly required to support AJ integrity during collective migration when junctions typically experience greater forces (Tambe *et al.*, 2011). Hence, it is likely that up-regulation of RhoGTPases and other actin regulatory proteins may be

a more widespread theme in collective migration to support actin turnover and

reorganization at cell-cell and/or cell-matrix adhesions.
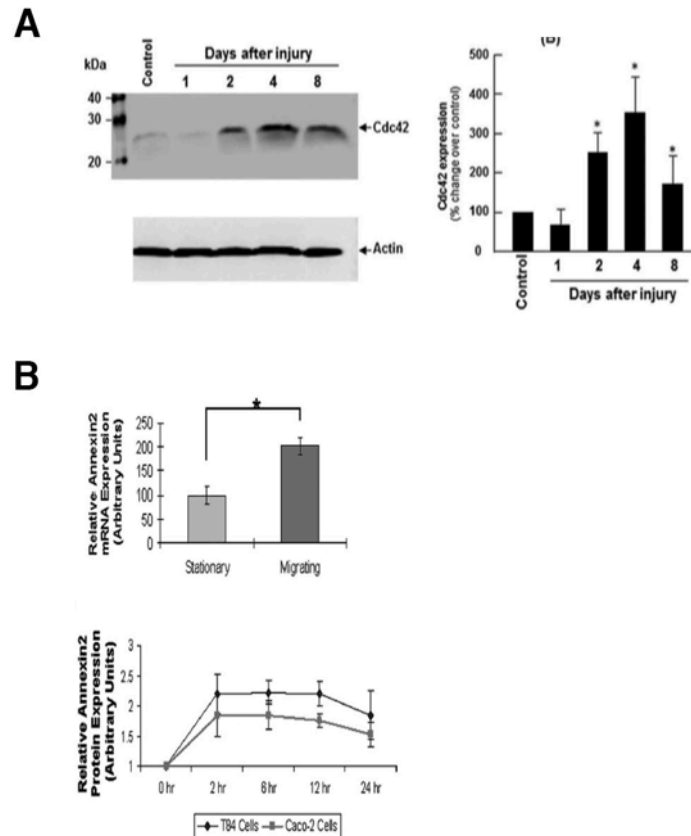
Figure 4.1: Up-regulation of Cdc42 and Annexin-2 expression during collective migration

(A) Change in Cdc42 expression during *in vivo* wound healing in rabbit corneal epithelia[1].

(B) Change in annexin-2 mRNA transcript levels in stationary vs. migrating T84 intestinal epithelial monolayers (top panel)[2]. Increase in annexin-2 protein levels in T84 and Caco2 intestinal epithelial cells associated with collective migration (bottom panel)[2].

[[1]Figure 4.1A reproduced with permission from (Pothula *et al.*, 2013) and Association for Research in Vision and Opthalmology (ARVO). [2]Figure 4.1B reproduced with permission from (Babbin *et al.*, 2007). Refer Appendix 6.2]

4.3 Mechano-sensitivity of formins

Cell-cell adhesions are mechano-sensitive structures, capable of sensing and transducing mechanical stimuli into biochemical responses. Linkage of E-cadherin to the actomyosin cytoskeleton is essential for this purpose, with resident AJ proteins (α-catenin, VASP, Zyxin, Testin) also contributing to the mechano-sensitivity of cell-cell junctions (Yonemura *et al.*, 2010; Leerberg *et al.*, 2014; Oldenburg *et al.*, 2015). For example, increase in junctional contractility leads to the recruitment of vinculin to the AJ, which in turn recruits the actin regulator Mena/VASP to promote actin assembly at cell-cell junctions and respond to contractile tension (Leerberg *et al.*, 2014). Here, we demonstrate tension-dependent recruitment of an actin nucleator, Fmnl3, to cell-cell junctions under strain during collective cell migration. In addition, with the aid of drugs to alter cellular contractility, we show direct recruitment of Fmnl3 to the AJ in a force-dependent manner. Our results add to the growing body of evidence illustrating the mechano-sensitive nature of formins. Single molecule tracking studies revealed stimulation of processive actin polymerization by mDia1 in response to a physical force (either cyclic stretch or needle manipulation) applied on cell surfaces (Higashida *et al.*, 2013). More recently, Inverted formin 2 (INF2) was reported to support the reversible assembly of a perinuclear actin rim following cell stimulation by application of local forces (Shao *et al.*, 2015). Hence, the ability of formins to sense forces and respond by promoting local actin polymerization can likely be extended to a variety of cellular processes and cell types. While the exact mechano-sensitive domain within a formin has not been fully characterized, evidence from (Higashida *et al.*, 2013) implicates the catalytic FH1 and FH2

domains as likely candidates. Further investigation will be required to test if the FH1/FH2 domains or others, in addition to formin-binding proteins (FBPs), enable formins to act as mechanotransducers.

4.4 Co-operation between formins for cellular actin polymerization

In a complex milieu where actin polymerization supports a variety of cellular structures and processes, it is not surprising to find instances when one or more members of the formin family act co-operatively. For example, in fission yeast, assembly of the contractile ring to facilitate cytokinesis is a function of two formins – For3 and Cdc12 (Coffman *et al.*, 2013). Indeed, double mutants for For3 and Cdc12 (truncation mutant) are completely defective in assembly and constriction of the contractile ring (Coffman *et al.*, 2013). Further, interaction between two formins can also result in an inhibition of the activity of one formin by the other. In a yeast two-hybrid screen, Inverted formin 2 (INF2) was found to interact with diaphanous related formins mDia1, mDia2 and mDia3 (Sun *et al.*, 2011). Detailed characterization of this interaction revealed an inhibitory effect of INF2 towards the Rho-dependent actin polymerization and serum response factor (SRF) activation properties of mDia1 (Sun *et al.*, 2011). Therefore, an interaction between formins could also serve as a negative regulatory mechanism for the control of actin polymerization in cells (Sun *et al.*, 2011; Sun *et al.*, 2013).

Due to the ability of formins to bind differentially to a wide variety of partners, there also exist instances when formins function non-redundantly in organizing the actin or microtubule cytoskeletons. Formins mDia1, mDia2 and mDia3 have been shown to interact with different binding partners to regulate in a non-redundant manner the capture of cortical microtubules for directed chemotaxis in breast carcinoma cells (Daou *et al.*, 2014). In the process of myofibrillogenesis in cardiomyocytes, formins mDia2, DAAM1, FMNL1 and FMNL2 localize differentially and function independently to support global assembly of myofibrils (Rosado *et al.*, 2014). Furthermore, FMNL1 and FMNL2 were also specifically involved in repair of myofibrils upon Latrunculin A induced actin depolymerization (Rosado *et al.*, 2014).

In this study, for the first time, we report functions for formins mDia1 and Fmnl3 in supporting F-actin polymerization at the AJ and in turn regulating E-cadherin stability in both quiescent and migrating monolayers. We demonstrate that combined inhibition of both mDia1 and Fmnl3 activities results in drastic failure in the formation of cell-cell junctions (refer **Figure 3.8**), indicating co-operation between these two formins at the AJ. We were successful in localizing Fmnl3 specifically at the AJ; however, difficulty in localizing mDia1 in epithelial cells remains a challenge to overcome. Due to our inability to localize endogenous or exogenously introduced mDia1, we were unable to identify co-localization, if any, between Fmnl3 and mDia1 in EpH4 cells, which might indicate interaction between these two formins.

As Fmnl3 and mDia1 share nearly 50% sequence similarity with each other, it is possible to hypothesize cross-activation of these formins mediated by their DID and DAD domains, akin to the interaction observed between INF2-DID and mDia1-DAD (Sun *et al.*, 2011). Performing co-immunoprecipitation experiments using full-length tagged (for instance, using myc- and flag-tags) Fmnl3 and mDia1 can confirm this possibility. Upon confirmation of an interaction between Fmnl3 and mDia1, further systematic analysis of interaction between specific domains of Fmnl3 and mDia1 can be carried out. In addition, performing co-immunoprecipitation experiments for endogenous Fmnl3 and mDia1 in non-transfected cells would confirm direct interaction between these two formins. Our data and observations suggest that Fmnl3 and mDia1 function co-operatively to polymerize actin at the AJ. Indeed with the knowledge of specific domains in these formins that interacts with each other, we could test for co-operative actin polymerization *in vitro* using the pyrene actin polymerization assay. Due to the inability in simultaneously visualizing both Fmnl3 and mDia1 in live cells, it is unclear if both formins contribute to polymerizing the same or distinct pools of actin at the AJ. Using new genome editing techniques such as the CRISPR/Cas9 system to differentially label these formins at endogenous loci could aid in dissecting their specific contributions to actin polymerization at the AJ.

Interestingly, in a collective cell migration model, we show a striking absence of lamellipodium formation associated with KD of both mDia1 and Fmnl3 (refer **Figure 3.15**). To our knowledge, this is the first evidence to show co-operation between two formins in supporting formation of lamellipodial

protrusions, and warrants further investigation. In a recent study, mDia1 was demonstrated to be an initiator of actin filament polymerization, which served as a template for the Arp2/3 complex to subsequently expand the lamellipodial structure (Isogai *et al.*, 2015). Conversely, in a different study, FMNL2 was found to function in the lamellipodium as an elongation factor of actin filaments that were initially nucleated by the Arp2/3 complex (Block *et al.*, 2012). Hence, it is likely that initiation and branching of actin filaments in a lamellipodium might be regulated by the concerted or sequential actions of more than one type of nucleator, including multiple formin proteins. Generation of cell lines with stable expression of Fmnl3 and mDia1, or labeling of these proteins at their endogenous loci, will be crucial to enable dissection of their roles in lamellipodium formation. Further, epidermal growth factor (EGF) application on single cells can be used to stimulate ruffling and lamellipodium generation to analyze localization and spatiotemporal recruitment of these formins to the cell edge. In addition, super-resolution imaging techniques (such as STORM) could assist in studying the localization of Fmnl3 and mDia1 in conjunction with lamellipodial actin labeling at the nano-scale.

4.5 Cellular tug-of-war between actin nucleators

Actin polymerization by a variety of nucleators is essential to support a multitude of cellular structures and processes including migration, morphogenesis, cytokinesis, and repair; as reviewed in (Welch and Mullins, 2002; Goode and Eck, 2007; Qualmann and Kessels, 2009; Campellone and Welch, 2010). Furthermore, in mammalian cells, several actin structures are

assembled via cooperation between different actin nucleators; for example, in stress fiber assembly (Hotulainen and Lappalainen, 2006; Tojkander *et al.*, 2012) and formation of lamellipodia (Svitkina and Borisy, 1999; Bear *et al.*, 2002; Block *et al.*, 2012).

More recent evidence also suggests the existence in cells of a fine balance between the activities of different nucleators that must compete for a common resource, that is, a limited pool of G-actin. For instance, in the fission yeast *Schizosaccharomyces pombe*, inhibiting the Arp2/3 complex promotes assembly of formin-polymerized actin cables, while formin inhibition results in increased Arp2/3-polymerized actin patches (Burke *et al.*, 2014). Further, the G-actin binding protein profilin is a key regulator of this balance, both in yeast as well as mammalian cells, by favoring formin or Ena/VASP-mediated actin polymerization over the Arp 2/3 complex (Rotty *et al.*, 2015; Suarez *et al.*, 2015). In our system, we find increased cell spreading upon inhibition of formin activity (SMIFH2) or KD of mDia1 or Fmnl3, which is abrogated with simultaneous inhibition of the Arp2/3 complex (CK666) (refer **Figure 3.2**). The sudden availability of a large pool of G-actin is likely responsible for enhanced activity of other actin nucleators, resulting in cell spreading and in turn an indirect effect on cell-cell junctions. Moreover, as demonstrated in a recent study by (Lomakin *et al.*, 2015), perturbation of myosin-II activity that results in the disassembly of cortical actomyosin bundles (such as those found at the AJ) is sufficient to switch cellular behavior from an epithelial to a protrusive migratory phenotype. Taking all these data into account, we reason that the phenotypes we observe at the epithelial AJ are not only a direct

consequence of formin activity at the AJ, but also due to promotion of Arp2/3-dependent spreading in the absence of formins.

As discussed previously, it is worthwhile to remember the important contributions of the Arp2/3 complex in regulating actin dynamics at the AJ (refer **Chapter 1, section 1.3.1**). In this context, it still remains unclear if the Arp2/3 complex and formins cooperate to polymerize the same or potentially distinct pools of actin filaments at the AJ. If these two classes of nucleators function independently at the AJ, how a balance is achieved between their activities given a common pool of G-actin is not understood. Development of reagents and methods to differentially label actin networks polymerized by distinct nucleators could aid in resolving these unanswered questions.
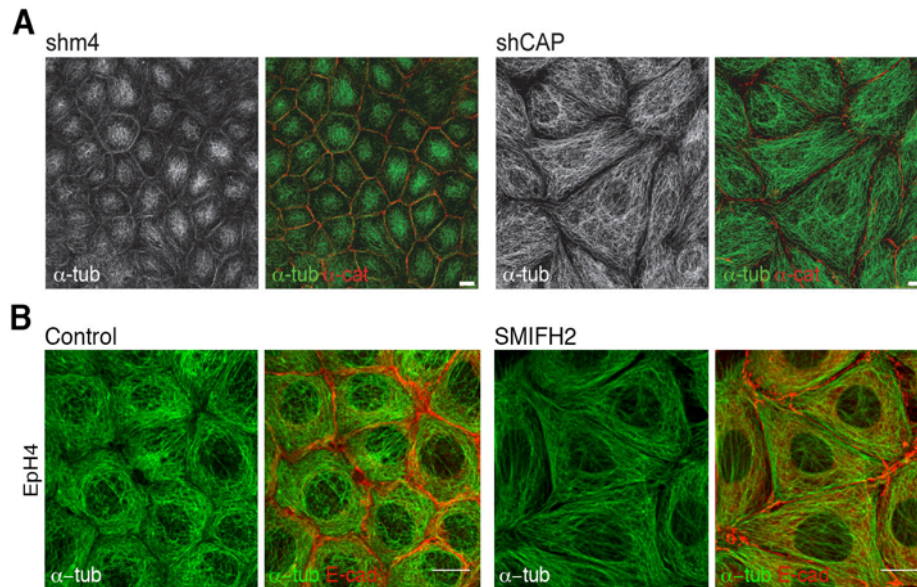
4.6 Maintenance of columnar shape in epithelial monolayers

As described in our results, suppression of formin activity resulted in the transition of a monolayer of columnar epithelial cells to one that was squamous (refer **Figure 3.1**). While we show that this phenomenon is primarily driven by increased activity of actin nucleators such as the Arp2/3 complex, we did not investigate other potential mechanisms for loss of columnar cell shape characteristic of epithelia.

In a recent study by (Gavilan *et al.*, 2015), the microtubule (MT)-binding protein CAP350 was shown to localize at the AJ in MDCK epithelial monolayers via binding to α-catenin, and enable the establishment of apico-basal MTs to support columnar cell architecture. shRNA-mediated KD of

CAP350 resulted in the failure of epithelial polarization, with KD monolayers containing flatter cells compared to control **(**shCAP in **Figure 4.2A)**, highly reminiscent of the phenotypes we observe with SMIFH2-treatment **(Figure 4.2B)**.

Several members of the formin family have been implicated in stabilizing MTs independent of their actin-polymerization functions; as reviewed in (Bartolini and Gundersen, 2010; Chesarone *et al.*, 2010). More specifically, mDia1 has been shown to stabilize and orient microtubules during wound healing (Palazzo *et al.*, 2001), while FMNL3 regulates endothelial MTs and supports angiogenesis in zebrafish (Hetheridge *et al.*, 2012). In our study, we assessed the localization and effects of depletion of mDia1 or Fmnl3 at the AJ with regards to actin polymerization and E-cad stabilization. However, we did not test directly the role for these formins in regulating MT function at the AJ. Further analysis of MT dynamics at the AJ could help understand if the loss of epithelial polarity upon SMIFH2 treatment is also a consequence of perturbed MT localization or stabilization at the AJ.

Figure 4.2: Maintenance of columnar shape in epithelial monolayers

(A) KD of microtubule-binding protein CAP350 results in loss of typical columnar epithelial architecture in MDCK monolayers[1].

(B) Inhibition of formin activity in EpH4 monolayers results in flattening of cells. Further investigation is required to understand the contributions of MTs in this process, if any. Scale bar, 20μm.

[[1]Figure 4.2A reproduced from (Gavilan *et al.*, 2015) published in PLOS Biology under the Creative Commons Attribution (CC BY) license. Terms of this license allowing free access and reuse of material, subject to citation, can be found at: http://journals.plos.org/plosbiology/s/content-license, or in Appendix section 6.2 of this thesis.]

4.7 Formins in EMT and cancer

EMT is a complex biological process associated with several dramatic changes including transcriptional down-regulation of E-cadherin, loss of cell-cell adhesion and reorganization of the actin cytoskeleton (Lamouille *et al.*, 2014). The role of formins in EMT and malignant transformation in cancers is poorly understood. A handful of studies have directly tested whether a role for formins exists in EMT and/or cancer progression. Formin Homology 2 Domain containing 1 (FHOD1) has been implicated in EMT in oral squamous cell cancers, where its up-regulation promotes cell migration and invasion

(Gardberg *et al.*, 2013). Higher expression levels of Formin-like 2 (FMNL2) are positively correlated with EMT and increased tumor cell invasion in models for colorectal carcinoma (Zhu *et al.*, 2008; Li *et al.*, 2010). On the contrary, our results demonstrate a protective role for FMNL3 in supporting epithelial phenotypes and preventing cell dispersion. We find, in a range of ovarian cancer cell lines, that mesenchymal cancer cells are associated with negligible expression of FMNL3.

The study of formin functions in EMT and cancer has remained challenging due to the diverse expression profile of fifteen different formins across several cell types (Krainer *et al.*, 2013). Further, we lack comparative expression data for formins in normal and malignant tissues, as well as specific antibodies and reagents to localize all members of the formin family. More detailed characterization of formin expression profiles in human tumors of various tissue types will enable better dissection of roles for formins in cancer cell migration. In addition, cancer metastases also requires adhesion of tumor cells to the endothelium lining blood vessels, as well as intravasation and extravasation to sites of secondary tumor formation. Interestingly, knockdown of FMNL1 in a human leukemia model resulted in lower ability of cancer cells to undergo trans-endothelial migration (Favaro *et al.*, 2013).

These studies highlight essential roles for formins in several stages of EMT and cancer progression, and undoubtedly require further investigation to potentially identify formin biomarkers associated with various kinds of human cancers.

4.8 Conclusions and future perspectives

Work outlined in this thesis provides novel insights into the functions of formins mDia1 and Fmnl3 at cell-cell junctions under conditions of homeostasis or migration. In particular, we focused on elucidating roles for these formins in regulating adhesion stability and strength in epithelial monolayers. Our findings have important implications in extending our understanding of diseases such as cancers that is associated with altered AJ turnover and cytoskeletal reorganization, and misregulation of formin expression.

Some broader outstanding questions, stated below, still remain in the study of formins and other actin nucleators, and will be essential to address in future studies:

1) What is the architecture of actin structures associated with AJ, and what is the contribution of each nucleator to this organization?

2) Do formins and the Arp2/3 complex act co-operatively or do they each nucleate specialized actin structures at the AJ?

3) How are the activities of multiple classes of actin nucleators integrated at the AJ (including the Arp2/3 complex, Formins and Mena/VASP)?

4) Finally, is there redundancy in the function of formins at cell-cell junctions or do they independently regulate various stages of AJ formation and maturation?

5. REFERENCES

Aberle, H., Butz, S., Stappert, J., Weissig, H., Kemler, R., and Hoschuetzky, H. (1994). Assembly of the cadherin-catenin complex in vitro with recombinant proteins. Journal of cell science *107 (Pt 12)*, 3655-3663.

Abu Taha, A., Taha, M., Seebach, J., and Schnittler, H.J. (2014). ARP2/3-mediated junction-associated lamellipodia control VE-cadherin-based cell junction dynamics and maintain monolayer integrity. Molecular biology of the cell *25*, 245-256.

Adams, C.L., Chen, Y.T., Smith, S.J., and Nelson, W.J. (1998). Mechanisms of epithelial cell-cell adhesion and cell compaction revealed by high-resolution tracking of E-cadherin-green fluorescent protein. The Journal of cell biology *142*, 1105-1119.

Alberts, A.S. (2001). Identification of a carboxyl-terminal diaphanous-related formin homology protein autoregulatory domain. The Journal of biological chemistry *276*, 2824-2830.

Anderson, J.M., and Van Itallie, C.M. (2009). Physiology and function of the tight junction. Cold Spring Harbor perspectives in biology *1*, a002584.

Aspenstrom, P., Richnau, N., and Johansson, A.S. (2006). The diaphanous-related formin DAAM1 collaborates with the Rho GTPases RhoA and Cdc42, CIP4 and Src in regulating cell morphogenesis and actin dynamics. Experimental cell research *312*, 2180-2194.

Babbin, B.A., Parkos, C.A., Mandell, K.J., Winfree, L.M., Laur, O., Ivanov, A.I., and Nusrat, A. (2007). Annexin 2 regulates intestinal epithelial cell spreading and wound closure through Rho-related signaling. The American journal of pathology *170*, 951-966.

Bartolini, F., and Gundersen, G.G. (2010). Formins and microtubules. Biochimica et biophysica acta *1803*, 164-173.

Bazellieres, E., Conte, V., Elosegui-Artola, A., Serra-Picamal, X., Bintanel-Morcillo, M., Roca-Cusachs, P., Munoz, J.J., Sales-Pardo, M., Guimera, R., and Trepat, X. (2015). Control of cell-cell forces and collective cell dynamics by the intercellular adhesome. Nature cell biology *17*, 409-420.

Bear, J.E., Svitkina, T.M., Krause, M., Schafer, D.A., Loureiro, J.J., Strasser, G.A., Maly, I.V., Chaga, O.Y., Cooper, J.A., Borisy, G.G., and Gertler, F.B. (2002). Antagonism between Ena/VASP proteins and actin filament capping regulates fibroblast motility. Cell *109*, 509-521.

Bertocchi, C., Vaman Rao, M., and Zaidel-Bar, R. (2012). Regulation of adherens junction dynamics by phosphorylation switches. Journal of signal transduction *2012*, 125295.

Block, J., Breitsprecher, D., Kuhn, S., Winterhoff, M., Kage, F., Geffers, R., Duwe, P., Rohn, J.L., Baum, B., Brakebusch, C., Geyer, M., Stradal, T.E., Faix, J., and Rottner, K. (2012). FMNL2 drives actin-based protrusion and migration downstream of Cdc42. Current biology : CB *22*, 1005-1012.

Buckley, C.D., Tan, J., Anderson, K.L., Hanein, D., Volkmann, N., Weis, W.I., Nelson, W.J., and Dunn, A.R. (2014). Cell adhesion. The minimal cadherin-catenin complex binds to actin filaments under force. Science *346*, 1254211.

Burke, T.A., Christensen, J.R., Barone, E., Suarez, C., Sirotkin, V., and Kovar, D.R. (2014). Homeostatic actin cytoskeleton networks are regulated by assembly factor competition for monomers. Current biology : CB *24*, 579-585.

Campellone, K.G., and Welch, M.D. (2010). A nucleator arms race: cellular control of actin assembly. Nature reviews. Molecular cell biology *11*, 237-251.

Carramusa, L., Ballestrem, C., Zilberman, Y., and Bershadsky, A.D. (2007). Mammalian diaphanous-related formin Dia1 controls the organization of E-cadherin-mediated cell-cell junctions. Journal of cell science *120*, 3870-3882.

Chang, Y.C., Nalbant, P., Birkenfeld, J., Chang, Z.F., and Bokoch, G.M. (2008). GEF-H1 couples nocodazole-induced microtubule disassembly to cell contractility via RhoA. Molecular biology of the cell *19*, 2147-2153.

Chesarone, M.A., DuPage, A.G., and Goode, B.L. (2010). Unleashing formins to remodel the actin and microtubule cytoskeletons. Nature reviews. Molecular cell biology *11*, 62-74.

Chhabra, E.S., and Higgs, H.N. (2006). INF2 Is a WASP homology 2 motif-containing formin that severs actin filaments and accelerates both polymerization and depolymerization. The Journal of biological chemistry *281*, 26754-26767.

Coffman, V.C., Sees, J.A., Kovar, D.R., and Wu, J.Q. (2013). The formins Cdc12 and For3 cooperate during contractile ring assembly in cytokinesis. The Journal of cell biology *203*, 101-114.

Copeland, J.W., Copeland, S.J., and Treisman, R. (2004). Homo-oligomerization is essential for F-actin assembly by the formin family FH2 domain. The Journal of biological chemistry *279*, 50250-50256.

Daou, P., Hasan, S., Breitsprecher, D., Baudelet, E., Camoin, L., Audebert, S., Goode, B.L., and Badache, A. (2014). Essential and nonredundant roles for Diaphanous formins in cortical microtubule capture and directed cell migration. Molecular biology of the cell *25*, 658-668.

Desai, B.V., Harmon, R.M., and Green, K.J. (2009). Desmosomes at a glance. Journal of cell science *122*, 4401-4407.

Desai, R., Sarpal, R., Ishiyama, N., Pellikka, M., Ikura, M., and Tepass, U. (2013). Monomeric alpha-catenin links cadherin to the actin cytoskeleton. Nature cell biology *15*, 261-273.

Doxzen, K., Vedula, S.R., Leong, M.C., Hirata, H., Gov, N.S., Kabla, A.J., Ladoux, B., and Lim, C.T. (2013). Guidance of collective cell migration by substrate geometry. Integrative biology : quantitative biosciences from nano to macro *5*, 1026-1035.

Drees, F., Pokutta, S., Yamada, S., Nelson, W.J., and Weis, W.I. (2005). Alpha-catenin is a molecular switch that binds E-cadherin-beta-catenin and regulates actin-filament assembly. Cell *123*, 903-915.

Erami, Z., Timpson, P., Yao, W., Zaidel-Bar, R., and Anderson, K.I. (2015). There are four dynamically and functionally distinct populations of E-cadherin in cell junctions. Biology open *4*, 1481-1489.

Esue, O., Harris, E.S., Higgs, H.N., and Wirtz, D. (2008). The filamentous actin cross-linking/bundling activity of mammalian formins. Journal of molecular biology *384*, 324-334.

Evans, W.H., and Martin, P.E. (2002). Gap junctions: structure and function (Review). Molecular membrane biology *19*, 121-136.

Favaro, P., Traina, F., Machado-Neto, J.A., Lazarini, M., Lopes, M.R., Pereira, J.K., Costa, F.F., Infante, E., Ridley, A.J., and Saad, S.T. (2013). FMNL1 promotes proliferation and migration of leukemia cells. Journal of leukocyte biology *94*, 503-512.

Fierro-Gonzalez, J.C., White, M.D., Silva, J.C., and Plachta, N. (2013). Cadherin-dependent filopodia control preimplantation embryo compaction. Nature cell biology *15*, 1424-1433.

Firat-Karalar, E.N., and Welch, M.D. (2011). New mechanisms and functions of actin nucleation. Current opinion in cell biology *23*, 4-13.

Friedl, P., and Gilmour, D. (2009). Collective cell migration in morphogenesis, regeneration and cancer. Nature reviews. Molecular cell biology *10*, 445-457.

Fukuhara, T., Shimizu, K., Kawakatsu, T., Fukuyama, T., Minami, Y., Honda, T., Hoshino, T., Yamada, T., Ogita, H., Okada, M., and Takai, Y. (2004). Activation of Cdc42 by trans interactions of the cell adhesion molecules nectins through c-Src and Cdc42-GEF FRG. The Journal of cell biology *166*, 393-405.

Gardberg, M., Kaipio, K., Lehtinen, L., Mikkonen, P., Heuser, V.D., Talvinen, K., Iljin, K., Kampf, C., Uhlen, M., Grenman, R., Koivisto, M., and Carpen, O. (2013). FHOD1, a formin upregulated in epithelial-mesenchymal transition, participates in cancer cell migration and invasion. PloS one *8*, e74923.

Gauvin, T.J., Young, L.E., and Higgs, H.N. (2015). The formin FMNL3 assembles plasma membrane protrusions that participate in cell-cell adhesion. Molecular biology of the cell *26*, 467-477.

Gavilan, M.P., Arjona, M., Zurbano, A., Formstecher, E., Martinez-Morales, J.R., Bornens, M., and Rios, R.M. (2015). Alpha-catenin-dependent recruitment of the centrosomal protein CAP350 to adherens junctions allows epithelial cells to acquire a columnar shape. PLoS biology *13*, e1002087.

Goley, E.D., and Welch, M.D. (2006). The ARP2/3 complex: an actin nucleator comes of age. Nature reviews. Molecular cell biology *7*, 713-726.

Goode, B.L., and Eck, M.J. (2007). Mechanism and function of formins in the control of actin assembly. Annual review of biochemistry *76*, 593-627.

Green, K.J., Getsios, S., Troyanovsky, S., and Godsel, L.M. (2010). Intercellular junction assembly, dynamics, and homeostasis. Cold Spring Harbor perspectives in biology *2*, a000125.

Grikscheit, K., Frank, T., Wang, Y., and Grosse, R. (2015). Junctional actin assembly is mediated by Formin-like 2 downstream of Rac1. The Journal of cell biology *209*, 367-376.

Guo, Z., Neilson, L.J., Zhong, H., Murray, P.S., Zanivan, S., and Zaidel-Bar, R. (2014). E-cadherin interactome complexity and robustness resolved by quantitative proteomics. Science signaling *7*, rs7.

Han, S.P., Gambin, Y., Gomez, G.A., Verma, S., Giles, N., Michael, M., Wu, S.K., Guo, Z., Johnston, W., Sierecki, E., Parton, R.G., Alexandrov, K., and Yap, A.S. (2014). Cortactin scaffolds Arp2/3 and WAVE2 at the epithelial zonula adherens. The Journal of biological chemistry *289*, 7764-7775.

Hanna, S., Miskolci, V., Cox, D., and Hodgson, L. (2014). A new genetically encoded single-chain biosensor for Cdc42 based on FRET, useful for live-cell imaging. PloS one *9*, e96469.

Harris, E.S., Li, F., and Higgs, H.N. (2004). The mouse formin, FRLalpha, slows actin filament barbed end elongation, competes with capping protein, accelerates polymerization from monomers, and severs filaments. The Journal of biological chemistry *279*, 20076-20087.

Harris, T.J., and Tepass, U. (2010). Adherens junctions: from molecules to morphogenesis. Nature reviews. Molecular cell biology *11*, 502-514.

Harrison, O.J., Jin, X., Hong, S., Bahna, F., Ahlsen, G., Brasch, J., Wu, Y., Vendome, J., Felsovalyi, K., Hampton, C.M., Troyanovsky, R.B., Ben-Shaul, A., Frank, J., Troyanovsky, S.M., Shapiro, L., and Honig, B. (2011). The extracellular architecture of adherens junctions revealed by crystal structures of type I cadherins. Structure *19*, 244-256.

Hetheridge, C., Scott, A.N., Swain, R.K., Copeland, J.W., Higgs, H.N., Bicknell, R., and Mellor, H. (2012). The formin FMNL3 is a cytoskeletal regulator of angiogenesis. Journal of cell science *125*, 1420-1428.

Higashida, C., Kiuchi, T., Akiba, Y., Mizuno, H., Maruoka, M., Narumiya, S., Mizuno, K., and Watanabe, N. (2013). F- and G-actin homeostasis regulates mechanosensitive actin nucleation by formins. Nature cell biology *15*, 395-405.

Homem, C.C., and Peifer, M. (2008). Diaphanous regulates myosin and adherens junctions to control cell contractility and protrusive behavior during morphogenesis. Development *135*, 1005-1018.

Hong, S., Troyanovsky, R.B., and Troyanovsky, S.M. (2013). Binding to F-actin guides cadherin cluster assembly, stability, and movement. The Journal of cell biology *201*, 131-143.

Hotulainen, P., and Lappalainen, P. (2006). Stress fibers are generated by two distinct actin assembly mechanisms in motile cells. The Journal of cell biology *173*, 383-394.

Huang, R.Y., Wong, M.K., Tan, T.Z., Kuay, K.T., Ng, A.H., Chung, V.Y., Chu, Y.S., Matsumura, N., Lai, H.C., Lee, Y.F., Sim, W.J., Chai, C., Pietschmann, E., Mori, S., Low, J.J., Choolani, M., and Thiery, J.P. (2013). An EMT spectrum defines an anoikis-resistant and spheroidogenic intermediate mesenchymal state that is sensitive to e-cadherin restoration by a src-kinase inhibitor, saracatinib (AZD0530). Cell death & disease *4*, e915.

Ilina, O., and Friedl, P. (2009). Mechanisms of collective cell migration at a glance. Journal of cell science *122*, 3203-3208.

Isogai, T., van der Kammen, R., Leyton-Puig, D., Kedziora, K.M., Jalink, K., and Innocenti, M. (2015). Initiation of lamellipodia and ruffles involves

cooperation between mDia1 and the Arp2/3 complex. Journal of cell science *128*, 3796-3810.

Kalluri, R., and Weinberg, R.A. (2009). The basics of epithelial-mesenchymal transition. The Journal of clinical investigation *119*, 1420-1428.

Koka, S., Minick, G.T., Zhou, Y., Westendorf, J.J., and Boehm, M.B. (2005). Src regulates the activity of the mammalian formin protein FHOD1. Biochemical and biophysical research communications *336*, 1285-1291.

Kovacs, E.M., Goodwin, M., Ali, R.G., Paterson, A.D., and Yap, A.S. (2002). Cadherin-directed actin assembly: E-cadherin physically associates with the Arp2/3 complex to direct actin assembly in nascent adhesive contacts. Current biology : CB *12*, 379-382.

Kovacs, E.M., Verma, S., Ali, R.G., Ratheesh, A., Hamilton, N.A., Akhmanova, A., and Yap, A.S. (2011). N-WASP regulates the epithelial junctional actin cytoskeleton through a non-canonical post-nucleation pathway. Nature cell biology *13*, 934-943.

Kovacs, M., Toth, J., Hetenyi, C., Malnasi-Csizmadia, A., and Sellers, J.R. (2004). Mechanism of blebbistatin inhibition of myosin II. The Journal of biological chemistry *279*, 35557-35563.

Krainer, E.C., Ouderkirk, J.L., Miller, E.W., Miller, M.R., Mersich, A.T., and Blystone, S.D. (2013). The multiplicity of human formins: Expression patterns in cells and tissues. Cytoskeleton *70*, 424-438.

Kuga, T., Hoshino, M., Nakayama, Y., Kasahara, K., Ikeda, K., Obata, Y., Takahashi, A., Higashiyama, Y., Fukumoto, Y., and Yamaguchi, N. (2008). Role of Src-family kinases in formation of the cortical actin cap at the dorsal cell surface. Experimental cell research *314*, 2040-2054.

Kuhn, S., and Geyer, M. (2014). Formins as effector proteins of Rho GTPases. Small GTPases *5*, e29513.

Lamouille, S., Xu, J., and Derynck, R. (2014). Molecular mechanisms of epithelial-mesenchymal transition. Nature reviews. Molecular cell biology *15*, 178-196.

le Duc, Q., Shi, Q., Blonk, I., Sonnenberg, A., Wang, N., Leckband, D., and de Rooij, J. (2010). Vinculin potentiates E-cadherin mechanosensing and is recruited to actin-anchored sites within adherens junctions in a myosin II-dependent manner. The Journal of cell biology *189*, 1107-1115.

Leerberg, J.M., Gomez, G.A., Verma, S., Moussa, E.J., Wu, S.K., Priya, R., Hoffman, B.D., Grashoff, C., Schwartz, M.A., and Yap, A.S. (2014). Tension-sensitive actin assembly supports contractility at the epithelial zonula adherens. Current biology : CB *24*, 1689-1699.

Levayer, R., Pelissier-Monier, A., and Lecuit, T. (2011). Spatial regulation of Dia and Myosin-II by RhoGEF2 controls initiation of E-cadherin endocytosis during epithelial morphogenesis. Nature cell biology *13*, 529-540.

Li, Y., Zhu, X., Zeng, Y., Wang, J., Zhang, X., Ding, Y.Q., and Liang, L. (2010). FMNL2 enhances invasion of colorectal carcinoma by inducing epithelial-mesenchymal transition. Molecular cancer research : MCR *8*, 1579-1590.

Lomakin, A.J., Lee, K.C., Han, S.J., Bui, D.A., Davidson, M., Mogilner, A., and Danuser, G. (2015). Competition for actin between two distinct F-actin

networks defines a bistable switch for cell polarization. Nature cell biology *17*, 1435-1445.

McLachlan, R.W., and Yap, A.S. (2007). Not so simple: the complexity of phosphotyrosine signaling at cadherin adhesive contacts. Journal of molecular medicine *85*, 545-554.

Mege, R.M., Gavard, J., and Lambert, M. (2006). Regulation of cell-cell junctions by the cytoskeleton. Current opinion in cell biology *18*, 541-548.

Miyake, Y., Inoue, N., Nishimura, K., Kinoshita, N., Hosoya, H., and Yonemura, S. (2006). Actomyosin tension is required for correct recruitment of adherens junction components and zonula occludens formation. Experimental cell research *312*, 1637-1650.

Moseley, J.B., Sagot, I., Manning, A.L., Xu, Y., Eck, M.J., Pellman, D., and Goode, B.L. (2004). A conserved mechanism for Bni1- and mDia1-induced actin assembly and dual regulation of Bni1 by Bud6 and profilin. Molecular biology of the cell *15*, 896-907.

Niediek, V., Born, S., Hampe, N., Kirchgessner, N., Merkel, R., and Hoffmann, B. (2012). Cyclic stretch induces reorientation of cells in a Src family kinase- and p130Cas-dependent manner. European journal of cell biology *91*, 118-128.

Oldenburg, J., van der Krogt, G., Twiss, F., Bongaarts, A., Habani, Y., Slotman, J.A., Houtsmuller, A., Huveneers, S., and de Rooij, J. (2015). VASP, zyxin and TES are tension-dependent members of Focal Adherens Junctions independent of the alpha-catenin-vinculin module. Scientific reports *5*, 17225.

Otani, T., Ichii, T., Aono, S., and Takeichi, M. (2006). Cdc42 GEF Tuba regulates the junctional configuration of simple epithelial cells. The Journal of cell biology *175*, 135-146.

Padmanabhan, A., Rao, M.V., Wu, Y., and Zaidel-Bar, R. (2015). Jack of all trades: functional modularity in the adherens junction. Current opinion in cell biology *36*, 32-40.

Palazzo, A.F., Cook, T.A., Alberts, A.S., and Gundersen, G.G. (2001). mDia mediates Rho-regulated formation and orientation of stable microtubules. Nature cell biology *3*, 723-729.

Pang, J.H., Kraemer, A., Stehbens, S.J., Frame, M.C., and Yap, A.S. (2005). Recruitment of phosphoinositide 3-kinase defines a positive contribution of tyrosine kinase signaling to E-cadherin function. The Journal of biological chemistry *280*, 3043-3050.

Paul, A.S., and Pollard, T.D. (2008). The role of the FH1 domain and profilin in formin-mediated actin-filament elongation and nucleation. Current biology : CB *18*, 9-19.

Phng, L.K., Gebala, V., Bentley, K., Philippides, A., Wacker, A., Mathivet, T., Sauteur, L., Stanchi, F., Belting, H.G., Affolter, M., and Gerhardt, H. (2015). Formin-mediated actin polymerization at endothelial junctions is required for vessel lumen formation and stabilization. Developmental cell *32*, 123-132.

Plutoni, C., Bazellieres, E., Le Borgne-Rochet, M., Comunale, F., Brugues, A., Seveno, M., Planchon, D., Thuault, S., Morin, N., Bodin, S., Trepat, X., and

Gauthier-Rouviere, C. (2016). P-cadherin promotes collective cell migration via a Cdc42-mediated increase in mechanical forces. The Journal of cell biology *212*, 199-217.

Pothula, S., Bazan, H.E., and Chandrasekher, G. (2013). Regulation of Cdc42 expression and signaling is critical for promoting corneal epithelial wound healing. Investigative ophthalmology & visual science *54*, 5343-5352.

Poujade, M., Grasland-Mongrain, E., Hertzog, A., Jouanneau, J., Chavrier, P., Ladoux, B., Buguin, A., and Silberzan, P. (2007). Collective migration of an epithelial monolayer in response to a model wound. Proceedings of the National Academy of Sciences of the United States of America *104*, 15988-15993.

Pring, M., Evangelista, M., Boone, C., Yang, C., and Zigmond, S.H. (2003). Mechanism of formin-induced nucleation of actin filaments. Biochemistry *42*, 486-496.

Pruyne, D., Evangelista, M., Yang, C., Bi, E., Zigmond, S., Bretscher, A., and Boone, C. (2002). Role of formins in actin assembly: nucleation and barbed-end association. Science *297*, 612-615.

Qualmann, B., and Kessels, M.M. (2009). New players in actin polymerization--WH2-domain-containing actin nucleators. Trends in cell biology *19*, 276-285.

Quinlan, M.E., Heuser, J.E., Kerkhoff, E., and Mullins, R.D. (2005). Drosophila Spire is an actin nucleation factor. Nature *433*, 382-388.

Raich, W.B., Agbunag, C., and Hardin, J. (1999). Rapid epithelial-sheet sealing in the Caenorhabditis elegans embryo requires cadherin-dependent filopodial priming. Current biology : CB *9*, 1139-1146.

Rajput, C., Kini, V., Smith, M., Yazbeck, P., Chavez, A., Schmidt, T., Zhang, W., Knezevic, N., Komarova, Y., and Mehta, D. (2013). Neural Wiskott-Aldrich syndrome protein (N-WASP)-mediated p120-catenin interaction with Arp2-Actin complex stabilizes endothelial adherens junctions. The Journal of biological chemistry *288*, 4241-4250.

Rao, M.V., Chu, P.H., Hahn, K.M., and Zaidel-Bar, R. (2013). An optogenetic tool for the activation of endogenous diaphanous-related formins induces thickening of stress fibers without an increase in contractility. Cytoskeleton *70*, 394-407.

Ren, G., Helwani, F.M., Verma, S., McLachlan, R.W., Weed, S.A., and Yap, A.S. (2009). Cortactin is a functional target of E-cadherin-activated Src family kinases in MCF7 epithelial monolayers. The Journal of biological chemistry *284*, 18913-18922.

Rizvi, S.A., Neidt, E.M., Cui, J., Feiger, Z., Skau, C.T., Gardel, M.L., Kozmin, S.A., and Kovar, D.R. (2009). Identification and characterization of a small molecule inhibitor of formin-mediated actin assembly. Chemistry & biology *16*, 1158-1168.

Romero, S., Le Clainche, C., Didry, D., Egile, C., Pantaloni, D., and Carlier, M.F. (2004). Formin is a processive motor that requires profilin to accelerate actin assembly and associated ATP hydrolysis. Cell *119*, 419-429.

Rosado, M., Barber, C.F., Berciu, C., Feldman, S., Birren, S.J., Nicastro, D., and Goode, B.L. (2014). Critical roles for multiple formins during cardiac myofibril development and repair. Molecular biology of the cell *25*, 811-827.

Rotty, J.D., Wu, C., Haynes, E.M., Suarez, C., Winkelman, J.D., Johnson, H.E., Haugh, J.M., Kovar, D.R., and Bear, J.E. (2015). Profilin-1 serves as a gatekeeper for actin assembly by Arp2/3-dependent and -independent pathways. Developmental cell *32*, 54-67.

Ryu, J.R., Echarri, A., Li, R., and Pendergast, A.M. (2009). Regulation of cell-cell adhesion by Abi/Diaphanous complexes. Molecular and cellular biology *29*, 1735-1748.

Sagot, I., Rodal, A.A., Moseley, J., Goode, B.L., and Pellman, D. (2002). An actin nucleation mechanism mediated by Bni1 and profilin. Nature cell biology *4*, 626-631.

Scarpa, E., and Mayor, R. (2016). Collective cell migration in development. The Journal of cell biology *212*, 143-155.

Schonichen, A., Mannherz, H.G., Behrmann, E., Mazur, A.J., Kuhn, S., Silvan, U., Schoenenberger, C.A., Fackler, O.T., Raunser, S., Dehmelt, L., and Geyer, M. (2013). FHOD1 is a combined actin filament capping and bundling factor that selectively associates with actin arcs and stress fibers. Journal of cell science *126*, 1891-1901.

Scott, J.A., Shewan, A.M., den Elzen, N.R., Loureiro, J.J., Gertler, F.B., and Yap, A.S. (2006). Ena/VASP proteins can regulate distinct modes of actin organization at cadherin-adhesive contacts. Molecular biology of the cell *17*, 1085-1095.

Seong, J., Lu, S., Ouyang, M., Huang, H., Zhang, J., Frame, M.C., and Wang, Y. (2009). Visualization of Src activity at different compartments of the plasma membrane by FRET imaging. Chemistry & biology *16*, 48-57.

Shao, X., Li, Q., Mogilner, A., Bershadsky, A.D., and Shivashankar, G.V. (2015). Mechanical stimulation induces formin-dependent assembly of a perinuclear actin rim. Proceedings of the National Academy of Sciences of the United States of America *112*, E2595-2601.

Shaw, T.J., and Martin, P. (2009). Wound repair at a glance. Journal of cell science *122*, 3209-3213.

Sprague, B.L., and McNally, J.G. (2005). FRAP analysis of binding: proper and fitting. Trends in cell biology *15*, 84-91.

Suarez, C., Carroll, R.T., Burke, T.A., Christensen, J.R., Bestul, A.J., Sees, J.A., James, M.L., Sirotkin, V., and Kovar, D.R. (2015). Profilin regulates F-actin network homeostasis by favoring formin over Arp2/3 complex. Developmental cell *32*, 43-53.

Sun, H., Schlondorff, J., Higgs, H.N., and Pollak, M.R. (2013). Inverted formin 2 regulates actin dynamics by antagonizing Rho/diaphanous-related formin signaling. Journal of the American Society of Nephrology : JASN *24*, 917-929.

Sun, H., Schlondorff, J.S., Brown, E.J., Higgs, H.N., and Pollak, M.R. (2011). Rho activation of mDia formins is modulated by an interaction with inverted formin 2 (INF2). Proceedings of the National Academy of Sciences of the United States of America *108*, 2933-2938.

Svitkina, T.M., and Borisy, G.G. (1999). Arp2/3 complex and actin depolymerizing factor/cofilin in dendritic organization and treadmilling of actin filament array in lamellipodia. The Journal of cell biology *145*, 1009-1026.

Taguchi, K., Ishiuchi, T., and Takeichi, M. (2011). Mechanosensitive EPLIN-dependent remodeling of adherens junctions regulates epithelial reshaping. The Journal of cell biology *194*, 643-656.

Takeichi, M. (2014). Dynamic contacts: rearranging adherens junctions to drive epithelial remodelling. Nature reviews. Molecular cell biology *15*, 397-410.

Takeya, R., Taniguchi, K., Narumiya, S., and Sumimoto, H. (2008). The mammalian formin FHOD1 is activated through phosphorylation by ROCK and mediates thrombin-induced stress fibre formation in endothelial cells. The EMBO journal *27*, 618-628.

Tambe, D.T., Hardin, C.C., Angelini, T.E., Rajendran, K., Park, C.Y., Serra-Picamal, X., Zhou, E.H., Zaman, M.H., Butler, J.P., Weitz, D.A., Fredberg, J.J., and Trepat, X. (2011). Collective cell guidance by cooperative intercellular forces. Nature materials *10*, 469-475.

Tardy, Y., McGrath, J.L., Hartwig, J.H., and Dewey, C.F. (1995). Interpreting photoactivated fluorescence microscopy measurements of steady-state actin dynamics. Biophysical journal *69*, 1674-1682.

Tatin, F., Varon, C., Genot, E., and Moreau, V. (2006). A signalling cascade involving PKC, Src and Cdc42 regulates podosome assembly in cultured endothelial cells in response to phorbol ester. Journal of cell science *119*, 769-781.

Thiery, J.P., Acloque, H., Huang, R.Y., and Nieto, M.A. (2009). Epithelial-mesenchymal transitions in development and disease. Cell *139*, 871-890.

Thumkeo, D., Shinohara, R., Watanabe, K., Takebayashi, H., Toyoda, Y., Tohyama, K., Ishizaki, T., Furuyashiki, T., and Narumiya, S. (2011). Deficiency of mDia, an actin nucleator, disrupts integrity of neuroepithelium and causes periventricular dysplasia. PloS one *6*, e25465.

Tojkander, S., Gateva, G., and Lappalainen, P. (2012). Actin stress fibers--assembly, dynamics and biological roles. Journal of cell science *125*, 1855-1864.

Tominaga, T., Sahai, E., Chardin, P., McCormick, F., Courtneidge, S.A., and Alberts, A.S. (2000). Diaphanous-related formins bridge Rho GTPase and Src tyrosine kinase signaling. Molecular cell *5*, 13-25.

Tzima, E., Kiosses, W.B., del Pozo, M.A., and Schwartz, M.A. (2003). Localized cdc42 activation, detected using a novel assay, mediates microtubule organizing center positioning in endothelial cells in response to fluid shear stress. The Journal of biological chemistry *278*, 31020-31023.

van Roy, F., and Berx, G. (2008). The cell-cell adhesion molecule E-cadherin. Cellular and molecular life sciences : CMLS *65*, 3756-3788.

Vasioukhin, V., Bauer, C., Yin, M., and Fuchs, E. (2000). Directed actin polymerization is the driving force for epithelial cell-cell adhesion. Cell *100*, 209-219.

Vavylonis, D., Kovar, D.R., O'Shaughnessy, B., and Pollard, T.D. (2006). Model of formin-associated actin filament elongation. Molecular cell *21*, 455-466.

Verma, S., Han, S.P., Michael, M., Gomez, G.A., Yang, Z., Teasdale, R.D., Ratheesh, A., Kovacs, E.M., Ali, R.G., and Yap, A.S. (2012). A WAVE2-Arp2/3 actin nucleator apparatus supports junctional tension at the epithelial zonula adherens. Molecular biology of the cell *23*, 4601-4610.

Verma, S., Shewan, A.M., Scott, J.A., Helwani, F.M., den Elzen, N.R., Miki, H., Takenawa, T., and Yap, A.S. (2004). Arp2/3 activity is necessary for efficient formation of E-cadherin adhesive contacts. The Journal of biological chemistry *279*, 34062-34070.

Wakayama, Y., Fukuhara, S., Ando, K., Matsuda, M., and Mochizuki, N. (2015). Cdc42 mediates Bmp-induced sprouting angiogenesis through Fmnl3-driven assembly of endothelial filopodia in zebrafish. Developmental cell *32*, 109-122.

Wang, Y., Botvinick, E.L., Zhao, Y., Berns, M.W., Usami, S., Tsien, R.Y., and Chien, S. (2005). Visualizing the mechanical activation of Src. Nature *434*, 1040-1045.

Watanabe, T., Sato, K., and Kaibuchi, K. (2009). Cadherin-mediated intercellular adhesion and signaling cascades involving small GTPases. Cold Spring Harbor perspectives in biology *1*, a003020.

Welch, M.D., and Mullins, R.D. (2002). Cellular control of actin nucleation. Annual review of cell and developmental biology *18*, 247-288.

Wu, Y., Kanchanawong, P., and Zaidel-Bar, R. (2015). Actin-delimited adhesion-independent clustering of E-cadherin forms the nanoscale building blocks of adherens junctions. Developmental cell *32*, 139-154.

Yamada, S., and Nelson, W.J. (2007). Localized zones of Rho and Rac activities drive initiation and expansion of epithelial cell-cell adhesion. The Journal of cell biology *178*, 517-527.

Yamada, S., Pokutta, S., Drees, F., Weis, W.I., and Nelson, W.J. (2005). Deconstructing the cadherin-catenin-actin complex. Cell *123*, 889-901.

Yap, A.S., Niessen, C.M., and Gumbiner, B.M. (1998). The juxtamembrane region of the cadherin cytoplasmic tail supports lateral clustering, adhesive strengthening, and interaction with p120ctn. The Journal of cell biology *141*, 779-789.

Yonemura, S. (2011). Cadherin-actin interactions at adherens junctions. Current opinion in cell biology *23*, 515-522.

Yonemura, S., Wada, Y., Watanabe, T., Nagafuchi, A., and Shibata, M. (2010). alpha-Catenin as a tension transducer that induces adherens junction development. Nature cell biology *12*, 533-542.

Zaidel-Bar, R. (2013). Cadherin adhesome at a glance. Journal of cell science *126*, 373-378.

Zhang, J., Betson, M., Erasmus, J., Zeikos, K., Bailly, M., Cramer, L.P., and Braga, V.M. (2005). Actin at cell-cell junctions is composed of two dynamic and functional populations. Journal of cell science *118*, 5549-5562.

Zhu, X.L., Liang, L., and Ding, Y.Q. (2008). Overexpression of FMNL2 is closely related to metastasis of colorectal cancer. International journal of colorectal disease *23*, 1041-1047.

6. APPENDIX

6.1 LIST OF PUBLICATIONS

1) **Rao MV** and Zaidel-Bar R (2016). Formin-mediated actin polymerization at cell-cell junctions stabilizes E-cadherin and maintains monolayer integrity during wound repair. *Molecular Biology of the Cell.* 2016 Jul 20. pii: mbc.E16-06-0429. [Epub ahead of print]

2) Zaidel-Bar R, **Rao MV**, Geiger B (2015). The Molecular Architecture of Cell–Cell Adhesions. *Encyclopedia of Cell Biology.* Elsevier Press.

3) Padmanabhan A, **Rao MV**, Wu Y, Zaidel-Bar R (2015). Jack of all trades: functional modularity in the adherens junction. *Current Opinion in Cell Biology.* 16; 36:32-40.

4) **Rao MV**, Chu PH, Hahn KM and Zaidel-Bar R (2013). A novel tool for the activation of endogenous diaphanous-related formins by light reveals thickening of stress fibers without an apparent increase in tension. *Cytoskeleton* Vol. 7, 394-407.

5) Bertocchi C, **Rao MV**, and Zaidel-Bar R (2012). Regulation of Adherens Junction Dynamics by Phosphorylation Switches. *Journal of Signal Transduction*, Article ID 125295.

6.2 COPYRIGHT PERMISSIONS

Related to Figure 1.1A

Copyright Clearance Center **RightsLink®**   Home | Account Info | Help | Live Chat

nature publishing group

Title:	Dynamic contacts: rearranging adherens junctions to drive epithelial remodelling
Author:	Masatoshi Takeichi
Publication:	Nature Reviews Molecular Cell Biology
Publisher:	Nature Publishing Group
Date:	May 14, 2014

Copyright © 2014, Rights Managed by Nature Publishing Group

Order Completed

Thank you very much for your order.

This is a License Agreement between Megha Vaman Rao ("You") and Nature Publishing Group ("Nature Publishing Group"). The license consists of your order details, the terms and conditions provided by Nature Publishing Group, and the payment terms and conditions.

Get the printable license.

License Number	3827500603760
License date	Mar 14, 2016
Licensed content publisher	Nature Publishing Group
Licensed content publication	Nature Reviews Molecular Cell Biology
Licensed content title	Dynamic contacts: rearranging adherens junctions to drive epithelial remodelling
Licensed content author	Masatoshi Takeichi
Licensed content date	May 14, 2014
Type of Use	reuse in a dissertation / thesis
Volume number	15
Issue number	6
Requestor type	academic/educational
Format	print and electronic
Portion	figures/tables/illustrations
Number of figures/tables/illustrations	1
High-res required	no
Figures	Figure 1
Author of this NPG article	no
Your reference number	None
Title of your thesis / dissertation	Functional Characterization of Formin-Dependent Actin Polymerization at Adherens Junctions
Expected completion date	Mar 2016
Estimated size (number of pages)	100
Total	0.00 USD

ORDER MORE... | CLOSE WINDOW

Related to Figure 1.1B

Copyright
Clearance
Center

Note: Copyright.com supplies permissions but not the copyrighted content itself.

1	2	3
PAYMENT	REVIEW	CONFIRMATION

Step 3: Order Confirmation

Thank you for your order! A confirmation for your order will be sent to your account email address. If you have questions about your order, you can call us at +1.855.239.3415 Toll Free, M-F between 3:00 AM and 6:00 PM (Eastern), or write to us at info@copyright.com. This is not an invoice.

Confirmation Number: 11547016
Order Date: 03/14/2016

If you paid by credit card, your order will be finalized and your card will be charged within 24 hours. If you choose to be invoiced, you can change or cancel your order until the invoice is generated.

Payment Information

Megha Vaman Rao
megha.vamanrao@gmail.com
+65 66018984
Payment Method: n/a

Order Details

Journal of cell science

Order detail ID:	69653893
Order License Id:	3827500226519
ISSN:	1477-9137
Publication Type:	e-Journal
Volume:	
Issue:	
Start page:	
Publisher:	COMPANY OF BIOLOGISTS LTD.
Author/Editor:	Company of Biologists

Permission Status: ✔ Granted

Permission type: Republish or display content
Type of use: Republish in a thesis/dissertation

Hide details

Requestor type	Academic institution
Format	Print, Electronic
Portion	chart/graph/table/figure
Number of charts/graphs/tables/figures	1
Title or numeric reference of the portion(s)	Poster Panel 1 - Linking the membrane to actin
Title of the article or chapter the portion is from	Cadherin adhesome at a glance
Editor of portion(s)	N/A
Author of portion(s)	Ronen Zaidel-Bar
Volume of serial or monograph	126
Page range of portion	373-378
Publication date of portion	2013
Rights for	Main product
Duration of use	Life of current edition
Creation of copies for the disabled	no
With minor editing privileges	no
For distribution to	Worldwide
In the following language(s)	Original language of publication

With incidental promotional use	no
Lifetime unit quantity of new product	Up to 499
Made available in the following markets	Education
The requesting person/organization	Megha Vaman Rao/National University of Singapore
Order reference number	
Author/Editor	Megha Vaman Rao
The standard identifier	Thesis/Dissertation (PhD)
Title	Functional characterization of formin-dependent actin polymerization at Adherens Junctions
Publisher	National University of Singapore
Expected publication date	Mar 2016
Estimated size (pages)	100

Note: This item will be invoiced or charged separately through CCC's **RightsLink** service. More info   **$ 0.00**

This is not an invoice.

Total order items: 1   **Order Total: 0.00 USD**

Related to Figure 1.2

Copyright Clearance Center **RightsLink®**

Home | Account Info | Help | Live Chat

Title:	Jack of all trades: functional modularity in the adherens junction
Author:	Anup Padmanabhan,Megha Vaman Rao,Yao Wu,Ronen Zaidel-Bar
Publication:	Current Opinion in Cell Biology
Publisher:	Elsevier
Date:	October 2015

Copyright © 2015 Elsevier Ltd. All rights reserved.

Logged in as:
Megha Vaman Rao
Account #:
3001008509

LOGOUT

Order Completed

Thank you very much for your order.

This is a License Agreement between Megha Vaman Rao ("You") and Elsevier ("Elsevier"). The license consists of your order details, the terms and conditions provided by Elsevier, and the payment terms and conditions.

Get the printable license.

License Number	3833371295216
License date	Mar 20, 2016
Licensed content publisher	Elsevier
Licensed content publication	Current Opinion in Cell Biology
Licensed content title	Jack of all trades: functional modularity in the adherens junction
Licensed content author	Anup Padmanabhan,Megha Vaman Rao,Yao Wu,Ronen Zaidel-Bar
Licensed content date	October 2015
Licensed content volume number	36
Licensed content issue number	n/a
Number of pages	9
Type of Use	reuse in a thesis/dissertation
Portion	figures/tables/illustrations
Number of figures/tables/illustrations	1
Format	both print and electronic
Are you the author of this Elsevier article?	Yes
Will you be translating?	No
Original figure numbers	Figure 3
Title of your thesis/dissertation	Functional Characterization of Formin-Dependent Actin Polymerization at Adherens Junctions
Expected completion date	Mar 2016
Estimated size (number of pages)	100
Elsevier VAT number	GB 494 6272 12
Permissions price	0.00 USD
VAT/Local Sales Tax	0.00 USD / 0.00 GBP
Total	0.00 USD

Related to Figures 1.3, 1.4 and 1.5B

Order Completed

Thank you very much for your order.

This is a License Agreement between Megha Vaman Rao ("You") and Nature Publishing Group ("Nature Publishing Group"). The license consists of your order details, the terms and conditions provided by Nature Publishing Group, and the payment terms and conditions.

Get the printable license.

License Number	3827050438745
License date	Mar 13, 2016
Licensed content publisher	Nature Publishing Group
Licensed content publication	Nature Reviews Molecular Cell Biology
Licensed content title	A nucleator arms race: cellular control of actin assembly
Licensed content author	Kenneth G. CampelloneandMatthew D. Welch
Licensed content date	Apr 1, 2010
Type of Use	reuse in a dissertation / thesis
Volume number	11
Issue number	4
Requestor type	academic/educational
Format	print and electronic
Portion	figures/tables/illustrations
Number of figures/tables/illustrations	3
High-res required	no
Figures	Figures 2, 4 and 5
Author of this NPG article	no
Your reference number	None
Title of your thesis / dissertation	Functional Characterization of Formin-Dependent Actin Polymerization at Adherens Junctions
Expected completion date	Mar 2016
Estimated size (number of pages)	100
Total	0.00 USD

ORDER MORE... | CLOSE WINDOW

Related to Figure 1.5A

npg nature publishing group

Title:	Unleashing formins to remodel the actin and microtubule cytoskeletons
Author:	Melissa A. Chesarone, Amy Grace DuPage and Bruce L. Goode
Publication:	Nature Reviews Molecular Cell Biology
Publisher:	Nature Publishing Group
Date:	Dec 9, 2009

Copyright © 2009, Rights Managed by Nature Publishing Group

Logged in as:
Megha Vaman Rao
Account #:
3001008509

LOGOUT

Order Completed

Thank you very much for your order.

This is a License Agreement between Megha Vaman Rao ("You") and Nature Publishing Group ("Nature Publishing Group"). The license consists of your order details, the terms and conditions provided by Nature Publishing Group, and the payment terms and conditions.

Get the printable license.

License Number	3827060933543
License date	Mar 13, 2016
Licensed content publisher	Nature Publishing Group
Licensed content publication	Nature Reviews Molecular Cell Biology
Licensed content title	Unleashing formins to remodel the actin and microtubule cytoskeletons
Licensed content author	Melissa A. Chesarone, Amy Grace DuPage and Bruce L. Goode
Licensed content date	Dec 9, 2009
Type of Use	reuse in a dissertation / thesis
Volume number	11
Issue number	1
Requestor type	academic/educational
Format	print and electronic
Portion	figures/tables/illustrations
Number of figures/tables/illustrations	1
High-res required	no
Figures	Figure 2
Author of this NPG article	no
Your reference number	None
Title of your thesis / dissertation	Functional Characterization of Formin-Dependent Actin Polymerization at Adherens Junctions
Expected completion date	Mar 2016
Estimated size (number of pages)	100
Total	0.00 USD

ORDER MORE... | CLOSE WINDOW

Related to Figure 4.1A

Related to Figure 4.1B

Title:	Annexin 2 Regulates Intestinal Epithelial Cell Spreading and Wound Closure through Rho-Related Signaling
Author:	Brian A. Babbin,Charles A. Parkos,Kenneth J. Mandell,L. Matthew Winfree,Oskar Laur,Andrei I. Ivanov,Asma Nusrat
Publication:	The American Journal of Pathology
Publisher:	Elsevier
Date:	March 2007

Copyright © 2007 American Society for Investigative Pathology. Published by Elsevier Inc. All rights reserved.

Order Completed

Thank you very much for your order.

This is a License Agreement between Megha Vaman Rao ("You") and Elsevier ("Elsevier"). The license consists of your order details, the terms and conditions provided by Elsevier, and the payment terms and conditions.

Get the printable license.

License Number	3826500312357
License date	Mar 12, 2016
Licensed content publisher	Elsevier
Licensed content publication	The American Journal of Pathology
Licensed content title	Annexin 2 Regulates Intestinal Epithelial Cell Spreading and Wound Closure through Rho-Related Signaling
Licensed content author	Brian A. Babbin,Charles A. Parkos,Kenneth J. Mandell,L. Matthew Winfree,Oskar Laur,Andrei I. Ivanov,Asma Nusrat
Licensed content date	March 2007
Licensed content volume number	170
Licensed content issue number	3
Number of pages	16
Type of Use	reuse in a thesis/dissertation
Portion	figures/tables/illustrations
Number of figures/tables/illustrations	1
Format	both print and electronic
Are you the author of this Elsevier article?	No
Will you be translating?	No
Original figure numbers	Figure 1
Title of your thesis/dissertation	Functional Characterization of Formin-Dependent Actin Polymerization at Adherens Junctions
Expected completion date	Mar 2016
Estimated size (number of pages)	100
Elsevier VAT number	GB 494 6272 12
Permissions price	0.00 USD
VAT/Local Sales Tax	0.00 USD / 0.00 GBP
Total	0.00 USD

Related to Figure 4.2A

Articles published in the following journal follow the Creative Commons Attributions (CC BY) license. This license was developed to facilitate open access – namely, free immediate access to, and unrestricted reuse of, original works of all types.

Under this license, authors agree to make articles legally available for reuse, without permission or fees, for virtually any purpose. Anyone may copy, distribute or reuse these articles, as long as the author and original source are properly cited.

Weblinks to journal(s) from where material has been re-used in this thesis under the CC BY license are provided here:

PLOS Biology
http://journals.plos.org/plosbiology/s/content-license